Modelling Calcite Dissolution in a Rotating Disc Reaction Vessel

by

Camelia Yazdani

A thesis submitted to the
School of Graduate and Postdoctoral Studies in partial
fulfillment of the requirements for the degree of

Master of Science in Modelling and Computational Science

Faculty of Science
University of Ontario Institute of Technology
(Ontario Tech University)

Oshawa, Ontario, Canada
June, 2021

Thesis Examination Information

Submitted by : **Camelia Yazdani**

Master of Science in **Modelling and Computational Science**

Thesis title: Modelling Calcite Dissolution in a Rotating Disc Reaction Vessel

An oral defense of this thesis took place on June 18, 2021 in front of the following examining committee:

Examining Committee

Chair of Examining Committee:	Dr. Lennaert van Veen
Research Supervisor:	Dr. C. Sean Bohun
Examining Committee Member:	Dr. Greg Lewis
Examining Committee Member:	Dr. Fedor Naumkin
Thesis Examiner:	Dr. Iain Moyles, York University

The above committee determined that the thesis is acceptable in form and content and that a satisfactory knowledge of the field covered by the thesis was demonstrated by the candidate during an oral examination. A signed copy of the Certificate of Approval is available from the School of Graduate and Postdoctoral Studies.

Abstract

The carbonate system is ubiquitous in nature, playing a role in many natural and industrial processes. For calcite dissolution, the kinetics and mass transport of the dissolved species reflect both the chemistry of the bulk, and the conditions at the dissolving interface. We formulate the dissolution problem as a set of coupled convection-reaction-diffusion equations that is not only consistent with the bulk chemistry, but is also connected with a Stefan condition for dissolution interface, treating it as a free boundary. The substantial difference in the order of magnitude of the various reaction rates decouples the system. The relatively slow speed of the moving interface allows for a quasi-steady solution. The model reproduces the experimentally observed behaviour without the need to introduce additional reactions occurring at the reacting surface.

keywords: calcite dissolution; rotating disc; Stefan Condition; advection-diffusion-reaction model; natural scaling

Author's Declaration

I declare that this work was carried out in accordance with the regulations of the University of Ontario Institute of Technology
(Ontario Tech University). The work is original except where indicated by special reference in the text and no part of this document has been submitted for any other degree. Any views expressed in the dissertation are those of the author and in no way represent those of the University of Ontario Institute of Technology
(Ontario Tech University). This document has not been presented to any other University for examination either in Canada or overseas.

Camelia Yazdani

Date: June 30, 2021

Statement of Contributions

Part of the work described in Chapter 3 and 4 was presented in:

1. Yazdani, Camelia and Bohun, C.Sean "Modelling Calcite Dissolution in a Rotating Disk Reaction Vessel." The IV AMMCS International Conference, Aug 20-25, 2017.

I hereby certify that I am the sole author of this thesis and that no part of this thesis has been published or submitted for publication. I have used standard referencing practices to acknowledge ideas, research techniques, or other materials that belong to others. Furthermore, I hereby certify that I am the sole source of the creative works and/or inventive knowledge described in this thesis.

Acknowledgements

First of all, I would like to sincerely thank my supervisor, Dr. C. Sean Bohun, who offered me this project to work on, has been my mentor, patiently guiding and helping me all the way, always encouraging and confident that everything would work out fine. Also, I would like to extend my gratitude to the advising committee that took their time to read and comment on this. Thanks to Corrie Geertsen for editing and proofreading, it is much appreciated. A big thank you to all the profs in the math program who taught me, and to my co- workers, past and present grad students in the Modelling and Computational Science program and in the CLAIM lab for their friendship and support. So grateful to my adopted country of Canada, that gave me opportunity to pursue an education, after I was barred a post-secondary education in my home land.

Deep gratitude to my parents for their unconditional, unwavering love and support throughout my life; my father, Dr. Keykhosro, who nurtured in me an admiration for intellectual power of human being and its manifestation in all forms of arts and science; my mother, Parichehre who taught me to embrace challenges and never stop learning; to Ashkan, Samin, and Nivedita, who are the delight of my heart and their beings was the most potent force for me not to give up. Finally, thanks a million to my best friend, my life companion, and pillar of support, Hamed, who never stopped believing in me, respected my desire and been my confident. None of this would have been possible without having him by my side. Thank you!

To those who endeavored to unravel the reality of things,
and those who labored to create beautiful things,
to uplift the world of being.

Contents

List of Tables

List of Figures

CHAPTER 1

Introduction

Calcium carbonate or calcite ($CaCO_3(s)$), is an extremely common mineral making up approximately 4% of the Earth's crust. It is considered one of the major carbon depositories on Earth. Over millions of years, carbon dioxide from the atmosphere has diffused into the oceans, then through the actions of precipitation and evaporation, been stored in limestone deposits. When subjected to heat and pressure, this limestone transforms into marble (a metamorphic rock) that is used extensively in construction due to its inherent beauty, abundance, and durability. The dissolution and precipitation of calcite plays a role in (i) monument degradation, (ii) karst landscape formation, and (iii) ocean acidification/coral reef dissolution.

Oil deposits are usually found in sedimentary rocks such as sandstone or limestone, the latter composed primarily of calcium carbonate ($CaCO_3(s)$) in the form of the mineral calcite. To increase the production of a petroleum reservoir, a commonly used stimulation technique is to inject acid into the pores of a rock formation to accelerate the dissolution of the matrix rock and/or materials encapsulating an oil deposit. This method, known as matrix acidization, enlarges the pores in the

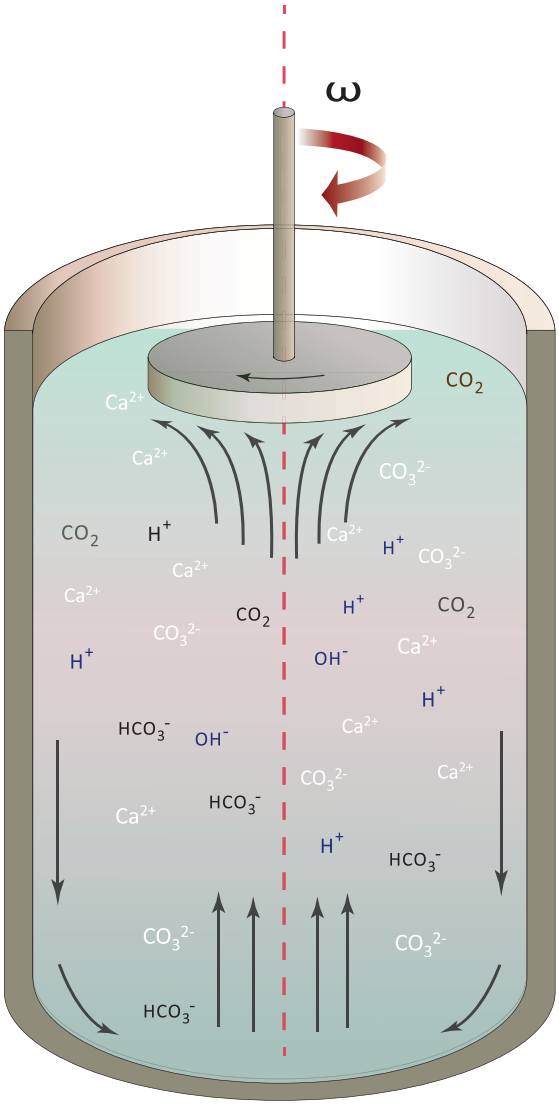

Figure 1.1: A rotating disc reaction vessel used to study the dissolution process.

rock, and is intimately tied to the process of calcite dissolution.[1]

A controlled way to study this dissolution process is the rotating disc reaction vessel. See Figure 1.1. With this method, the rock sample is attached to a rotating shaft, and is submerged in a solution of reactant. The temperature, pressure, and rotation rate can also be controlled. The rotation of the disc creates a uniform thickness boundary layer across the sample surface that is independent of its distance

[1]In contrast, the Alberta oil sands consist of a mixture of sand, water, and bitumen. The latter material consists of oil that is too heavy or thick to flow on its own. Bitumen requires extraction from underneath the boreal forest, either through surface mining or in-situ recovery.

from the axis of rotation. Levich in [23] derived an expression for the magnitude of the mass flux due to diffusion (diffusional mass flux) as

$$J = -D \left.\frac{\partial c}{\partial z}\right|_{z=0} \simeq 0.62048 D^{2/3} \nu^{-1/6} \omega^{1/2} c_\infty, \tag{1.1}$$

where D is the diffusion coefficient of the solution, ν is the kinematic viscosity, ω is the angular velocity, and c_∞ is the constituent concentration in the bulk. This result ignores any chemical kinetics, assumes that the fluid is unbounded, and outside of the boundary layer, and that fluid only flows in the axial (vertical) direction.

The rotating disc apparatus, along with the result of Levich, are utilized in the petroleum industry to characterize the matrix acidization process during drilling. This method can indicate, with some processing, the dissolution rate, reaction rate constants, and the reaction order specific to each unique rock formation. Rather than the classical Levich equation (1.1), a modified expression for large Schmidt numbers ($\mathrm{Sc} = \nu/D$) is used [28]

$$J_{\text{corr}} = \frac{0.62048 D^{2/3} \nu^{-1/6} \omega^{1/2} c_\infty}{1 - 0.2980\,\mathrm{Sc}^{-1/3} + 0.1451\,\mathrm{Sc}^{-2/3}}. \tag{1.2}$$

Despite this correction, there has been significant variability in the observed reaction rate data of the reservoir rock. In essence, different laboratories using similar experimental techniques, and utilizing the Levich equation, should produce consistent results with rock samples from the same formation. However, this is not the case. Taylor and H.A. Nasr-El-Din [40] quantify this surprising variability, which cannot be easily justified. It is suspected that many of the experimental results are obtained in chemical environments that violate the assumptions used to arrive at Levich's result. For example, when a very strong acid such as HCl is used in a sample of calcite and dolomite,[2] and the pH is monitored over time, the reaction rates

[2] Dolomite is a carbonate mineral composed of calcium magnesium carbonate, $\mathrm{CaMg(CO_3)_2}$.

of the calcite and dolomite can be determined through the stiochiometry. However, directly applying the Levich equation, or its correction, is an oversimplification of this complex chemical system.

To address this variability, we will focus on calcite and the specific chemistry involved in its dissolution. A starting point for this is the work of Dreybrodt which details the dissolution and precipitation of calcite in open [4] and closed [5] systems. In this work, the surface reactions and the mass transport for the basic $CaCO_3$(s)-CO_2-H_2O system are combined with a rate equation to find the boundary values for the ion species. This rate equation is known as the PWP equation, and is a result of the contribution made by Plummer, Wigley, and Parkhurst (PWP) in their experimental investigations on surface controlled reactions. Rather than using the experimentally determined PWP boundary conditions, this research uses a Stefan condition at the dissolving interface, that preserves mass as the material dissolves. This gives results that are consistent with those that use the PWP equation.

The aim of this thesis, and the research it contains, is to fill a gap that bridges the classical Levich result with modern mathematical modelling of the process of dissolution. Motivated to build a comprehensive model to describe calcite dissolution in the setting of a rotating disc vessel, we include the specific chemical kinetics, as well as imposing mass conservation at the dissolution interface. We must consider the chemical reactions taking place in the bulk fluid and at the rock surface. This will require a careful analysis of the fluid flow and the resulting transport of various ion species.

We start in Chapter 2 with a detailed explanation of the setting and specifications of the rotating disc reaction vessel. We derive the equations for the fluid flow using the Navier-Stokes equation in a cylindrical coordinate system. We solve for the velocity distribution, swirling von Kármán flow, as explained in Appendix A. The classical Levich solution and its applications are discussed. In Chapter 3, we

discuss the equilibrium chemistry of the carbonate system, and the $CaCO_3(s)$ dissolution process. Two equilibrium regimes: (i) no calcium in solution, and (ii) saturated with calcium in solution are analyzed. Changes in the behaviour of the system with respect to acidity, and partial pressure of CO_2 are explored. We construct the full model we each of the chemical species in Chapter 4. This includes the chemical system, the fluid motion, and the Stefan condition arising from the dissolution process itself. A system of equations are proposed, boundary conditions are defined, and characteristic scalings are used to find a set of dimensionless quantities. It is shown that the system splits into a set of slow reactions, and a collection of algebraic equilibrium conditions. In Chapter 5, the numerical solution of the model will be explored for a fixed pressure and acidity. In Chapter 6, the dependence on pressure and solution acidity is presented, and compared with a set of experimental data. This is the same data that has been used to define the PWP model, which is typically used as an experimentally derived boundary condition for the carbonate system in dissolution problems. Finally, the thesis is concluded in Chapter 7.

CHAPTER 2

The Rotating Disc Reaction Vessel

The rotating disc apparatus is usually used to study chemical kinetics under laboratory conditions. It consists of a rock disc, attached to a rotating shaft, inside a cylindrical vessel. If the disc is made of the material under consideration, it can serve as the reaction site, a technique used in many electrochemical laboratory experiments.

2.1 Classical Levich

In these experiments, the fluid moves due to a rotating disc and is assumed to reach equilibrium, necessitating the search for a stationary, axi-symmetric solution of the incompressible Navier-Stokes equations. The pioneering study of this problem was carried out by von Kármán [42], where he formulated the fluid flow problem in terms of a natural similarity variable, and was able to convert the system of partial differential equations into a system of nonlinear ordinary differential equations. Subsequently, Cochran [7] advanced von Kármán's result, and obtained asymptotic

solutions for the steady hydrodynamic problem.

To pick up the geometric aspects of the rotating vessel, a similarity solution is attempted. In particular, a similarity variable ζ is identified, and the Navier-Stokes equations, (A.2)–(A.5), detailed in Appendix A, are nondimensionalized by applying the transformation

$$z = \sqrt{\frac{\nu}{\omega}}\zeta, \quad u_r = r\omega F(\zeta), \quad u_\theta = r\omega G(\zeta), \quad u_z = \sqrt{\nu\omega}H(\zeta), \quad p = -\rho\nu\omega P(\zeta). \quad (2.1)$$

This reduces the system (A.2)–(A.5) for the fluid flow $\mathbf{u} = \langle u_r, u_\theta, u_z \rangle$, to a system of non-linear coupled ordinary differential equations

$$F'' = F^2 - G^2 + F'H, \quad (2.2)$$

$$G'' = 2FG + G'H, \quad (2.3)$$

$$H' = -2F. \quad (2.4)$$

The primes denote derivatives with respect to the variable ζ. A unique solution to the system (2.2)–(2.4) requires five conditions. These are provided by the initial conditions

$$F(0) = 0, \qquad G(0) = 1, \qquad H(0) = 0, \quad (2.5)$$

and terminal conditions

$$\lim_{\zeta\to\infty} F(\zeta) = 0, \qquad \lim_{\zeta\to\infty} G(\zeta) = 0. \quad (2.6)$$

With the solution specified, the limiting value of $\lim_{z\to\infty} u_z(z) = -U_0$ becomes, under the transformation (2.1), the condition

$$\lim_{\zeta\to\infty} H(\zeta) = -(\nu\omega)^{-1/2}U_0. \quad (2.7)$$

See Appendix A for more details.

Plots of the dimensionless quantities F, G, and H can be found in Figure 2.1. It shows, that with increasing ζ, the tangential velocity component, $G(\zeta)$, decreases exponentially, the axial velocity component increases, though in the negative direction. The radial velocity component, $F(\zeta)$, initially increases, but eventually approaches zero. At a distance from the disc surface near the value of $\zeta = 3.6$, corresponding to $z = 3.6(\nu/\omega)^{1/2}$, the quantity $H(\zeta)$ reaches 80% of its ultimate value of U_0, and $G(\zeta)$ decreases to 5% of its value at the disc surface. This layer, adjacent to the rotating disc surface, is the hydrodynamic boundary layer, the thickness of which we denote as δ_0 so that $\delta_0 = 3.6(\nu/\omega)^{1/2}$. Within this layer, the tangential and radial velocity components are not zero, and beyond this layer, the flow motion is primarily axial. The disc as been assumed to be of infinite extent. For a finite disc, the edge effects of the disc are negligible for the central flow, up to a few boundary layer thicknesses away from the edge.

In the rotating disc flow, the material is transferred from one location to the other through the combined processes of diffusion and advection. Diffusion is due to the random movement of particles from high concentrations to lower concentrations, while advection, is due to the particles being carried along with the motion of the fluid itself. Also called advection-diffusion, its derivation comes from a basic application of the conservation of mass. In this case, the quantity $P = P(\mathbf{x}, t)$ is the mass per unit volume or the concentration $c = c(\mathbf{x}, t)$, while the corresponding flux, $\mathbf{Q} = \mathbf{Q}(\mathbf{x}, t) = \mathbf{u}c - D\nabla c$, has units of mass per area per time. The first term, corresponding to the motion of the material due to the velocity field $\mathbf{u}$, and the second term is due to the diffusion of material from regions of high to low concentration, with diffusivity D. The expression for the conservation of mass is

$$\frac{\partial P}{\partial t} + \nabla \circ \mathbf{Q} = R \tag{2.8}$$

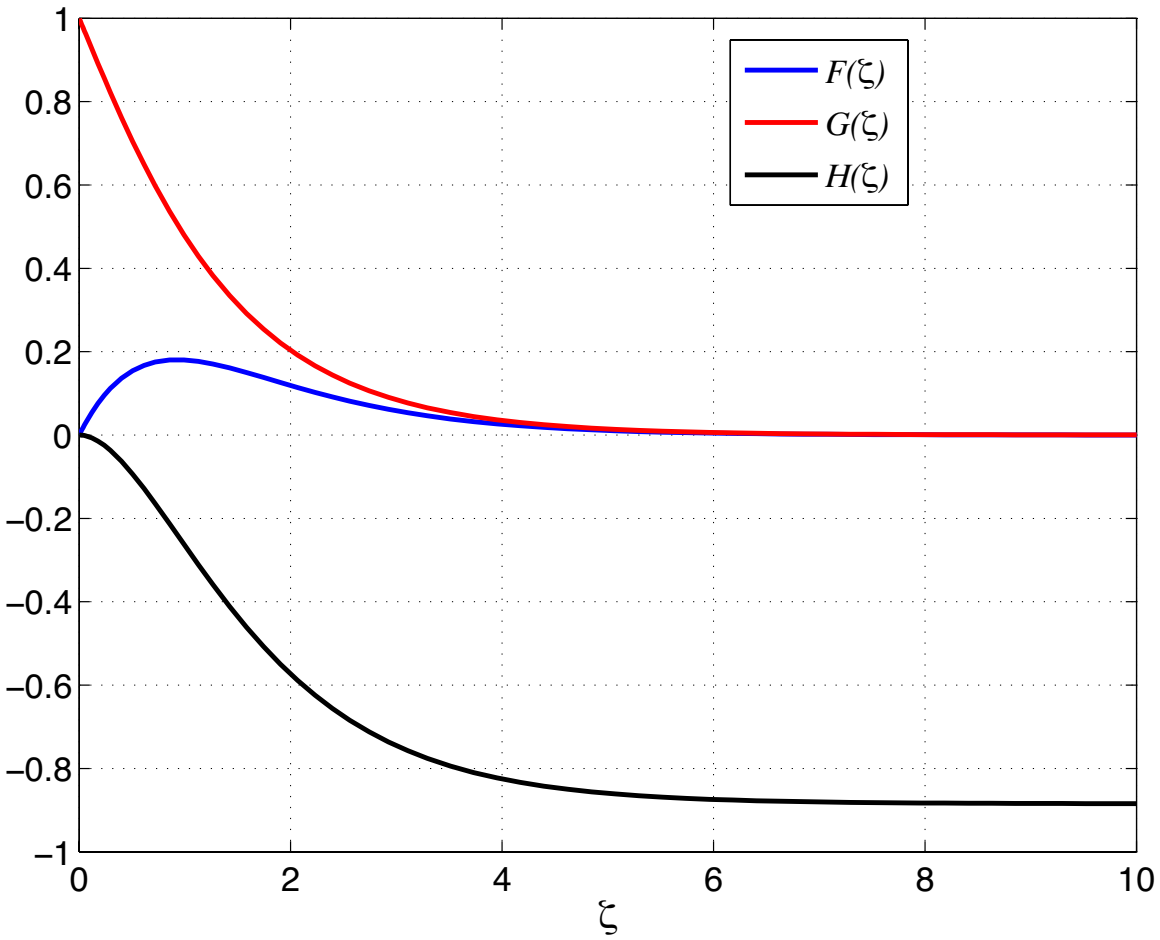

Figure 2.1: Components $F(\zeta), G(\zeta)$ and $H(\zeta)$ of the system (2.2). This results in the asymptotic value of $\lim_{\zeta\to\infty} H(\zeta) = -\alpha \simeq 0.884919$.

which is the advection-diffusion-reaction equations, where $R = R(\mathbf{x}, t)$ is the rate of production $(R > 0)$ or consumption $(R < 0)$ for the given quantity c. For an incompressible fluid, so that $\nabla \circ \mathbf{u} = 0$, and no production or consumption of the material $(R = 0)$, equation (2.8) becomes

$$\frac{\partial c}{\partial t} + \mathbf{u} \circ \nabla c - \nabla \circ (D \nabla c) = 0. \tag{2.9}$$

Further simplification can be made if we assume D is constant and in a steady state so that $\partial c/\partial t = 0$. In cylindrical coordinates and using these simplifying assump-

tions, equation (2.9) takes the form

$$u_r\frac{\partial c}{\partial r}+\frac{u_\theta}{r}\frac{\partial c}{\partial \theta}+u_z\frac{\partial c}{\partial z}=D\left(\frac{\partial^2 c}{\partial z^2}+\frac{\partial^2 c}{\partial r^2}+\frac{1}{r}\frac{\partial c}{\partial r}+\frac{1}{r^2}\frac{\partial^2 c}{\partial \theta^2}\right). \tag{2.10}$$

To reproduce the classical result due to Levich [23], we assume that the concentration is only a function of distance from the disc surface, z, and doesn't depend on either the radial or angular coordinates r and θ. This reduces (2.10) to the classical problem

$$u_z\frac{\mathrm{d}c}{\mathrm{d}z}=D\frac{\mathrm{d}^2 c}{\mathrm{d}z^2}, \qquad c(0)=0, \qquad \lim_{z\to\infty}c(z)=c_\infty, \tag{2.11}$$

where c_∞ is the concentration of the substance in the bulk solution, and the concentration at the disc surface is set to zero. Integrating once yields

$$\frac{\mathrm{d}c}{\mathrm{d}z}=A_1\exp\left(\frac{1}{D}\int_0^z u_z(w)\,\mathrm{d}w\right) \tag{2.12}$$

and once again to get

$$c(z)=A_1\int_0^z\exp\left(\frac{1}{D}\int_0^x u_z(w)\,\mathrm{d}w\right)\mathrm{d}x+A_2. \tag{2.13}$$

Considering the set boundary conditions, since $c(0)=0$, $A_2=0$. In a similar fashion, letting $\lim_{z\to\infty}c(z)=c_\infty$ we find

$$c_\infty=A_1\int_0^\infty\exp\left(\frac{1}{D}\int_0^x u_z(w)\,\mathrm{d}w\right)\mathrm{d}x, \tag{2.14}$$

and consequently

$$c(z)=c_\infty\frac{\displaystyle\int_0^z\exp\left(\frac{1}{D}\int_0^x u_z(w)\,\mathrm{d}w\right)\mathrm{d}x}{\displaystyle\int_0^\infty\exp\left(\frac{1}{D}\int_0^x u_z(w)\,\mathrm{d}w\right)\mathrm{d}x}. \tag{2.15}$$

An expression for the magnitude of the mass flux at the disc surface is now given by

$$J = D\left.\frac{\partial c}{\partial z}\right|_{z=0} = Dc_\infty\left(\int_0^\infty \exp\left(\frac{1}{D}\int_0^x u_z(w)\,\mathrm{d}w\right)\mathrm{d}x\right)^{-1}. \tag{2.16}$$

To calculate this improper integral, we will divide it into two regions, one within the boundary layer, and one beyond

$$\frac{c_\infty}{A_1} = \underbrace{\int_0^{\delta_0} \exp\left(\frac{1}{D}\int_0^x u_z(w)\,\mathrm{d}w\right)\mathrm{d}x}_{I_1} + \underbrace{\int_{\delta_0}^\infty \exp\left(\frac{1}{D}\int_0^x u_z(w)\,\mathrm{d}w\right)\mathrm{d}x}_{I_2}. \tag{2.17}$$

For evaluating the first integral, we will use an asymptotic expansion for u_z near $z = 0$, see Appendix A, expression (A.26), and neglect the higher order terms so that

$$u_z(z) = -a_1\sqrt{\frac{\omega^3}{\nu}}z^2 + \mathcal{O}\left(\left(\frac{\omega}{\nu}\right)^{3/2} z^3\right) \tag{2.18}$$

where $a_1 \simeq 0.510232618867$. Plugging this result into the first integral gives

$$I_1 = \int_0^{\delta_0} \exp\left(\frac{1}{D}\int_0^x u_z(w)\,\mathrm{d}w\right)\mathrm{d}x \simeq \int_0^{\delta_0} \exp\left(-\frac{a_1}{3}D^{-1}\nu^{-1/2}\omega^{3/2}x^3\right)\mathrm{d}x. \tag{2.19}$$

To further simplify first let $s = (a_1/3)^{1/3}D^{-1/3}\nu^{-1/6}\omega^{1/2}x$ and note that for $\lambda = \mathcal{O}(1)$, $\delta_0 = \lambda(\nu/\omega)^{1/2}$, we have[1]

$$I_1 \simeq \left(\frac{3}{a_1}\right)^{1/3} D^{1/3}\nu^{1/6}\omega^{-1/2}\int_0^{\overline{s}} \mathrm{e}^{-s^3}\,\mathrm{d}s, \qquad \overline{s} = \lambda\left(\frac{a_1}{3}\right)^{1/3}\left(\frac{\nu}{D}\right)^{1/3}. \tag{2.20}$$

For an aqueous solution, the kinematic viscosity of water is $\nu = 10^{-6}\ \mathsf{m}^2\,\mathsf{s}^{-1}$, and the diffusion coefficient of molecules dissolved in the liquid are in the range of

[1] The thickness of the hydrodynamic boundary layer is defined as that distance where the velocity reaches 80% of its limiting value, or $u_z(\delta_0) = 0.8\lim_{z\to\infty} u_z(z)$. This corresponds to $\lambda \simeq 3.6$.

$10^{-10}\,\mathrm{m^2\,s^{-1}} < D < 10^{-9}\,\mathrm{m^2\,s^{-1}}$, so that $4.64\times10^{-2} < (D/\nu)^{1/3} < 10^{-1}$. For the upper bound of the integral, the dimensionless ratio $\nu/D = \mathcal{O}(10^3)$. Since $\lambda(a_1/3)^{1/3} = \mathcal{O}(1)$, and the integrand decreases rapidly, we can replace this the upper bound with infinity, effectively losing the dependence on the boundary layer thickness. Through a change of variable and integration by parts,[2]

$$\int_0^\infty \mathrm{e}^{-s^3}\,\mathrm{d}s = \frac{1}{3}\int_0^\infty \mathrm{e}^{-x}x^{-2/3}\,\mathrm{d}x = \int_0^\infty \mathrm{e}^{-x}x^{1/3}\,\mathrm{d}x = \Gamma\left(\frac{4}{3}\right), \tag{2.21}$$

and we have that[3]

$$I_1 \simeq \left(\frac{3}{a_1}\right)^{1/3}\Gamma\left(\frac{4}{3}\right)D^{1/3}\nu^{1/6}\omega^{-1/2}. \tag{2.22}$$

A similar strategy follows for evaluating the second integral, corresponding to the region beyond the boundary layer. For this term, the approximation for u_z is taken as $z\to\infty$. From Appendix A, expression (A.34), the asymptotic expansion for u_z as $z\to\infty$,

$$u_z(z) = -\alpha\sqrt{\nu\omega} + \mathcal{O}\left(\mathrm{e}^{-\alpha(\omega/\nu)^{1/2}z}\right), \qquad \alpha = 0.884919. \tag{2.23}$$

In this case, the estimate for I_2 becomes

$$\begin{aligned} I_2 &= \int_{\delta_0}^\infty \exp\left(\frac{1}{D}\int_0^x u_z(w)\,\mathrm{d}w\right)\mathrm{d}x \simeq \int_{\delta_0}^\infty \exp\left(-\frac{\alpha\sqrt{\nu\omega}}{D}x\right)\mathrm{d}x \\ &= \frac{D}{\alpha\sqrt{\nu\omega}}\mathrm{e}^{-\lambda\alpha\nu/D}. \end{aligned} \tag{2.24}$$

As discussed earlier, for $\nu \gg D$, which is the case for most water based solutions,

[2] $\Gamma(z) = \int_0^\infty \mathrm{e}^{-x}x^{z-1}\,dx$, $\Re z > 0$.

[3] Note that $\left(\frac{3}{a_1}\right)^{1/3}\Gamma\left(\frac{4}{3}\right) \simeq 1.61166$.

the value of I_2 is negligible comparing to I_1, so it is justified to state

$$\int_0^\infty \exp\left(\frac{1}{D}\int_0^x u_z(w)\,\mathrm{d}w\right)\mathrm{d}x \simeq \left(\frac{3}{a_1}\right)^{1/3}\Gamma\left(\frac{4}{3}\right)D^{1/3}\nu^{1/6}\omega^{-1/2}. \tag{2.25}$$

The expression for the magnitude of the mass flux, (2.16), simplifies to

$$J = D\left.\frac{\partial c}{\partial z}\right|_{z=0} \simeq \frac{(a_1/3)^{1/3}}{\Gamma(4/3)}D^{2/3}\nu^{-1/6}\omega^{1/2}c_\infty \tag{2.26}$$

which is the classical [23] result due to Levich.

From Levich [23], the thickness of the diffusion layer, δ, is defined by setting $\partial c/\partial z|_{z=0} \simeq c_\infty/\delta$, and from both (2.15) and $\delta_0 = \lambda(\nu/\omega)^{1/2}$,

$$\delta \simeq I_1 \simeq \left(\frac{3}{a_1}\right)^{1/3}\Gamma\left(\frac{4}{3}\right)\frac{1}{\lambda}\left(\frac{D}{\nu}\right)^{1/3}\delta_0, \qquad \left(\frac{3}{a_1}\right)^{1/3}\Gamma\left(\frac{4}{3}\right)\frac{1}{\lambda} \simeq 0.447683. \tag{2.27}$$

We see that for aqueous systems this diffusion boundary layer, δ, is thinner than the hydrodynamic boundary layer, δ_0, adjacent to the disc surface. An interesting feature of the diffusion boundary layer in a rotating disc flow setting, is that its thickness does not depend on the distance from the axis of rotation. It has the same thickness for the entire surface of the disc, except near the edges. This behaviour is termed a uniformly accessible surface from a diffusional standpoint.

2.2 An Electrochemical Interpretation

Another example of von Kármán swirling flow at work is the rotating disc electrode (RDE). The rotating disc apparatus is a hydrodynamic device used in voltammetry, a subcategory of electrochemical methods in which information about the analyte (the chemical compound of interest) is obtained, by measuring the electric current as the voltage (electric potential) is varied. The spinning disc introduces convection

into the chemical cell, and as long as the rotational speed is within a certain limit, it creates predictable laminar flow across the surface, as described in the previous section. This method is used in electrochemical studies when investigating reaction mechanisms related to reduction/oxidation chemistry.

The RDE is the working electrode used in a three electrode system. The working electrode makes contact with the analyte, applies the desired potential in a controlled way, and facilitates transfer of charge to and from the analyte. The second electrode is the standard/reference electrode, acts as reference in measuring and controlling the potential of the working electrode. It has a known and constant potential, and no current passes through this electrode. The third electrode passes all the current needed to balance the circuit at the working electrode. The working electrode includes a conductive disc (typically platinum or gold) embedded in the top face of a rod of insulating material such as Teflon, epoxy or resin, that can be attached to an electric motor. In this arrangement, the solution is brought in contact with the surface of the electrode, and as the result of the rotation it moves away from the center of the electrode in the radial direction, toward the edge of the cylinder. The configuration is shown in Figure 2.2.

The result is a laminar flow of analyte toward and across the electrode. Provided that the rotational speed is low enough, the laminar flow can be maintained and predicted. This flow is a von Kármán flow, as in the previous section, and the convection-diffusion equation in cylindrical coordinates can be used to solve for the reagent concentration that indicates the number of electrons. The flux of electrons to or from the electrode surface, due to the reactions occurring at the electrode, creates a current, i. In this setting, with a fixed rotational speed of angular velocity ω, a steady-state velocity profile is quickly attained. By using Fick's law of diffusion

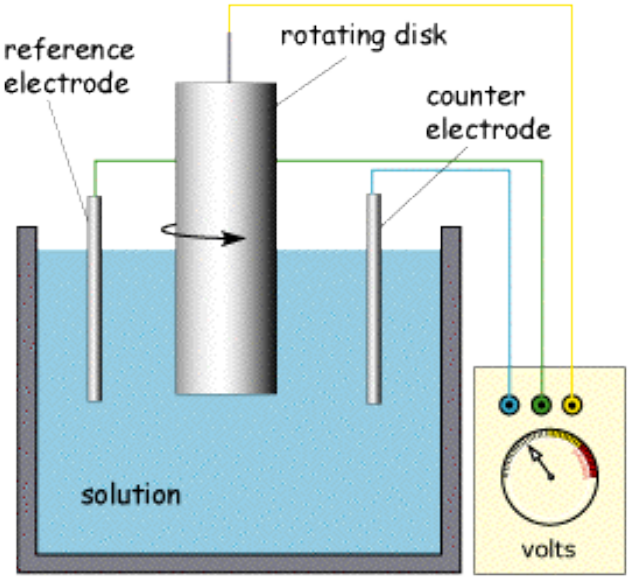

Figure 2.2: The rotating disc apparatus for a three electrode system.

and the boundary conditions, the current is given by

$$i = nFAD \left.\frac{\partial c}{\partial z}\right|_{z=0}. \tag{2.28}$$

In this expression, c is the concentration of the reducible analyte in the bulk of the solution measured in $\mathrm{mol\,m^{-3}}$, n is the number of electrons involved in the electrochemical reaction, $F = 96485.3321\ \mathrm{C\,mol^{-1}}$ is the Faraday constant, A is the electrode surface area measured in $\mathrm{m^2}$, and D is the diffusion coefficient of the solute species expressed in $\mathrm{m^2\,s^{-1}}$.

On the other hand, the total flux of a quantity is defined as the rate of flow of the quantity per unit area and is given by

$$\mathbf{J} = c\mathbf{u} - D\nabla c \tag{2.29}$$

consisting of a term regarding the advection of material due to the fluid velocity $\mathbf{u}$ and a term due to diffusion. Within the hydrodynamic boundary layer, the axial fluid velocity is negligible so that the total flux is effectively only due to diffusion.

This is consistent with how the current i is measured considering the number of the electrons passing per unit surface area which the concentration gradient is based. For the concentration profile, the convection-diffusion equation is used as in the previous section and in the steady state, the equation reduces to

$$u_z \frac{\partial c}{\partial z} = D \frac{\partial^2 c}{\partial z^2}, \qquad c(0) = 0, \qquad \lim_{z \to \infty} c(z) = c_\infty. \tag{2.30}$$

Combining the solution of (2.30) and finding the magnitude of the limiting flux given by (2.26) with the expression for the current (2.28), gives

$$i_{l,c} \simeq \frac{(a_1/3)^{1/3}}{\Gamma(4/3)} nFAD^{2/3}\nu^{-1/6}\omega^{1/2}c_\infty \simeq 0.620nFAD^{2/3}\nu^{-1/6}\omega^{1/2}c_\infty \tag{2.31}$$

where $i = i_{l,c}$ denotes the limiting current. The electric current created is directly proportional to the electrode area of the disc.

2.3 Beyond Levich

By fixing the chemical system (we will choose the carbonate system) sources and sinks of the various chemical quantities may change the standard result as predicted by Levich. In the classical Levich solution for the rotating disc, the disc is treated as an impervious surface and not as a surface that is undergoing dissolution. In addition, the original derivation has no connection to any particular chemical system.

The Levich equation is used extensively for RDE experiments. In order to apply the theory, while remaining cognizant of the dissolution process, the surface boundary condition needs to be revised. Contrary to the classical Levich derivation, the concentration of the critical species at the dissolution surface is not zero

so that

$$c(S(t), t) = c_0, \qquad S(0) = 0. \tag{2.32}$$

where $S(t)$ denotes the position of the dissolving surface as a function of time. The substance at the surface has a maximum concentration. In the bulk, before dissolution begins, the concentration would be zero. That is,

$$\lim_{z \to \infty} c(z, 0) = 0. \tag{2.33}$$

What was defined previously as the horizontal axis where $z = 0$ would require an additional expression that captured the moving boundary. This is known as a Stefan condition, and is effectively a result of mass conservation applied at the dissolution interface.

These aspects will be explored in Chapter 4 but first we consider the carbonate chemical system in detail so that it can be incorporated into the dissolution process.

CHAPTER 3

The Carbonate System

3.1 Aqueous Carbonate Solutions

Carbon dioxide, with the chemical formula of CO_2, is a colourless gas which makes up less than 0.05% of the gases present in the Earth's atmosphere. Natural sources for CO_2 includes ocean release, respiration, organic matter decomposition, forest fires, and volcanic eruptions. It is also added to the air via human activities such as burning fossil fuels, and agriculture. The concentration of CO_2 has been substantially increasing since the industrial revolution [38]. For 800,000 years prior to this, the level had remained relatively constant at about 320 ppm (parts per million) and has been steadily increasing since the the 19^{th} century to 413 ppm in 2020.

Since it is a water soluble gas, CO_2 is also present in groundwater, rivers and lakes, ice caps, glaciers, and seawater. CO_2 is a greenhouse gas that absorbs the long wave radiation in the atmosphere from sunlight and releases it gradually over time. Another reason for the global significance of carbon dioxide, is its reaction with water molecules producing carbonic acid, and lowering the ocean's pH. Since the

start of the Industrial Revolution, the pH of the ocean's surface waters has dropped from 8.21 to 8.04 [13]. This drop in pH is called ocean acidification.

The number of H^+ ions present in a solution is the measure for acidity or basicity of the solution, and is defined as

$$\mathrm{pH} = -\log_{10}[\mathsf{H}^+]. \tag{3.1}$$

In $\mathsf{H_2O}$, pure water, and at standard temperature $(25°\mathsf{C})$, there are about 10^{-7} moles of H^+ ions per liter ($[\mathsf{H}^+] = 10^{-7}$ M)[1] this corresponds to a pH value of 7, which denotes a neutral environment. For an aqueous (water based) solution, the pH scale typically ranges from 1 to 14, from strongest acid to strongest base.

The carbonate system is composed of a number of interrelated chemical reactions which we now describe individually. Beginning with carbon dioxide, $\mathsf{CO_2}$, this species dissolves into free surface waters open to the atmosphere and takes its aqueous form $\mathsf{CO_2(aq)}$. This is represented with the reaction

$$\mathsf{CO_2(g)} \overset{K_\mathrm{H}}{\longleftrightarrow} \mathsf{CO_2(aq)}. \tag{3.2}$$

This equality assumes an equilibrium. Once the molecules have crossed the phase boundary, diffusion in the aqueous phase will distribute them throughout the fluid. Their concentration can be modified spatially due to chemical reactions with the other chemical species. A sophisticated treatment of these modelling aspects can be found in the literature [36]. The solubility of $\mathsf{CO_2}$ decreases with temperature and increases with the partial pressure of $\mathsf{CO_2(g)}$. For pressure up to 5 atm, the solubility follows Henry's law with a temperature dependent Henry's constant, K_H.[2]

From this point forward, all of the chemical components will be assumed to be

[1] The notation $[\cdot]$ denotes the concentration of a particular quantity in moles/litre or M.

[2] By Henry's law, at a constant temperature, the amount of a given gas dissolved in a volume of liquid is directly proportional to the partial pressure of that gas in equilibrium with that liquid.

aqueous and therefore the notation (aq) will be dropped. Dissolved in the water, the aqueous carbon dioxide, through a reversible slow reaction with water molecules, H_2O, forms carbonic acid, H_2CO_3, which rapidly decomposes to release hydrogen ions, H^+, and bicarbonate ions, HCO_3^-, through the reactions

$$CO_2 + H_2O \underset{k_{-1}}{\overset{k_1}{\rightleftharpoons}} {H_2CO_3}^0, \tag{3.3}$$

$${H_2CO_3}^0 \overset{K_1}{\longleftrightarrow} H^+ + HCO_3^-. \tag{3.4}$$

Concurrently, CO_2 molecules react with hydroxide ions to form bicarbonate ions, HCO_3^-. This reaction is slow and reversible, given by

$$CO_2 + OH^- \underset{k_{-2}}{\overset{k_2}{\rightleftharpoons}} HCO_3^-. \tag{3.5}$$

Subsequent to their formation, bicarbonate ions, HCO_3^-, depending upon the pH of the solution, dissociate into hydrogen ions, H^+, and carbonate ions, CO_3^{2-}, via a fast reaction

$$HCO_3^- \overset{K_2}{\longleftrightarrow} H^+ + CO_3^{2-}. \tag{3.6}$$

Another source of hydrogen ions, H^+, or hydroxide ions, OH^-, is the dissociation of water molecules

$$H_2O \overset{K_W}{\longleftrightarrow} H^+ + OH^- \tag{3.7}$$

and the setting of the initial pH level through addition of either HCl or $NaOH$.

This series of reactions form the carbonic acid system. Through this system, the absorption of CO_2 into the water increases the concentration of hydrogen ions, H^+, and creates a weakly acidic environment.

If calcite, $CaCO_3(s)$, also referred to as calcium carbonate, is present then, depending on the concentration of CO_3^{2-} in the solution, it would either dissolve or precipitate, by the reaction

$$CaCO_3(s) \overset{K_{sp}}{\longleftrightarrow} Ca^{2+} + CO_3^{2-}. \tag{3.8}$$

The solubility product constant,[3] K_{sp}, describes the dynamic equilibrium state of this reaction. K_{sp} is used to describe saturated solutions of ionic compounds with relatively low solubility. During the dissolution, the ions contained within the remaining undissolved solid are in a state of dynamic equilibrium with the dissociated ions. For the dissolution of calcite in water,

$$K_{sp} = [Ca^{2+}][CO_3^{2-}] \tag{3.9}$$

at the point where $CaCO_3(s)$ precipitates out of solution. Calcium carbonate also reacts with H^+ ions, to release CO_2 through

$$CaCO_3(s) + H^+ \rightarrow Ca^{2+} + HCO_3^- \tag{3.10}$$

with an overall dissolution reaction that takes the form

$$CaCO_3(s) + 2H^+ \longleftrightarrow Ca^{2+} + H_2O + CO_2 \tag{3.11}$$

obtained by using (3.3) and (3.4). Calcium carbonate will also react with CO_2 saturated water to form the soluble calcium bicarbonate

$$CaCO_3(s) + CO_2 + H_2O \rightarrow Ca(HCO_3^-)_2, \tag{3.12}$$

[3] K_{sp} is defined as the mathematical product of its dissolved ion concentrations raised to the power of their stoichiometric coefficients.

which encapsulates the major causes of ocean acidification when saturated with CO_2. This last reaction, relation (3.12), is also important in the erosion of the carbonate rock, forming caverns and karst landscapes, as well as leading to hard water in many regions.

3.2 The Carbonic Acid System

Collecting together the reactions from the previous section, gives the basic carbonic acid system which can be summarized as follow

$$CO_2(g) \xleftrightarrow{K_H} CO_2, \tag{3.13}$$

$$CO_2 + H_2O \underset{k_{-1}}{\overset{k_1}{\rightleftharpoons}} {H_2CO_3}^0, \tag{3.14}$$

$${H_2CO_3}^0 \xleftrightarrow{K_1} H^+ + HCO_3^-, \tag{3.15}$$

$$CO_2 + OH^- \underset{k_{-2}}{\overset{k_2}{\rightleftharpoons}} HCO_3^-, \tag{3.16}$$

$$HCO_3^- \xleftrightarrow{K_2} H^+ + CO_3^{2-}, \tag{3.17}$$

$$H_2O \xleftrightarrow{K_W} H^+ + OH^-. \tag{3.18}$$

The slower reactions are characterized by lowercase rate constants and the fast reactions are given by uppercase equilibrium constants. The superscript '0' on ${H_2CO_3}^0$ refers to carbonic acid in equilibrium with both the bicarbonate ion and the aqueous carbon dioxide, and will be clarified below.

In reaction (3.13), $CO_2(g)$ is dissolved and either forms bicarbonate ions directly through (3.16), or is effectively catalyzed through the formation of carbonic acid in (3.14)–(3.15). Bicarbonate ions can then disassociate with (3.17) to form carbonate ions. The final reaction, (3.18), is the equilibrium of water with hydrogen and hydroxide ions. The overall pH of the reaction can be changed though the addition of a strong acid or base, for example, $HCl \rightarrow H^+ + Cl^-$ or $NaOH \rightarrow Na^+ + OH^-$,

which effectively completely disassociate into their respective ions with either the Cl^- or Na^+ providing the charge balance. Any resulting reactions would have to be included.

If calcite is present then there is an additional reaction

$$CaCO_3(s) \overset{K_{sp}}{\longleftrightarrow} Ca^{2+} + CO_3^{2-} \tag{3.19}$$

which illustrates that as $CaCO_3(s)$ is dissolved by (3.19), the calcium ions that are injected into the solution are influenced by the carbonate ions already present, affecting its solubility.

Variants on the system (3.13)–(3.19) appear in the literature. A closely related system that neglects (3.16) and (3.18) is studied in [26] with respect to ocean acidification, and it is shown that despite the seeming complexity of the system, there is a natural decoupling of time scales due to the rate coefficients differing by many orders of magnitude. All of the rate and equilibrium constants are temperature dependent, but at this stage of the current work only their values at 25°C are used and can be found in Table 3.1. Expressions that include the full temperature dependence can be found in Appendix C.

3.3 Charge Balance and Equilibrium States

3.3.1 Law of mass action

The law of mass action states that the rate of any chemical reaction is proportional to the product of the activities, or concentration, of the reacting substances with often each mass raised to a power equal to the coefficient that occurs in the chemical equation. Consider, as a first example, the simple transformation, $A \underset{k_{-1}}{\overset{k_1}{\rightleftharpoons}} B$, with the

Table 3.1: Rate and equilibrium constants associated with the carbonic acid system, and the dissolution of calcium carbonate.

Quantity (Q)	$Q(T = 298.15\ \mathsf{K})$	Units	Ref.
k_1	2.62×10^{-2}	s^{-1}	[41]
k_{-1}	2.67×10^{1}	s^{-1}	[41]
k_2	8.42×10^{3}	$\mathsf{M}^{-1}\,\mathsf{s}^{-1}$	[41]
k_{-2}	1.94×10^{-4}	s^{-1}	[41]
K_1	4.49×10^{-4}	M	$\frac{k_{-1}k_2}{k_1k_{-2}}K_{\mathrm{W}}$
K_2	4.68×10^{-11}	M	[33]
K_{W}	1.01×10^{-14}	M^2	[17]
K_{H}	3.40×10^{-2}	$\mathsf{M\,atm}^{-1}$	[33]
K_{sp}	4.47×10^{-9}	M^2	[30]

corresponding differential equations

$$\frac{\mathrm{d}[A]}{\mathrm{d}t} = -k_1[A] + k_{-1}[B], \qquad \frac{\mathrm{d}[B]}{\mathrm{d}t} = k_1[A] - k_{-1}[B], \tag{3.20}$$

and initial concentrations $[A](0) = A_0$ and $[B](0) = B_0$. In this case $[A] + [B]$ is constant and equals $A_0 + B_0$, and the equation for $[A]$ becomes

$$\frac{\mathrm{d}[A]}{\mathrm{d}t} = -(k_1 + k_{-1})[A] + k_{-1}(A_0 + B_0), \quad [A](0) = A_0. \tag{3.21}$$

The solution to this set of equations is

$$[A](t) = A_0\mathrm{e}^{-(k_1+k_{-1})t} + \frac{k_{-1}}{k_1 + k_{-1}}(A_0 + B_0)\left(1 - \mathrm{e}^{-(k_1+k_{-1})t}\right), \tag{3.22}$$

$$[B](t) = B_0 + A_0\left(1 - \mathrm{e}^{-(k_1+k_{-1})t}\right) - \frac{k_{-1}}{k_1 + k_{-1}}(A_0 + B_0)\left(1 - \mathrm{e}^{-(k_1+k_{-1})t}\right). \tag{3.23}$$

As $t \to \infty$, the concentrations approach their limiting values,

$$A_\infty = \lim_{t\to\infty}[A](t) = \frac{k_{-1}}{k_1 + k_{-1}}(A_0 + B_0), \quad B_\infty = \lim_{t\to\infty}[B](t) = \frac{k_1}{k_1 + k_{-1}}(A_0 + B_0), \tag{3.24}$$

and

$$\frac{k_{-1}}{k_1} = \frac{A_\infty}{B_\infty}. \tag{3.25}$$

Relationship (3.25) can be accessed directly with (3.20) by assuming equilibrium, and finding the degenerate relation $k_1 A_\infty - k_{-1} B_\infty = 0$.

Now consider the more general reaction

$$aA + bB \underset{k_{-1}}{\overset{k_1}{\rightleftharpoons}} cC + dD, \tag{3.26}$$

where k_1 and k_{-1} are respectively the forward and backward reaction rate constants, and a, b, c, d are the stoichiometric coefficients. This reaction gives rise to a conservation law for each of the species given by

$$\frac{1}{a}\frac{\mathrm{d}[A]}{\mathrm{d}t} = \frac{1}{b}\frac{\mathrm{d}[B]}{\mathrm{d}t} = -k_1[A]^a[B]^b + k_{-1}[C]^c[D]^d = -\frac{1}{c}\frac{\mathrm{d}[C]}{\mathrm{d}t} = -\frac{1}{d}\frac{\mathrm{d}[D]}{\mathrm{d}t}. \tag{3.27}$$

Rather than solving for the time dependence, the equilibrium concentrations must satisfy

$$\frac{k_{-1}}{k_1} = \frac{[A]^a[B]^b}{[C]^c[D]^d}. \tag{3.28}$$

As mentioned earlier in Section 3.2, $H_2CO_3{}^0$ refers to carbonic acid that is in equilibrium with both the dissolved carbon dioxide, and the bicarbonate ion. Because of this, the equilibrium coefficient K_1 can be calculated from the other rate constants. The confusion arises because there are two distinct values that are quoted in the literature: (i) a true ionization constant, and (ii) an apparent equilibrium constant.

In either case, suppose that (3.14)–(3.16), and (3.18) are in equilibrium so that

$$k_1[\mathrm{CO_2}] = k_{-1}[\mathrm{H_2CO_3}^0], \quad k_2[\mathrm{CO_2}][\mathrm{OH^-}] = k_{-2}[\mathrm{HCO_3^-}], \quad K_\mathrm{W} = [\mathrm{H^+}][\mathrm{OH^-}]. \tag{3.29}$$

Combining these gives the true ionization constant for $\mathrm{H_2CO_3}^0$

$$K_1 = \frac{[\mathrm{H^+}][\mathrm{HCO_3^-}]}{[\mathrm{H_2CO_3}^0]} = \frac{k_{-1}k_2}{k_1k_{-2}}K_\mathrm{W} \sim 4.49 \times 10^{-4}. \tag{3.30}$$

The apparent equilibrium constant, due to most of the carbonic acid converting into aqueous carbon dioxide, is[4]

$$K_1' = \frac{[\mathrm{H^+}][\mathrm{HCO_3^-}]}{[\mathrm{CO_2} + \mathrm{H_2CO_3}^0]} = \frac{k_1}{k_1 + k_{-1}}K_1 \sim 4.40 \times 10^{-7}. \tag{3.31}$$

Applying the law of mass action to the chemical reactions given in (3.13)–(3.19) yields a number of relationships amongst the various chemical species. Those reactions, with a given equilibrium constant, reach their state of equilibrium quickly and give rise to the algebraic equations

$$K_1 = \frac{[\mathrm{H^+}][\mathrm{HCO_3^-}]}{[\mathrm{H_2CO_3}^0]}, \qquad K_2 = \frac{[\mathrm{H^+}][\mathrm{CO_3^{2-}}]}{[\mathrm{HCO_3^-}]}, \qquad K_\mathrm{W} = [\mathrm{H^+}][\mathrm{OH^-}]. \tag{3.32}$$

Rearranging these gives expressions for $\{\mathrm{OH^-}, \mathrm{H_2CO_3}^0, \mathrm{CO_3^{2-}}\}$, each considered a rapidly evolving species gives

$$[\mathrm{OH^-}] = \frac{K_\mathrm{W}}{[\mathrm{H^+}]}, \quad [\mathrm{H_2CO_3}^0] = \frac{[\mathrm{H^+}][\mathrm{HCO_3^-}]}{K_1}, \quad [\mathrm{CO_3^{2-}}] = \frac{K_2[\mathrm{HCO_3^-}]}{[\mathrm{H^+}]}, \tag{3.33}$$

where $[\mathrm{CO_2}] = K_\mathrm{H}P_{\mathrm{CO_2(g)}}$ if the $[\mathrm{CO_2}]$ is in equilibrium. The slower reactions, which have forward and backward rates, take more time to reach the state of equilibrium. Using the law of mass action gives the set of expressions for the remaining species

[4] See Kern [20] for more details.

as

$$\frac{\mathrm{d}[\mathrm{CO_2}]}{\mathrm{d}t} = -k_1[\mathrm{CO_2}] + k_{-1}[\mathrm{H_2CO_3}^0] - k_2[\mathrm{CO_2}][\mathrm{OH^-}] + k_{-2}[\mathrm{HCO_3^-}], \tag{3.34}$$

$$\frac{\mathrm{d}[\mathrm{OH^-}]}{\mathrm{d}t} = -k_2[\mathrm{CO_2}][\mathrm{OH^-}] + k_{-2}[\mathrm{HCO_3^-}], \tag{3.35}$$

$$\frac{\mathrm{d}[\mathrm{H_2CO_3}^0]}{\mathrm{d}t} = k_1[\mathrm{CO_2}] - k_{-1}[\mathrm{H_2CO_3}^0], \tag{3.36}$$

$$\frac{\mathrm{d}[\mathrm{HCO_3^-}]}{\mathrm{d}t} = k_2[\mathrm{CO_2}][\mathrm{OH^-}] - k_{-2}[\mathrm{HCO_3^-}]. \tag{3.37}$$

The set of differential equations (3.34)–(3.37), together with the algebraic equations (3.33), describe the evolution of the carbonate system given by (3.14)–(3.18). The system is closed with an expression for $[\mathrm{H^+}]$ which will be discussed in the following section.

One final observation is a consequence of the decoupling into slow and fast reactions. From (3.34)–(3.37) the conditions for equilibrium are $k_1[\mathrm{CO_2}] = k_{-1}[\mathrm{H_2CO_3}^0]$ and $k_2[\mathrm{CO_2}][\mathrm{OH^-}] = k_{-2}[\mathrm{HCO_3^-}]$. However, from the fast reactions (3.33),

$$\begin{aligned}[\mathrm{H^+}]\left(k_2[\mathrm{CO_2}][\mathrm{OH^-}] - k_{-2}[\mathrm{HCO_3^-}]\right) &= k_2K_\mathrm{W}[\mathrm{CO_2}] - k_{-2}K_1[\mathrm{H_2CO_3}^0] \\ &= \frac{k_2K_\mathrm{W}}{k_1}\left(k_1[\mathrm{CO_2}] - \underbrace{\frac{k_1k_{-2}K_1}{k_2K_\mathrm{W}}}_{k_{-1}}[\mathrm{H_2CO_3}^0]\right).\end{aligned} \tag{3.38}$$

This implies that the carbonate system is in equilibrium if either of these conditions are satisfied, since they imply one another.

3.3.2 Chemical activity

At high solute concentrations, typical of the acidization process, ion complexes form between the dissolved molecules and ions. This inhibits the dissolved species

from participating in the thermodynamic equilibrium. The consequence of this is that the equilibrium constants depend not only on the temperature but also on the ionic environment. This can be characterized by the ionic strength of the solution

$$I = \frac{1}{2}\sum_i [\mathsf{A}_i] q_i^2, \tag{3.39}$$

where q_i denotes the electric charge of species A_i, and the sum is taken over all of the ion species. To model these Coulumbic interactions between ions, one defines the activity of a compound A, denoted by (A), as $(\mathsf{A}) = \gamma_{\mathsf{A}}[\mathsf{A}]$ where $\gamma_{\mathsf{A}} = \gamma_{\mathsf{A}}(I)$, known as the activity coefficient of A, is a function of the ionic strength of the solution.

Up to this point we have used the concentration of a species in place of the activity which assumes an ideal condition of infinite dilution. Deviations from the ideal condition are corrected with this activity coefficient and replacing the concentrations with activities, or "effective" concentrations. In fact, when in thermodynamic equilibrium, concentrations should be replaced by the activities.

Even though the large variation in the equilibrium constants dominates the chemical behaviour of the carbonate system, there are a variety of models in the literature that attempt to compensate for nontrivial activation coefficients. In the model described by Kaufmann et al. [19], an extended Debye-Hückel model is used to account for the differing ion sizes. The natural limitation of using only this approximation, limits this models applicability to only moderate ionic strengths ($I < 10^{-1}$ M). At higher ionic strengths (10^{-1} M $< I < 0.5$ M), other models are applied, for example (Davies [10], Pitzer & Brewer [24, 32]). At their core, these models correct the logarithm of the activity with a term proportional to the square of the charge on the species, indicative of the electrical energy of the species. For a

chemical species A,

$$\log_{10}\gamma_q(I;\mathsf{A}) = q^2 G(I), \qquad G(0) = 0, \tag{3.40}$$

where G is a continuous function, independent of the species. The function G primarily depends on the ionic strength of the solution, and since $G(0) = 0$, $\gamma_q(I;\mathsf{A}) \to 1$ as $I \to 0$.

Using the chemical activity to define the equilibrium values

$$K_1 = \frac{(\mathsf{H^+})(\mathsf{HCO_3^-})}{(\mathsf{H_2CO_3}^0)}, \quad K_2 = \frac{(\mathsf{H^+})(\mathsf{CO_3^{2-}})}{(\mathsf{HCO_3^-})}, \quad K_\mathrm{W} = (\mathsf{H^+})(\mathsf{OH^-}). \tag{3.41}$$

From the definition of the activity coefficients,

$$K_1 = \frac{\gamma_1^2[\mathsf{H^+}][\mathsf{HCO_3^-}]}{\gamma_0[\mathsf{H_2CO_3}^0]}, \quad K_2 = \frac{\gamma_2[\mathsf{H^+}][\mathsf{CO_3^{2-}}]}{[\mathsf{HCO_3^-}]}, \quad K_\mathrm{W} = \gamma_1^2[\mathsf{H^+}][\mathsf{OH^-}]. \tag{3.42}$$

Absorbing the activity coefficients into the rate constant defines a compensated equilibrium constant. For the specific reactions in this paper, using $\gamma_0 = 1$, and $\gamma_2 = \gamma_1^4$ from the form of (3.40), gives

$$K_1^c = \frac{K_1}{\gamma_1^2} = \frac{[\mathsf{H^+}][\mathsf{HCO_3^-}]}{[\mathsf{H_2CO_3}^0]}, \quad K_2^c = \frac{K_2}{\gamma_1^4} = \frac{[\mathsf{H^+}][\mathsf{CO_3^{2-}}]}{[\mathsf{HCO_3^-}]}, \quad K_\mathrm{W}^c = \frac{K_\mathrm{W}}{\gamma_1^2} = [\mathsf{H^+}][\mathsf{OH^-}] \tag{3.43}$$

where γ_1 is determined experimentally. In the absence of experimental data, and since this is a secondary effect,[5] a value of $\gamma_1 = 1$ is used in all of the numerical solutions. To denote this effect, a superscript c is used throughout.

[5] This is secondary in comparison to the variation of the equilibrium values over many orders of magnitude in this chemical system.

3.3.3 Charge neutrality and equilibrium conditions

To ensure that there is no net charge on the solution, all of the positive charges must balance the negative charges. If we consider the carbonic system with initially added $[\mathsf{Cl}^-]$ to specify the initial acidity of the solvent and the experimental environment, then the charge neutrality condition is

$$[\mathsf{H}^+] + 2[\mathsf{Ca}^{2+}] - [\mathsf{OH}^-] - [\mathsf{HCO}_3^-] - 2[\mathsf{CO}_3^{2-}] - [\mathsf{Cl}^-] = 0. \tag{3.44}$$

By using the expressions for the rapidly evolving species (3.33) with the activity compensation notation in (3.43)

$$[\mathsf{H}^+] + 2[\mathsf{Ca}^{2+}] - \frac{K_{\mathsf{W}}^c}{[\mathsf{H}^+]} - \frac{K_1^c[\mathsf{H_2CO_3}^0]}{[\mathsf{H}^+]} - \frac{2K_1^cK_2^c[\mathsf{H_2CO_3}^0]}{[\mathsf{H}^+]^2} - [\mathsf{Cl}^-] = 0. \tag{3.45}$$

The dependency on the calcium comes from the solubility product (3.9) written in the form

$$[\mathsf{Ca}^{2+}] = \frac{\lambda K_{\mathrm{sp}}}{[\mathsf{CO}_3^{2-}]} \leq \frac{K_{\mathrm{sp}}}{[\mathsf{CO}_3^{2-}]}, \tag{3.46}$$

where $0 \leq \lambda \leq 1$ is a slack variable corresponding to the extreme cases of $\lambda = 0$ (no calcium) and $\lambda = 1$ (saturated calcium). Incorporating (3.46) into (3.45) gives a fourth degree polynomial in terms of $[\mathsf{H}^+]$

$$\frac{2\lambda K_{\mathrm{sp}}[\mathsf{H}^+]^4}{K_2^c\mathcal{K}} + [\mathsf{H}^+]^3 - [\mathsf{Cl}^-][\mathsf{H}^+]^2 - (K_{\mathsf{W}}^c + \mathcal{K})[\mathsf{H}^+] - 2K_2^c\mathcal{K} = 0 \tag{3.47}$$

with $\mathcal{K} = K_1^c[\mathsf{H_2CO_3}^0] = [\mathsf{H}^+][\mathsf{HCO}_3^-]$.

Equation (3.47) does not only depend on $[\mathsf{H}^+]$, and to achieve this, further assumptions are required. At this point we assume that the chemical system (3.34)–(3.37) is at equilibrium, so that $k_1[\mathsf{CO}_2] = k_{-1}[\mathsf{H_2CO_3}^0]$ (see equation (3.38)) and

that the species are well mixed[6], which implies that $[\mathsf{CO_2}] = K_{\mathrm{H}} P_{\mathsf{CO_{2(g)}}}$ throughout the domain. With these additional assumptions

$$\mathcal{K} = \frac{k_1}{k_{-1}} K_1^c [\mathsf{CO_2}] = \frac{k_2}{k_{-2}} K_{\mathrm{W}}^c K_{\mathrm{H}} P_{\mathsf{CO_{2(g)}}} = K_{\mathrm{P}}, \tag{3.48}$$

a constant depending on the pressure level, $P_{\mathsf{CO_{2(g)}}}$. For a given partial pressure of $\mathsf{CO_2(g)}$, the polynomial (3.47) gives the corresponding equilibrium hydrogen concentration consistent with the carbonate system.

Two situations are of interest, the case with no calcium in solution, $\lambda = 0$, and the case when the solution is saturated with calcium, $\lambda = 1$. Before starting this analysis, it is instructive to estimate the size of the coefficients in (3.47) with $\mathcal{K} = K_{\mathrm{P}}$. For a pressure of 1 atm and 400 ppm of $\mathsf{CO_2(g)}$ one has $K_{\mathrm{P}} \simeq 5.99 \times 10^{-12}$ M^2 or $\log_{10} K_{\mathrm{P}} = -11.22$.

Figure 3.1 shows the equilibrium concentrations of the various ionic species when there is no calcium in the solution ($\lambda = 0$), and $[\mathsf{Cl^-}] = 10^{-2}$ M. The equilibrium concentration of $[\mathsf{H^+}]$, denoted by $[\mathsf{H^+}]_0$ to indicate $\lambda = 0$, satisfies

$$[\mathsf{H^+}]_0^3 - [\mathsf{Cl^-}][\mathsf{H^+}]_0^2 - (K_{\mathrm{W}}^c + K_{\mathrm{P}})[\mathsf{H^+}]_0 - 2K_2^c K_{\mathrm{P}} = 0. \tag{3.49}$$

Viewing the solution as a function of K_{P}, there are two distinct regions with a transition point that depends on $[\mathsf{Cl^-}]$. In the low pressures region, $K_{\mathrm{P}} < K_{\mathrm{P0}} = [\mathsf{Cl^-}]/2 + ([\mathsf{Cl^-}]^2/4 + K_{\mathrm{W}}^c)^{1/2}$,

$$[\mathsf{H^+}] \sim \max\{[\mathsf{Cl^-}], (K_{\mathrm{W}}^c + K_{\mathrm{P}})^{1/2}\}, \tag{3.50}$$

and balances with $[\mathsf{Cl^-}]$.[7] The concentration of other negative ions, $[\mathsf{HCO_3^-}]$ and $[\mathsf{CO_3^{2-}}]$ are negligible, though they increase with increasing pressure. Finally, $[\mathsf{OH^-}]$

[6] If there is a spatial dependence then $K_{\mathrm{H}} P_{\mathsf{CO_{2(g)}}} = [\mathsf{CO_2}]$ only at the fluid-gas interface.

[7] For small amounts of $\mathsf{Cl^-}$, $[\mathsf{Cl^-}] < 2(K_{\mathrm{W}}^c + K_{\mathrm{P}})^{1/2}$, we have the estimate $[\mathsf{H^+}] \sim (K_{\mathrm{W}}^c + K_{\mathrm{P}})^{1/2}$.

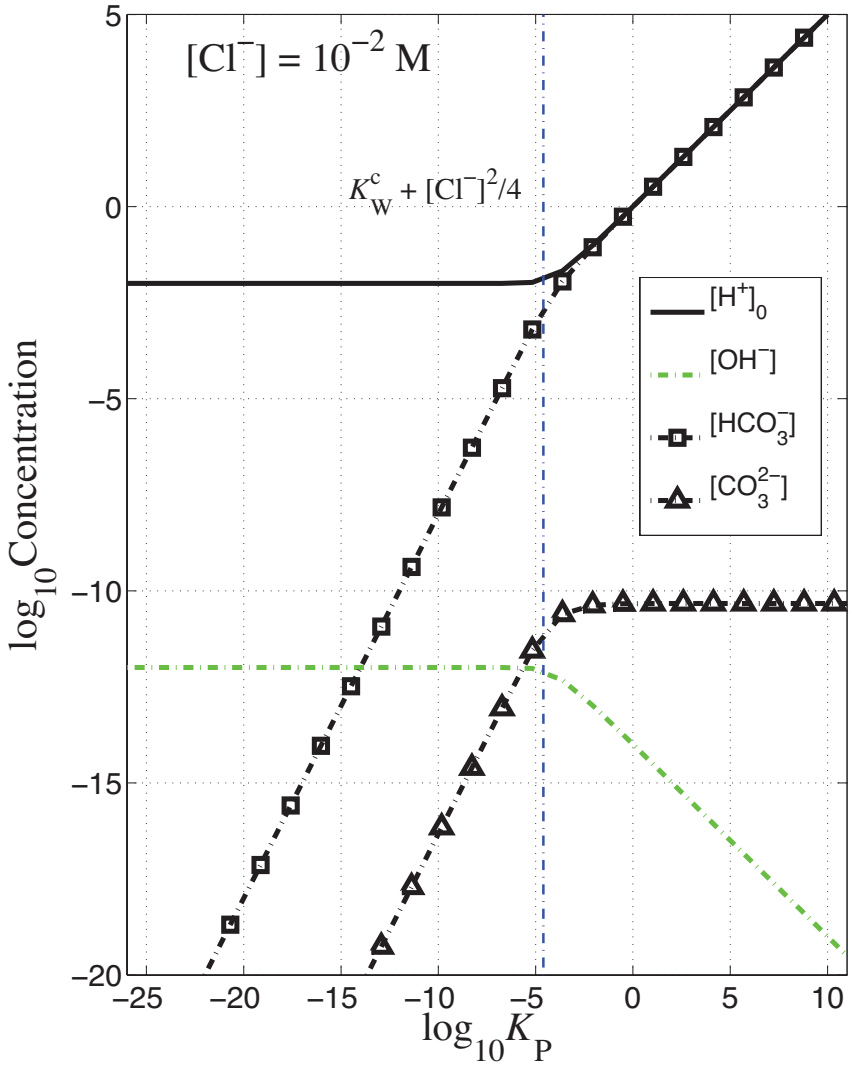

Figure 3.1: Concentrations versus $K_{\mathrm{P}} = \frac{k_2}{k_{-2}} K_{\mathrm{W}}^c K_{\mathrm{H}} P_{\mathrm{CO_2(g)}}$ in a calcium free carbonic solution with $[\mathrm{Cl}^-] = 10^{-2}$ M.

remains constant so that the product $[\mathrm{OH}^-][\mathrm{H}^+] = K_{\mathrm{W}}^c$. Quantitatively, at $\log_{10} K_{\mathrm{P}} = -11.22$, (pressure of 1 atm with 400 ppm of $\mathrm{CO_2(g)}$),

$$\begin{aligned} [\mathrm{H}^+]_0 &\simeq [\mathrm{Cl}^-] = 1.00 \times 10^{-2}\ \mathrm{M}, & [\mathrm{OH}^-] &= \frac{K_{\mathrm{W}}^c}{[\mathrm{H}^+]_0} = 1.01 \times 10^{-12}\ \mathrm{M}, \\ [\mathrm{HCO}_3^-] &= \frac{K_{\mathrm{P}}}{[\mathrm{H}^+]_0} = 5.99 \times 10^{-10}\ \mathrm{M}, & [\mathrm{CO}_3^{2-}] &= \frac{K_2^c K_{\mathrm{P}}}{[\mathrm{H}^+]_0^2} = 2.81 \times 10^{-18}\ \mathrm{M} \end{aligned} \tag{3.51}$$

with an ionic strength of $I = 1.0 \times 10^{-2}$ M^2. In the high pressure regime, $K_{\mathrm{P}} > K_{\mathrm{P0}} = [\mathrm{Cl}^-]/2 + ([\mathrm{Cl}^-]^2/4 + K_{\mathrm{W}}^c)^{1/2}$, $[\mathrm{H}^+]$ balances $[\mathrm{HCO}_3^-]$ and $[\mathrm{H}^+] \sim K_{\mathrm{P}}^{1/2}$. In this regime,

$[\mathrm{CO_3^{2-}}]$ remains constant while the $[\mathrm{OH^-}]$ decreases to match the increasing $[\mathrm{H^+}]$ level.

All of the above analysis has assumed that $[\mathrm{Cl^-}]$ determines the chemistry. In natural waters, $[\mathrm{Cl^-}]$ is typically near zero, so this situation should be carefully delineated. When $[\mathrm{Cl^-}] = 0$, carbon dioxide gas, $\mathrm{CO_2(g)}$, plays a much more dominant role and it is the corresponding value of K_P that determines the solutions maximum pH. Further increases in pH are possible, but would require the addition of another chemical, such as NaOH. This possibility lies outside the current model. In the case of no added calcium, $(K_\mathrm{W}^c + K_\mathrm{P})^{1/2} < [\mathrm{H^+}]_0 < [\mathrm{Cl^-}]$, so that $-\log_{10}[\mathrm{Cl^-}] \lesssim \mathrm{pH} \lesssim -\frac{1}{2}\log_{10}(K_\mathrm{W}^c + K_\mathrm{P})$. For a pressure of 1 atm with 400 ppm of $\mathrm{CO_2(g)}$, this gives an upper bound on the pH of 5.61. For 0.97 atm of $\mathrm{CO_2(g)}$, we find $\mathrm{pH} \lesssim 3.92$. In this latter case, the associated characteristic concentrations are

$$\begin{aligned} &[\mathrm{H^+}]_0 \simeq (K_\mathrm{W}^c + K_\mathrm{P})^{1/2} = 1.21 \times 10^{-4}\ \mathrm{M}, \quad [\mathrm{OH^-}] = \frac{K_\mathrm{W}^c}{[\mathrm{H^+}]_0} = 8.40 \times 10^{-11}\ \mathrm{M}, \\ &[\mathrm{HCO_3^-}] = \frac{K_\mathrm{P}}{[\mathrm{H^+}]_0} = 1.21 \times 10^{-4}\ \mathrm{M}, \qquad [\mathrm{CO_3^{2-}}] = \frac{K_2^c K_\mathrm{P}}{[\mathrm{H^+}]_0^2} = 4.68 \times 10^{-11}\ \mathrm{M} \end{aligned} \tag{3.52}$$

with an ionic strength of $I = 1.2 \times 10^{-4}\ \mathrm{M}^2$.

The situation when the solution is saturated with $[\mathrm{Ca^{2+}}]$ ($\lambda = 1$) is described in Figure 3.2. This differs significantly from the previous case due to the coupling of the $\mathrm{CO_3^{2-}}$ ions with both the $\mathrm{Ca^{2+}}$ and the rest of the carbonate system. In this case the equilibrium concentration of $[\mathrm{H^+}]$, denoted by $[\mathrm{H^+}]_\infty$, satisfies

$$\underbrace{\frac{2K_\mathrm{sp}}{K_2^c K_\mathrm{P}}[\mathrm{H^+}]_\infty^4}_{[\mathrm{Ca^{2+}}]} + \underbrace{[\mathrm{H^+}]_\infty^3}_{[\mathrm{H^+}]} - \underbrace{[\mathrm{Cl^-}][\mathrm{H^+}]_\infty^2}_{[\mathrm{Cl^-}]} - (\underbrace{K_\mathrm{W}^c}_{[\mathrm{OH^-}]} + \underbrace{K_\mathrm{P}}_{[\mathrm{HCO_3^-}]})[\mathrm{H^+}]_\infty - 2\underbrace{K_2^c K_\mathrm{P}}_{[\mathrm{CO_3^{2-}}]} = 0, \tag{3.53}$$

where their associated ionic species is represented below each term. Four regimes exist in this situation [3]. The corresponding chemical balances are observered in Figure 3.2. For low pressures, as seen in the figure (region I), $[\mathrm{Ca^{2+}}] \sim [\mathrm{OH^-}]$, the

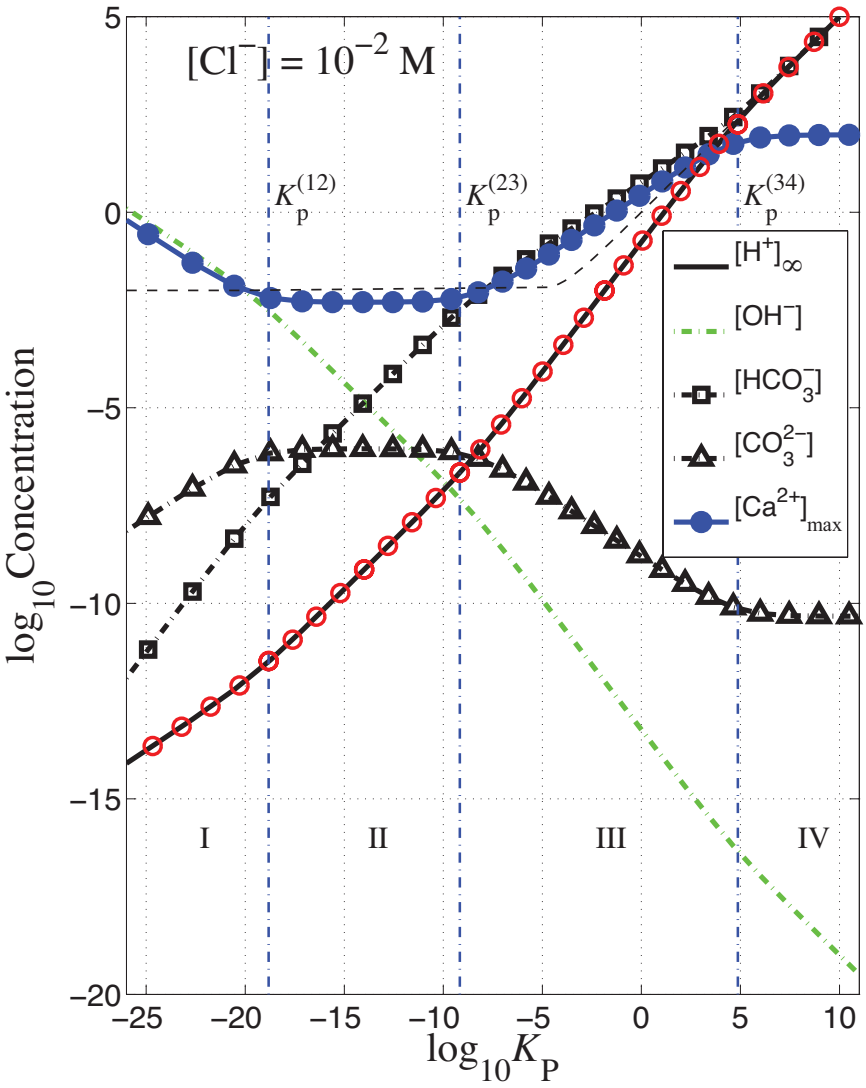

Figure 3.2: Concentrations versus $K_P = \frac{k_2}{k_{-2}} K_W^c K_H P_{CO_2(g)}$ in a saturated calcium carbonic solution with $[Cl^-] = 10^{-2}$ M. The $[H^+]_0$ curve is also indicated with a dashed line for comparison.

calcium ions balance hydroxide so that

$$\frac{2K_{sp}}{K_2^c K_P}[H^+]_\infty^4 \sim K_W^c [H^+]_\infty \Longrightarrow [H^+]_\infty \sim \left(\frac{K_2^c K_W^c K_P}{2K_{sp}}\right)^{1/3} \tag{3.54}$$

or $[H^+]_\infty = \mathcal{O}\left(K_P^{1/3}\right)$. The balance of the other species follow from the equilibrium

equations (3.43), (3.48) giving[8]

$$\begin{aligned}&[\mathsf{OH}^-] = \mathcal{O}\left(K_{\mathrm{P}}^{-1/3}\right), \quad [\mathsf{HCO}_3^-] = \mathcal{O}\left(K_{\mathrm{P}}^{2/3}\right), \quad [\mathsf{CO}_3^{2-}] = \mathcal{O}\left(K_{\mathrm{P}}^{1/3}\right),\\ &[\mathsf{Ca}^{2+}] = \mathcal{O}\left(K_{\mathrm{P}}^{-1/3}\right).\end{aligned} \tag{3.55}$$

Further increasing $P_{\mathsf{CO}_2(\mathsf{g})}$ causes the $[\mathsf{Ca}^{2+}]$ to balance with $[\mathsf{Cl}^-]$ in region II, implying that

$$\frac{2K_{\mathrm{sp}}}{K_2^c K_{\mathrm{P}}}[\mathsf{H}^+]_\infty^4 \sim [\mathsf{Cl}^-][\mathsf{H}^+]_\infty^2 \Longrightarrow [\mathsf{H}^+]_\infty \sim \left(\frac{K_2^c[\mathsf{Cl}^-]K_{\mathrm{P}}}{2K_{\mathrm{sp}}}\right)^{1/2} \tag{3.56}$$

or $[\mathsf{H}^+]_\infty = \mathcal{O}\left(K_{\mathrm{P}}^{1/2}\right)$. Again, by using the equilibrium relationships,

$$\begin{aligned}&[\mathsf{OH}^-] = \mathcal{O}\left(K_{\mathrm{P}}^{-1/2}\right), \quad [\mathsf{HCO}_3^-] = \mathcal{O}\left(K_{\mathrm{P}}^{1/2}\right), \quad [\mathsf{CO}_3^{2-}] = \mathcal{O}\left(K_{\mathrm{P}}^{0}\right),\\ &[\mathsf{Ca}^{2+}] = \mathcal{O}\left(K_{\mathrm{P}}^{0}\right).\end{aligned} \tag{3.57}$$

Continuing with the increase in pressure, the calcium begins to balance with the bicarbonate ions in region III, and

$$\frac{2K_{\mathrm{sp}}}{K_2^c K_{\mathrm{P}}}[\mathsf{H}^+]_\infty^4 \sim K_{\mathrm{P}}[\mathsf{H}^+]_\infty \Longrightarrow [\mathsf{H}^+]_\infty \sim \left(\frac{K_2^c K_{\mathrm{P}}^2}{2K_{\mathrm{sp}}}\right)^{1/3} \tag{3.58}$$

or $[\mathsf{H}^+]_\infty = \mathcal{O}\left(K_{\mathrm{P}}^{2/3}\right)$. This is the same limiting behaviour when the concentration of chlorine is low. That is, when $[\mathsf{Cl}^-] < (2K_{\mathrm{sp}}K_{\mathrm{P}}/K_2^c)^{1/3}$, $[\mathsf{H}^+]_\infty \sim (K_2^c K_{\mathrm{P}}^2/(2K_{\mathrm{sp}}))^{1/3}$. Consequently in this region,

$$\begin{aligned}&[\mathsf{OH}^-] = \mathcal{O}\left(K_{\mathrm{P}}^{-2/3}\right), \quad [\mathsf{HCO}_3^-] = \mathcal{O}\left(K_{\mathrm{P}}^{1/3}\right), \quad [\mathsf{CO}_3^{2-}] = \mathcal{O}\left(K_{\mathrm{P}}^{-1/3}\right),\\ &[\mathsf{Ca}^{2+}] = \mathcal{O}\left(K_{\mathrm{P}}^{1/3}\right).\end{aligned} \tag{3.59}$$

In the highest pressure regime, region IV, the calcium ions are suppressed resulting

[8] If $[\mathsf{H}^+]_\infty = \mathcal{O}(K_{\mathrm{P}}^n)$ then $[\mathsf{OH}^-] = \mathcal{O}\left(K_{\mathrm{P}}^{-n}\right)$, $[\mathsf{HCO}_3^-] = \mathcal{O}\left(K_{\mathrm{P}}^{1-n}\right)$, $[\mathsf{CO}_3^{2-}] = \mathcal{O}\left(K_{\mathrm{P}}^{1-2n}\right)$, and $[\mathsf{Ca}^{2+}] = \mathcal{O}\left(K_{\mathrm{P}}^{2n-1}\right)$.

in a balance between $[\mathsf{H}^+]$ and $[\mathsf{HCO}_3^-]$ and

$$[\mathsf{H}^+]_\infty^3 \sim K_\mathrm{P}[\mathsf{H}^+]_\infty \Longrightarrow [\mathsf{H}^+]_\infty \sim K_\mathrm{P}^{1/2} \tag{3.60}$$

resulting in a reproduction of (3.57).

The transitions between these various behaviours are characterized by particular K_P values, $K_\mathrm{P}^{(12)} < K_\mathrm{P}^{(23)} < K_\mathrm{P}^{(34)}$ where the superscript indicates which transition. For example, $K_\mathrm{P}^{(12)}$ indicates the K_P value marking the transition from the first to the second region. An approximate estimate of each value can be obtained by equating the behaviour for each of the regions. For example, where the first and second regions overlap,

$$\left(\frac{K_2^c K_\mathrm{W}^c K_\mathrm{P}^{(12)}}{2K_\mathrm{sp}}\right)^{1/3} \sim \left(\frac{K_2^c[\mathsf{Cl}^-]K_\mathrm{P}^{(12)}}{2K_\mathrm{sp}}\right)^{1/2} \Longrightarrow K_\mathrm{P}^{(12)} \sim \frac{2K_\mathrm{sp}{K_\mathrm{W}^c}^2}{K_2^c[\mathsf{Cl}^-]^3}. \tag{3.61}$$

A careful analysis of the asymptotic expansions results in the relationships

$$K_\mathrm{P}^{(12)} = \frac{2f^{(12)}K_\mathrm{sp}{K_\mathrm{W}^c}^2}{K_2^c[\mathsf{Cl}^-]^3}, \qquad K_\mathrm{P}^{(23)} = \frac{f^{(23)}K_2^c[\mathsf{Cl}^-]^3}{2K_\mathrm{sp}}, \qquad K_\mathrm{P}^{(34)} = \frac{4f^{(34)}K_\mathrm{sp}^2}{{K_2^c}^2}, \tag{3.62}$$

with

$$f^{(12)} \simeq 7.723474474, \qquad f^{(23)} \simeq 0.1294754069, \qquad f^{(34)} \simeq 2.041336172. \tag{3.63}$$

The details can be found in [3] and reproduced in Appendix B.

Examining $K_\mathrm{P}^{(12)}$, $K_\mathrm{P}^{(23)}$, and $K_\mathrm{P}^{(34)}$, it is apparent that the second region increases as the amount of $[\mathsf{Cl}^-]$ increases (to increase the acidity). The nominal value of $[\mathsf{Cl}^-] = 10^{-2}$ M gives

$$K_\mathrm{P}^{(12)} = 1.51 \times 10^{-19}, \qquad K_\mathrm{P}^{(23)} = 6.78 \times 10^{-10}, \qquad K_\mathrm{P}^{(34)} = 7.47 \times 10^{4}. \tag{3.64}$$

In addition, as stated earlier, for 400 ppm of $\mathsf{CO_2(g)}$ in 1 atm of air, $K_{\rm P} \simeq 5.99 \times 10^{-12}$ M^2 or $\log_{10} K_{\rm P} = -11.22$, so the system is well within the second region. This gives the estimated ionic concentrations of [9]

$$\begin{aligned} &[\mathsf{H^+}]_\infty \simeq \left(\frac{K_2^c K_{\rm P}[\mathsf{Cl^-}]}{2K_{\rm sp}}\right)^{1/2} = 1.77 \times 10^{-8}\ \mathsf{M}, \quad [\mathsf{OH^-}] = \frac{K_{\rm W}^c}{[\mathsf{H^+}]_\infty} \simeq 5.72 \times 10^{-7}\ \mathsf{M}, \\ &[\mathsf{HCO_3^-}] = \frac{K_{\rm P}}{[\mathsf{H^+}]_\infty} \simeq 3.38 \times 10^{-4}\ \mathsf{M}, \qquad\qquad [\mathsf{CO_3^{2-}}] = \frac{K_2^c K_{\rm P}}{[\mathsf{H^+}]_\infty^2} \simeq 8.94 \times 10^{-7}\ \mathsf{M}, \end{aligned} \tag{3.65}$$

with an ionic strength of $I = 1.5 \times 10^{-2}$ M^2, and with a corresponding $\rm pH = 8 - \log_{10} 1.77 = 7.75$. When $[\mathsf{Cl^-}]$ drops, the pH, in this case, to rise to its maximum of $\rm pH = -\frac{1}{3}\log_{10}(K_2^c K_{\rm P}^2/2/K_{\rm sp}) = 8.24$. When $[\mathsf{Cl^-}]$ drops $[\mathsf{H^+}]_\infty$ is determined by $\mathsf{CO_2(g)}$. Corresponding to (3.65) with 0.97 atm of $\mathsf{CO_2(g)}$,

$$\begin{aligned} &[\mathsf{H^+}]_\infty \simeq \left(\frac{K_2^c K_{\rm P}^2}{2K_{\rm sp}}\right)^{1/3} = 1.03 \times 10^{-6}\ \mathsf{M}, \quad [\mathsf{OH^-}] = \frac{K_{\rm W}^c}{[\mathsf{H^+}]_\infty} \simeq 9.80 \times 10^{-9}\ \mathsf{M}, \\ &[\mathsf{HCO_3^-}] = \frac{K_{\rm P}}{[\mathsf{H^+}]_\infty} \simeq 1.41 \times 10^{-2}\ \mathsf{M}, \qquad [\mathsf{CO_3^{2-}}] = \frac{K_2^c K_{\rm P}}{[\mathsf{H^+}]_\infty^2} \simeq 6.36 \times 10^{-7}\ \mathsf{M} \end{aligned} \tag{3.66}$$

with an ionic strength of $I = 2.1 \times 10^{-2}$ M^2

The estimate for $[\mathsf{H^+}]_\infty$ gives a corresponding maximal $\mathsf{Ca^{2+}}$ concentration. There are two cases, depending on the level of $[\mathsf{Cl^-}]$. In particular, this estimate is

$$\begin{aligned} [\mathsf{Ca^{2+}}]_{\rm max} = \frac{K_{\rm sp}}{[\mathsf{CO_3^{2-}}]} &= \frac{K_{\rm sp}[\mathsf{H^+}]_\infty^2}{K_2^c K_{\rm P}} \\ &\simeq \begin{cases} \dfrac{[\mathsf{Cl^-}]}{2}, & [\mathsf{Cl^-}] > \Gamma_{\mathsf{Ca^{2+}}}, \\ \dfrac{\Gamma_{\mathsf{Ca^{2+}}}}{2}, & [\mathsf{Cl^-}] < \Gamma_{\mathsf{Ca^{2+}}}, \end{cases} \quad \Gamma_{\mathsf{Ca^{2+}}} = \left(\frac{2K_{\rm P}K_{\rm sp}}{K_2^c}\right)^{1/3}. \end{aligned} \tag{3.67}$$

Associated with (3.65), $[\mathsf{Ca^{2+}}]_{\rm max} \simeq [\mathsf{Cl^-}]/2 = 5.00 \times 10^{-3}$ M, and from the values in (3.66), $[\mathsf{Ca^{2+}}]_{\rm max} \simeq [\mathsf{HCO_3^-}]/2 = 7.03 \times 10^{-3}$ M In either case, throughout the four

[9] The exact numerical values are $[\mathsf{H^+}]_\infty = 1.80 \times 10^{-8}$ M, $[\mathsf{OH^-}] = 5.62 \times 10^{-7}$ M, $[\mathsf{HCO_3^-}] = 3.33 \times 10^{-4}$ M, $[\mathsf{CO_3^{2-}}] = 8.65 \times 10^{-7}$ M, $[\mathsf{Ca^{2+}}] = 5.17 \times 10^{-3}$ M.

regions, $[H^+]$ increases while $[OH^-]$ decreases with rising pressure.

3.4 Natural Scalings

One of the difficulties when analyzing chemical processes within the field of applied mathematics is to find an appropriate scaling for each of the chemical species. For the carbonate system, there are essentially two extreme equilibrium states. The first is when there is no calcium in solution, and the second is when the calcium is saturated, at its solubility limit. All other cases lie between these two extremes.

We close this chapter by comparing the two equilibrium states for the pressure levels and range of $[Cl^-]$. From the results of (3.51), (3.52) and (3.65), (3.66), $[H^+]$ should be scaled with $[H^+]_0$, since this is largest value that it can attain. For all the other chemical species the largest values are found with using $[H^+]_\infty$.

Considering the reaction equations (3.34)–(3.37), we only need to consider the ionic species H^+, HCO_3^-, and Ca^{2+}. The amounts of the remaining species are available through the equilibrium expressions (3.33) and the structure of (3.34)–(3.37). In particular,

$$\frac{\mathrm{d}}{\mathrm{d}t}\left([OH^-] + [HCO_3^-]\right) = 0, \qquad \frac{\mathrm{d}}{\mathrm{d}t}\left([CO_2] + [H_2CO_3{}^0] + [HCO_3^-]\right) = 0, \tag{3.68}$$

so that considered only as a function in t,

$$[OH^-](t) = [OH^-](0) + [HCO_3^-](0) - [HCO_3^-](t), \tag{3.69}$$

$$[H_2CO_3{}^0](t) = [H_2CO_3{}^0](0) + [HCO_3^-](0) + [CO_2](0) - [HCO_3^-](t) - [CO_2](t). \tag{3.70}$$

A natural scaling for the concentration of CO_2 is the partial pressure of CO_2(g).

Collecting all these scales together gives

$$\begin{aligned} [\mathsf{H}^+] &= [\mathsf{H}^+]_0 h, & [\mathsf{HCO}_3^-] &= \frac{K_\mathrm{P}}{[\mathsf{H}^+]_\infty} b, \\ [\mathsf{Ca}^{2+}] &= \frac{K_\mathrm{sp}[\mathsf{H}^+]_\infty^2}{K_2^c K_\mathrm{P}} c, & [\mathsf{CO}_2] &= K_\mathrm{H} P_{\mathsf{CO}_2(\mathsf{g})} u, \end{aligned} \tag{3.71}$$

where $\{h, b, c, u\}$ are the corresponding dimensionless species.

With respect to these scalings, the charge balance relation (3.44) becomes

$$h^2 + \left(\frac{2\lambda K_\mathrm{sp}[\mathsf{H}^+]_\infty^2}{K_2^c K_\mathrm{P}[\mathsf{H}^+]_0} c - \frac{K_\mathrm{P}}{[\mathsf{H}^+]_0[\mathsf{H}^+]_\infty} b - \frac{[\mathsf{Cl}^-]}{[\mathsf{H}^+]_0} \right) h - \frac{K_\mathrm{W}^c}{[\mathsf{H}^+]_0^2} - \frac{2K_2^c K_\mathrm{P}}{[\mathsf{H}^+]_0^2 [\mathsf{H}^+]_\infty} b = 0, \tag{3.72}$$

where for $[\mathsf{Cl}^-] = 0.01$ and 400 ppm of CO_2(g),

$$\begin{aligned} &\frac{2K_\mathrm{sp}[\mathsf{H}^+]_\infty^2}{K_2^c K_\mathrm{P}[\mathsf{H}^+]_0} \simeq 1.03, \quad \frac{K_\mathrm{P}}{[\mathsf{H}^+]_0[\mathsf{H}^+]_\infty} \simeq 3.33 \times 10^{-2}, \quad \frac{[\mathsf{Cl}^-]}{[\mathsf{H}^+]_0} \simeq 1, \\ &\frac{K_\mathrm{W}^c}{[\mathsf{H}^+]_0^2} \simeq 1.01 \times 10^{-10}, \quad \frac{2K_2 K_\mathrm{P}}{[\mathsf{H}^+]_0^2 [\mathsf{H}^+]_\infty} \simeq 3.12 \times 10^{-12}. \end{aligned} \tag{3.73}$$

and for $[\mathsf{Cl}^-] = 0$ and 0.97 atm of CO_2(g),

$$\begin{aligned} &\frac{2K_\mathrm{sp}[\mathsf{H}^+]_\infty^2}{K_2^c K_\mathrm{P}[\mathsf{H}^+]_0} \simeq 1.17 \times 10^2, \quad \frac{K_\mathrm{P}}{[\mathsf{H}^+]_0[\mathsf{H}^+]_\infty} \simeq 1.17 \times 10^2, \quad \frac{[\mathsf{Cl}^-]}{[\mathsf{H}^+]_0} \simeq 0, \\ &\frac{K_\mathrm{W}^c}{[\mathsf{H}^+]_0^2} \simeq 6.97 \times 10^{-7}, \quad \frac{2K_2 K_\mathrm{P}}{[\mathsf{H}^+]_0^2 [\mathsf{H}^+]_\infty} \simeq 1.09 \times 10^{-8}. \end{aligned} \tag{3.74}$$

It is an easy exercise to extract the original two equilibrium states from (3.72)–(3.74) by setting

$$k_2[\mathsf{CO}_2][\mathsf{OH}^-] = k_{-2}[\mathsf{HCO}_3^-], \qquad [\mathsf{H}^+]_0 bh = [\mathsf{H}^+]_\infty u, \tag{3.75}$$

the second expression in dimensionless variables. In equilibrium, the solution is saturated with CO_2(g) ($u = 1$), and we have $[\mathsf{H}^+]_0 bh = [\mathsf{H}^+]_\infty$. In the case of no

calcium ($c = 0$) and $[\mathsf{H}^+] = [\mathsf{H}^+]_0$, ($h = 1$) then $b = [\mathsf{H}^+]_\infty/[\mathsf{H}^+]_0$ and (3.72) becomes (3.49). In the case of saturated calcium ($c = 1$) and $[\mathsf{H}^+] = [\mathsf{H}^+]_\infty$, ($h = [\mathsf{H}^+]_\infty/[\mathsf{H}^+]_0$) then $b = 1$ and (3.72) becomes (3.53).

CHAPTER 4

The Advection-Diffusion-Reaction Model

4.1 What is the ADR Model?

An advection-diffusion-reaction (ADR) model is used to model the flow of material as it undergoes changes due to its advection through the surroundings, diffusion into the domain, and reactions within its environment. Diffusion is the movement of a substance (molecules or particles) from an area with a high concentration to an area with a low concentration, while advection refers to the transport of a substance or quantity by bulk motion. If we denote the amount of substance per unit volume as P, with a corresponding flux[1] $\mathbf{Q}$, then the rate of change of the material[2] is given by $\partial P/\partial t + \nabla \circ \mathbf{Q}$. The advective and diffusive behaviours are captured by this flux and the equation governing the time evolution of the quantity undergoing these

[1] The units of flux are quantity per unit area per unit time.
[2] This assumes that the quantities are sufficiently smooth so that these derivatives exist.

processes. For a conserved quantity, there is no net change of the quantity over time so this expression would equal zero. For our process, the chemical reactions provide another source of creating or removing material. These reactions, that are specific to the chemical reactions, replace the zero in these non-equilibrium processes. The specific terms for the carbonic system are (3.34)–(3.37), derived in the previous chapter through the law of mass action.

For the carbonic system, the quantity under consideration is the amount of each chemical species, so that $P = c$ corresponds to the concentration. The corresponding flux, in the dilute limit, which includes both advective (due to the motion of the fluid), and diffusive (with diffusion coefficient D) terms is $\mathbf{Q} = c\mathbf{u} - D\nabla c$. Assuming that the fluid is incompressible, and has uniform density,

$$\frac{\partial P}{\partial t} + \nabla \circ \mathbf{Q} = \frac{\partial c}{\partial t} + \mathbf{u} \circ \nabla c - \nabla \circ (D\nabla c) = R, \tag{4.1}$$

where R stands for changes due to reactions that may add or remove a particular chemical species.

4.2 ADR Model for the Carbonate System

In the experimental setup, a sample of $CaCO_3$(s) is attached to the surface of a rotating disc, within a reaction vessel, containing a fluid of a given acidity (determined by HCl), and prescribed partial pressure of CO_2. The disc spins at a constant angular velocity ω, creating a von Kármán swirling flow that fans out over the surface of the dissolving sample. The surface of the $CaCO_3$(s) dissolves as it rotates, and the ionic components are transported into the bulk.

Figure 4.1 shows the domain of interest, Ω, fluid flow streamlines, and some of ion species in the solution. The domain is bounded by $\partial\Omega = \Gamma_S \cup \Gamma_\infty \cup \Gamma_R$ consisting of Γ_S, the free boundary of the dissolving sample, Γ_∞, an inflow boundary where

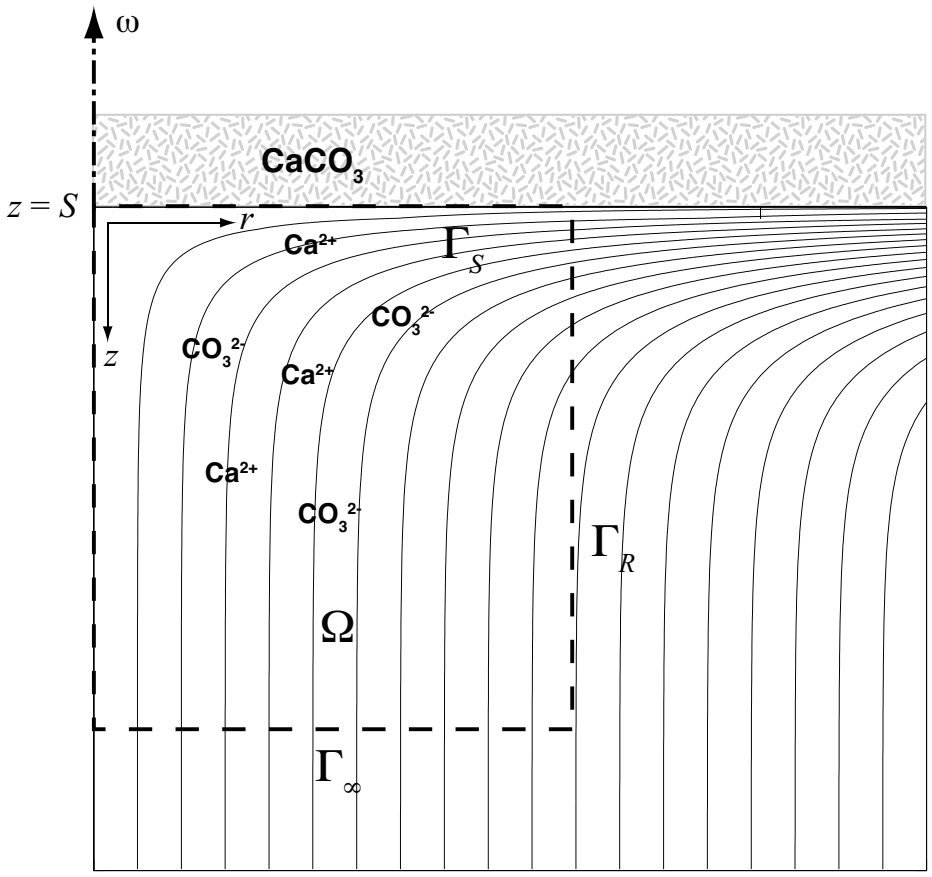

Figure 4.1: General features of the domain, Ω, within the reaction vessel.

the well mixed fluid enters, and Γ_R, an outflow boundary where the fluid leaves.

Throughout the domain, the presence of CO_2 in the solution, as well as the initial acidity, determined by adding HCl, creates the initial conditions for the carbonate system in the vessel. Dissolution of a $CaCO_3(s)$ disc disperses both Ca^{2+} and CO_3^{2-} into the solution. For the system under consideration, the Ca^{2+} does not react, but CO_3^{2-} interacts with the other constituents which complicates the chemistry. The dissolution of $CaCO_3(s)$ can be modelled using an advection-diffusion-reaction as described above.

Within the bulk, the solution is assumed to be well mixed, and the concentration of the slowly evolving species are given by the system (3.34)–(3.37) in Chapter 3. To include spatial dependence, we use a set of ADR equations. As discussed at the

end of Chapter 3, the carbonate system in the presence of Ca^{2+} can be described by solving for the concentrations of CO_2, HCO_3^-, and Ca^{2+}. Each of these species defines a part of a system of ADR equations

$$\frac{\partial U_i}{\partial t} + \mathbf{u} \circ \nabla U_i - D_i \nabla^2 U_i = R_i, \qquad \mathbf{x} \in \Omega, \quad t > 0, \tag{4.2}$$

where $U = ([CO_2], [HCO_3^-], [Ca^{2+}])$ is a vector of concentrations, with corresponding diffusion constants $D = (D_{[CO_2]}, D_{[HCO_3^-]}, D_{[Ca^{2+}]})$. The $\mathbf{u}$ denotes the von Kármán flow discussed in Chapter 2, and $R = (R_{CO_2}, R_{HCO_3^-}, R_{Ca^{2+}})$ refers to the time rate of change of these constituents based on equations (3.34)–(3.37) in Chapter 3. Considering (3.34), (3.37), and that there are no reactions involving Ca^{2+} in the bulk,

$$R_{CO_2} = -k_1[CO_2] + k_{-1}[H_2CO_3{}^0] - k_2[CO_2][OH^-] + k_{-2}[HCO_3^-], \tag{4.3}$$

$$R_{HCO_3^-} = k_2[CO_2][OH^-] - k_{-2}[HCO_3^-], \tag{4.4}$$

$$R_{Ca^{2+}} = 0. \tag{4.5}$$

Associated with this set of ADR equations, are boundary conditions that represent the dissolving interface, and the conditions far from the interface in the well mixed bulk region. The position of the dissolution interface, denoted by Γ_S, is a function of time given by $S(\mathbf{x}, t)$ so that

$$F(\mathbf{x}, z, t) = z - S(\mathbf{x}, t) = 0, \qquad x \in \Gamma_S. \tag{4.6}$$

At this interface, the calcium concentration is saturated, and there is no flux of CO_2. This is because the dissolving surface only produces Ca^{2+} and CO_3^{2-}. For the level of $[CO_2](S, t)$, we note that if $\mathbf{n}$ denotes the outward unit normal of the surface $z - S(\mathbf{x}, t) = 0$ then

$$\mathbf{Q} \circ \mathbf{n}|_{\Gamma_S} = \left([CO_2](\mathbf{x}, t)\mathbf{u}(\mathbf{x}) - D\frac{\partial}{\partial \mathbf{n}}[CO_2](\mathbf{x}, t) \right) \circ \mathbf{n} = 0, \qquad \mathbf{x} \in \Gamma_S. \tag{4.7}$$

To find the concentration of H^+ at this interface, we assume a charge balance (3.45), and use the associated value of $[\mathsf{CO}_2](S(t),t)$. This results in the condition

$$[\mathsf{H}^+] + \frac{2k_{-2}K_{\mathrm{sp}}[\mathsf{H}^+]^2}{k_2K_{\mathrm{W}}^cK_2^c[\mathsf{CO}_2]} - \frac{K_{\mathrm{W}}^c}{[\mathsf{H}^+]} - \frac{k_2K_{\mathrm{W}}^c}{k_{-2}}\frac{[\mathsf{CO}_2]}{[\mathsf{H}^+]} - \frac{2k_2K_{\mathrm{W}}^cK_2^c}{k_{-2}}\frac{[\mathsf{CO}_2]}{[\mathsf{H}^+]^2} - [\mathsf{Cl}^-] = 0, \quad (4.8)$$

where it is understood that $[\mathsf{H}^+] = [\mathsf{H}^+](\mathbf{x},t)$ and $[\mathsf{CO}_2] = [\mathsf{CO}_2](\mathbf{x},t)$, $\mathbf{x} \in \Gamma_S$, and $[\mathsf{Cl}^-]$ is constant. The level of $[\mathsf{HCO}_3^-](\mathbf{x},t)$ where $\mathbf{x} \in \Gamma_S$ satisfies the assumption of equilibrium[3]

$$[\mathsf{HCO}_3^-](\mathbf{x},t) = \frac{k_2K_{\mathrm{W}}^c}{k_{-2}}\frac{[\mathsf{CO}_2](\mathbf{x},t)}{[\mathsf{H}^+](\mathbf{x},t)}, \qquad \mathbf{x} \in \Gamma_S, \quad (4.9)$$

given in Chapter 3, and from (3.65)–(3.67) the level of calcium at the dissolving interface is

$$[\mathsf{Ca}^{2+}](\mathbf{x},t) = [\mathsf{Ca}^{2+}]_{\max} = \frac{k_{-2}K_{\mathrm{sp}}[\mathsf{H}^+]^2(\mathbf{x},t)}{k_2K_{\mathrm{W}}^cK_2^c[\mathsf{CO}_2](\mathbf{x},t)}, \qquad \mathbf{x} \in \Gamma_S. \quad (4.10)$$

At the inflow boundary Γ_∞, that is away from the dissolving interface, the chemical species are again in equilibrium. The value of $[\mathsf{Ca}^{2+}](\mathbf{x},t)$, with $\mathbf{x} \in \Gamma_\infty$, is given by the condition that the bulk calcium concentration is consistent with amount of (well mixed) calcium that has dissolved. That is,

$$\int_{\mathbf{A}\in\Gamma_S} c_s\,|S(\mathbf{x},0) - S(\mathbf{x},t)|\,\mathrm{d}\mathbf{A} = \int_{V_v\cup\Gamma_\infty} [\mathsf{Ca}^{2+}](\mathbf{x},t)\,\mathrm{d}V \quad (4.11)$$

with c_s being the density of calcium in $\mathsf{CaCO}_3(\mathsf{s})$ in units of M, $\mathrm{d}\mathbf{A}$ is an infinitesimal element of the dissolution surface, and V_v is the volume of the reaction vessel. The amount of dissolved CO_2 is in equilibrium with the applied pressure so that

$$[\mathsf{CO}_2](\mathbf{x},t) = K_{\mathrm{H}}P_{\mathsf{CO}_2(\mathsf{g})}, \qquad \mathbf{x} \in \Gamma_\infty. \quad (4.12)$$

[3] An equivalent condition is $k_1[\mathsf{CO}_2] = k_{-1}[\mathsf{H}_2\mathsf{CO}_3{}^0]$.

The charge balance relationship (3.47) becomes

$$[\mathsf{H}^+] + 2[\mathsf{Ca}^{2+}] - \frac{K_{\mathrm{W}}^c}{[\mathsf{H}^+]} - \frac{K_{\mathrm{P}}}{[\mathsf{H}^+]} - \frac{2K_{\mathrm{P}}K_2^c}{[\mathsf{H}^+]^2} - [\mathsf{Cl}^-] = 0, \tag{4.13}$$

where it is understood that $[\mathsf{H}^+] = [\mathsf{H}^+](\mathbf{x}, t)$ and $[\mathsf{Ca}^{2+}] = [\mathsf{Ca}^{2+}](\mathbf{x}, t)$, $\mathbf{x} \in \Gamma_\infty$. Using these values, the level of $[\mathsf{HCO}_3^-](\mathbf{x}, t)$ satisfies

$$[\mathsf{HCO}_3^-](\mathbf{x}, t) = \frac{K_{\mathrm{P}}}{[\mathsf{H}^+](\mathbf{x}, t)}, \qquad \mathbf{x} \in \Gamma_\infty. \tag{4.14}$$

Finally, we require an expression that determines the motion of the dissolution interface, which starts at $z = S(\mathbf{x}, 0)$, and moves upward ($\partial S/\partial t < 0$ for $t > 0$) as material is dissolved. The dissolving interface is assumed to be flat so from (4.7) the advective term contains only the axial velocity. However, at the dissolving interface this velocity vanishes. Therefore, the motion of the interface, governed by a Stefan condition, takes the form

$$\Big(c_s - [\mathsf{Ca}^{2+}](\mathbf{x}, t)\Big)\, \mathbf{v}_n \circ \mathbf{n} = D_{[\mathsf{Ca}^{2+}]} \frac{\partial}{\partial \mathbf{n}} [\mathsf{Ca}^{2+}] \circ \mathbf{n}, \qquad \mathbf{x} \in \Gamma_S, \tag{4.15}$$

where c_s is the concentration of the calcium in the solid $\mathsf{CaCO}_3(\mathsf{s})$ disc, and $\mathbf{v}_n = v_n \mathbf{n}$, is the velocity of the interface. The condition (4.15) is a conservation law applied at the dissolution interface. The flux of material, as it is carried away from the interface, must match the jump in concentration as the material dissolves. This naturally limits the speed at which this dissolution can occur. Generally, if $\partial S/\partial t$ denotes the speed of the interface in the $\mathbf{k}$ direction, then

$$\mathbf{v}_n \circ \mathbf{n} = \frac{\partial S}{\partial t} \mathbf{k} \circ \mathbf{n} = v_n. \tag{4.16}$$

Since both the vessel and the rotating disc are cylindrical, we write these equations in cylindrical coordinates, and assume cylindrical symmetry. Before doing this we

will construct a set of characteristic sizes for all of the quantities.

4.3 Nondimensionalization

In Chapter 3, the chemistry of the carbonate system was considered for the equilibrium situations of 'no calcium' and 'saturated calcium' environments for the pressures and temperatures at which we are operating. This provides the insight to identify the dominating reactions and determines how the chemical concentrations should be scaled to capture both of these behaviours. Referring to the experimental conditions stated in Tables 3.1 and 4.1, the concentration of hydronium in these two cases are $[\mathsf{H}^+]_0 = 10^{-2}$ M from (3.51) and $[\mathsf{H}^+]_\infty = 1.77 \times 10^{-8}$ M from (3.65) respectively.[4]

Referring back to Chapter 3, the scaling for the various chemical species is given by (3.71) which is repeated here for convenience

$$\begin{aligned} [\mathsf{H}^+] &= [\mathsf{H}^+]_0 h, & [\mathsf{HCO}_3^-] &= \frac{K_\mathrm{P}}{[\mathsf{H}^+]_\infty} b, \\ [\mathsf{Ca}^{2+}] &= \frac{K_\mathrm{sp}[\mathsf{H}^+]_\infty^2}{K_2^c K_\mathrm{P}} c, & [\mathsf{CO}_2] &= K_\mathrm{H} P_{\mathsf{CO}_2(\mathsf{g})} u. \end{aligned} \tag{4.17}$$

For the spatial and velocity scaling, we use the (2.1) from the von Kármán's flow that defines the fluid velocity for the experiment. Collecting these expressions here,

$$z = \sqrt{\frac{\nu}{\omega}}\zeta, \qquad S = \sqrt{\frac{\nu}{\omega}}\hat{S}, \qquad r = R_d \hat{r} \tag{4.18}$$

$$u_r = r\omega F(\zeta), \qquad u_\theta = r\omega G(\zeta), \qquad u_z = \sqrt{\nu\omega} H(\zeta). \tag{4.19}$$

One of the purposes of the nondimensionalization procedure is to find dimensionless collections of parameters that characterize the process being examined. In

[4] $[\mathsf{H}^+]_0$ is the equilibrium concentration of $[\mathsf{H}^+]$ with no calcium in solution and $[\mathsf{H}^+]_\infty$ refers to equilibrium concentration of $[\mathsf{H}^+]$ in a solution saturated with calcium.

Table 4.1: Physical parameters for the dissolution process.

Data	Symbol	Units	Value	Ref.
Calcium concentration within calcite	c_s	M	27.08	[30]
Chlorine concentration to set the initial pH	$[\mathrm{Cl}^-]$	M	10^{-2}	–
CO_2(g) partial pressure in air at 1 atm	$P_{\mathrm{CO_2(g)}}$	atm	4.0×10^{-4}	–
Rotational speed of the disc	ω	rpm	100	–
Kinetic viscosity of water	ν	$\mathrm{m^2\,s^{-1}}$	9.82×10^{-7}	[21]
Area of the sample[5]	πR_d^2	$\mathrm{m^2}$	1.15×10^{-3}	–
Volume of the reaction vessel	$\pi R_v^2 H_v$	$\mathrm{m^3}$	10^{-3}	–
Diffusion coefficient of CO_2	$D_{[\mathrm{CO_2}]}$	$\mathrm{m^2\,s^{-1}}$	2.07×10^{-9}	[48]
Diffusion coefficient of H^+	$D_{[\mathrm{H}^+]}$	$\mathrm{m^2\,s^{-1}}$	9.31×10^{-9}	[46]
Diffusion coefficient of Cl^-	$D_{[\mathrm{Cl}^-]}$	$\mathrm{m^2\,s^{-1}}$	2.03×10^{-9}	[46]
Diffusion coefficient of Ca^{2+}	$D_{[\mathrm{Ca}^{2+}]}$	$\mathrm{m^2\,s^{-1}}$	7.93×10^{-10}	[46]

what follows, a few of these dimensionless collections arise naturally and will be discussed in advance.

- The **Reynolds** number, Re, is defined as the ratio of inertial forces to viscous forces within a fluid. It is helpful for predicting flow patterns and the level of disorder within a flow. For this work,

$$\mathrm{Re} = \frac{\omega R_d^2}{\nu} \simeq 3.87 \times 10^3, \tag{4.20}$$

  and is associated with the rotational velocity of the flow.

- The **Schmidt** number, Sc, is defined as the ratio of the momentum diffusivity (kinematic viscosity)to the mass diffusivity. Physically, it relates the relative thickness of the hydrodynamic and the diffusive boundary layers. A large value of Sc indicates that advection dominates diffusion with respect to the dynamics. In this process, we compute the Schmidt number with respect to

[5]The typical stone sample is 1.5 inches in diameter, and held within a 5 inch diameter reaction vessel.

the representative diffusion coefficient for the dissolved CO_2 and find that

$$\mathrm{Sc} = \frac{\nu}{D_{[\mathsf{CO}_2]}} \simeq 474. \tag{4.21}$$

- The **Stefan** number, St, in the current context indicates the relative velocity of the dynamics of a process compared to the speed of an associated moving interface. For the two cases discussed in Chapter 3, (i) a pressure of 1 atm with 400 ppm CO_2(g) with $[\mathsf{Cl}^-] = 0.01$, and (ii) a pressure of 0.97 atm CO_2(g) with $[\mathsf{Cl}^-] = 0$, expression (3.67) gives $\Gamma_{\mathsf{Ca}^{2+}} = 1.05 \times 10^{-3}$ and 1.41×10^{-2} respectively. As a result,

$$[\mathsf{Ca}^{2+}]_{\max} = \frac{K_{\mathrm{sp}}[\mathsf{H}^+]_\infty^2}{K_2^c K_{\mathrm{P}}} \simeq \begin{cases} \dfrac{[\mathsf{Cl}^-]}{2} = 5.00 \times 10^{-3}\ \mathsf{M}, \ \text{ case (i)}, \\ \dfrac{\Gamma_{\mathsf{Ca}^{2+}}}{2} = 7.03 \times 10^{-3}\ \mathsf{M}, \ \text{ case (ii)}, \end{cases} \tag{4.22}$$

with corresponding Stefan numbers of

$$\mathrm{St} = \frac{c_s - [\mathsf{Ca}^{2+}]_{\max}}{[\mathsf{Ca}^{2+}]_{\max}} \simeq \begin{cases} 5415, \ \text{ case (i)}, \\ 3851, \ \text{ case (ii)}. \end{cases} \tag{4.23}$$

A large Stefan number, $\mathrm{St} = \mathcal{O}(10^3)$, indicates that the dissolution occurs on a much faster time scale than the rate at which the boundary is moving. This type of situation is typically referred to as quasi-steady.

Returning to the process of determining effective scaling parameters, it is convenient to use the Schmidt number with the rotation frequency and take

$$t = \frac{\mathrm{Sc}}{\omega}\hat{t}. \tag{4.24}$$

4.4 ADR Equations in Cylindrical Coordinates

4.4.1 State equations

With the non-dimensionalized form of each of the species defined, the model can be written in these quantities in cylindrical coordinates. Starting with the original equation (4.1), repeated here for convenience,

$$\frac{\partial U_i}{\partial t} + \mathbf{u} \circ \nabla U_i - \nabla \circ (D \nabla U_i) = R_i. \tag{4.25}$$

The terms of this expression, written in cylindrical coordinates, and with the scaling, become

$$\frac{\partial U_i}{\partial t} + \mathbf{u} \circ \nabla = \frac{\omega}{\mathrm{Sc}} \frac{\partial U_i}{\partial \hat{t}} + \omega \left(\hat{r} F(\zeta) \frac{\partial U_i}{\partial \hat{r}} + H(\zeta) \frac{\partial U_i}{\partial \zeta} \right), \tag{4.26}$$

and

$$D \nabla^2 U_i = \frac{D}{R_d^2} \frac{1}{\hat{r}} \frac{\partial U_i}{\partial \hat{r}} \left(\hat{r} \frac{\partial U_i}{\partial \hat{r}} \right) + \frac{D\omega}{\nu} \frac{\partial^2 U_i}{\partial \zeta^2} = \frac{\omega}{\mathrm{Sc}} \left(\frac{1}{\mathrm{Re}} \left(\hat{r} \frac{\partial U_i}{\partial \hat{r}} \right) + \frac{\partial^2 U_i}{\partial \zeta^2} \right). \tag{4.27}$$

This facilitates the definition of the differential operator $\mathcal{L}$ with

$$\mathcal{L} f = \frac{1}{\mathrm{Sc}} \frac{\partial f}{\partial \hat{t}} + \hat{r} F(\zeta) \frac{\partial f}{\partial \hat{r}} + H(\zeta) \frac{\partial f}{\partial \zeta} - \frac{1}{\mathrm{Sc}\,\mathrm{Re}} \left(\hat{r} \frac{\partial f}{\partial \hat{r}} \right) - \frac{1}{\mathrm{Sc}} \frac{\partial^2 f}{\partial \zeta^2}. \tag{4.28}$$

For the reaction terms, starting with $R_{\mathsf{CO_2}}$, using (4.3),

$$\begin{aligned}
R_{\mathsf{CO_2}} &= -k_1[\mathsf{CO_2}] + k_{-1}[\mathsf{H_2CO_3}^0] - R_{\mathsf{HCO_3^-}} \\
&= -\left(\frac{k_1[\mathsf{H^+}]}{k_2 K_{\mathrm{W}}^c} + 1 \right) \left(k_2[\mathsf{CO_2}][\mathsf{OH^-}] - k_{-2}[\mathsf{HCO_3^-}] \right) \\
&= -k_1 \left(h + \frac{k_2 K_{\mathrm{W}}^c}{k_1[\mathsf{H^+}]_0} \right) \left(\frac{K_{\mathrm{H}} P_{\mathsf{CO_2(g)}} u}{h} - \frac{k_{-2} K_{\mathrm{P}} [\mathsf{H^+}]_0 b}{k_2 K_{\mathrm{W}}^c [\mathsf{H^+}]_\infty} \right) \\
&= -k_1 K_{\mathrm{H}} P_{\mathsf{CO_2(g)}} \frac{[\mathsf{H^+}]_0}{[\mathsf{H^+}]_\infty} \left(h + \frac{k_2 K_{\mathrm{W}}^c}{k_1[\mathsf{H^+}]_0} \right) \left(\frac{[\mathsf{H^+}]_\infty}{[\mathsf{H^+}]_0} \frac{u}{h} - b \right).
\end{aligned} \tag{4.29}$$

Similarly for $R_{\mathsf{HCO_3^-}}$, using (4.4),

$$R_{\mathsf{HCO_3^-}} = k_2[\mathsf{CO_2}][\mathsf{OH^-}] - k_{-2}[\mathsf{HCO_3^-}] = \frac{k_{-2}K_{\mathrm{P}}}{[\mathsf{H^+}]_\infty}\left(\frac{[\mathsf{H^+}]_\infty}{[\mathsf{H^+}]_0}\frac{u}{h} - b\right), \tag{4.30}$$

and for $R_{\mathsf{Ca^{2+}}}$,

$$R_{\mathsf{Ca^{2+}}} = 0. \tag{4.31}$$

From (4.29)–(4.31), and (4.28), the expression (4.26) becomes

$$\mathcal{L}u = -\frac{k_1}{\omega}\frac{[\mathsf{H^+}]_0}{[\mathsf{H^+}]_\infty}\left(h + \frac{k_2K_{\mathrm{W}}^c}{k_1[\mathsf{H^+}]_0}\right)\left(\frac{[\mathsf{H^+}]_\infty}{[\mathsf{H^+}]_0}\frac{u}{h} - b\right), \tag{4.32}$$

$$\mathcal{L}b = \frac{k_{-2}}{\omega}\left(\frac{[\mathsf{H^+}]_\infty}{[\mathsf{H^+}]_0}\frac{u}{h} - b\right), \tag{4.33}$$

$$\mathcal{L}c = 0. \tag{4.34}$$

Finally, the Stefan condition that governs the speed of the moving interface satisfies

$$\mathrm{St}\,\frac{\partial \hat{S}}{\partial \hat{t}}\mathbf{k}\circ\mathbf{n} = \frac{\partial c}{\partial \mathbf{n}}, \qquad \mathbf{x}\in\Gamma_S, \quad S(\mathbf{x},0) = 0, \tag{4.35}$$

where an initial flat interface at $z = 0$ is assumed.

4.4.2 Non-dimensional charge neutrality equation

Associated with (4.32)–(4.23) is an expression for h that comes from the charge balance. From the previous chapter, expressions (3.72)–(3.74), repeated here for convenience,

$$h^2 + \left(\frac{2K_{\mathrm{sp}}[\mathsf{H^+}]_\infty^2}{K_2^cK_{\mathrm{P}}[\mathsf{H^+}]_0}c - \frac{K_{\mathrm{P}}}{[\mathsf{H^+}]_0[\mathsf{H^+}]_\infty}b - \frac{[\mathsf{Cl^-}]}{[\mathsf{H^+}]_0}\right)h - \frac{K_{\mathrm{W}}^c}{[\mathsf{H^+}]_0^2} - \frac{2K_2^cK_{\mathrm{P}}}{[\mathsf{H^+}]_0^2[\mathsf{H^+}]_\infty}b = 0, \tag{4.36}$$

and for $[\mathsf{Cl}^-] = 0.01$ and 400 ppm of CO_2(g),

$$\begin{aligned} &\frac{2K_{\mathrm{sp}}[\mathsf{H}^+]_\infty^2}{K_2^c K_{\mathrm{P}}[\mathsf{H}^+]_0} \simeq 1.03, \qquad \frac{K_{\mathrm{P}}}{[\mathsf{H}^+]_0[\mathsf{H}^+]_\infty} \simeq 3.33 \times 10^{-2}, \qquad \frac{[\mathsf{Cl}^-]}{[\mathsf{H}^+]_0} \simeq 1, \\ &\frac{K_{\mathrm{W}}^c}{[\mathsf{H}^+]_0^2} \simeq 1.01 \times 10^{-10}, \quad \frac{2K_2 K_{\mathrm{P}}}{[\mathsf{H}^+]_0^2[\mathsf{H}^+]_\infty} \simeq 3.12 \times 10^{-12}. \end{aligned} \tag{4.37}$$

while for $[\mathsf{Cl}^-] = 0$ and 0.97 atm of CO_2(g),

$$\begin{aligned} &\frac{2K_{\mathrm{sp}}[\mathsf{H}^+]_\infty^2}{K_2^c K_{\mathrm{P}}[\mathsf{H}^+]_0} \simeq 1.17 \times 10^{2}, \quad \frac{K_{\mathrm{P}}}{[\mathsf{H}^+]_0[\mathsf{H}^+]_\infty} \simeq 1.17 \times 10^{2}, \qquad \frac{[\mathsf{Cl}^-]}{[\mathsf{H}^+]_0} \simeq 0, \\ &\frac{K_{\mathrm{W}}^c}{[\mathsf{H}^+]_0^2} \simeq 6.97 \times 10^{-7}, \qquad \frac{2K_2 K_{\mathrm{P}}}{[\mathsf{H}^+]_0^2[\mathsf{H}^+]_\infty} \simeq 1.09 \times 10^{-8}. \end{aligned} \tag{4.38}$$

There are two conditions that play a special role in determining the state of the chemical species. The first is the condition for equilibrium, that in Chapter 3 was identified as either $k_2[\mathsf{CO}_2][\mathsf{OH}^-] = k_{-2}[\mathsf{HCO}_3^-]$ or $k_1[\mathsf{CO}_2] = k_{-1}[\mathsf{H}_2\mathsf{CO}_3{}^0]$ as they were shown to be equivalent. Using the former,

$$b = \frac{[\mathsf{H}^+]_\infty}{[\mathsf{H}^+]_0}\frac{u}{h}, \qquad (\text{from} \quad k_2[\mathsf{CO}_2][\mathsf{OH}^-] = k_{-2}[\mathsf{HCO}_3^-]) \tag{4.39}$$

with the second relation being the dimensionless form. This can be confirmed by observing that this is the same condition that makes the right hand side of (4.32)–(4.33) vanish. The second condition is when the fluid is saturated with $[\mathsf{Ca}^{2+}]$. This condition ($\lambda = 1$) corresponds to

$$\frac{[\mathsf{H}^+]_\infty}{[\mathsf{H}^+]_0} cb = h, \qquad (\text{from} \quad [\mathsf{Ca}^{2+}][\mathsf{CO}_3^{2-}] = K_{\mathrm{sp}}) \tag{4.40}$$

again with the second relation being the dimensionless form.

At this point we can reconstruct the dimensionless versions of the equilibrium conditions detailed in Chapter 3. The first, corresponding to expression (3.49), occurs when there is no calcium in solution, $c = 0$, and the system is in equilibrium,

$[\mathsf{H}^+]_0 bh = [\mathsf{H}^+]_\infty u$. Placing these conditions into (4.36) yields

$$[\mathsf{H}^+]_0^3 h^3 - [\mathsf{Cl}^-][\mathsf{H}^+]_0^2 h^2 - K_{\mathrm{W}}^c [\mathsf{H}^+]_0 h - K_{\mathrm{P}} [\mathsf{H}^+]_0 uh - 2K_2 K_{\mathrm{P}} u = 0. \tag{4.41}$$

When the dissolved $[\mathsf{CO}_2]$ is uniform, and equal to its value at the boundary of the domain, then $u = 1$ everywhere. Expression (4.41), with $u = 1$, reproduces equation (3.49), and therefore its solution is $h = 1$ or $[\mathsf{H}^+] = [\mathsf{H}^+]_0$.

The other extreme case is when the calcium is saturated, $[\mathsf{H}^+]_\infty cb = [\mathsf{H}^+]_0 h$, and the system is in equilibrium, $[\mathsf{H}^+]_0 bh = [\mathsf{H}^+]_\infty u$. In this case (4.36) becomes

$$\frac{2K_{\mathrm{sp}}[\mathsf{H}^+]_0^4}{K_2^c K_{\mathrm{P}}} \frac{h^4}{u} + [\mathsf{H}^+]_0^3 h^3 - [\mathsf{Cl}^-][\mathsf{H}^+]_0^2 h^2 - (K_{\mathrm{W}}^c + K_{\mathrm{P}} u)[\mathsf{H}^+]_0 h - 2K_2^c K_{\mathrm{P}} u = 0 \tag{4.42}$$

corresponding to (3.53). The solution when $u = 1$ is $h = [\mathsf{H}^+]_\infty / [\mathsf{H}^+]_0$.

4.4.3 Boundary conditions

To uniquely solve the system (4.28), (4.32)–(4.23), requires a set of boundary conditions. At the dissolution surface, Γ_S, the Ca^{2+} concentration is saturated and the solution is in a state of chemical equilibrium. Denoting the concentration of $\{[\mathsf{CO}_2]$, $[\mathsf{HCO}_3^-]$, $[\mathsf{Ca}^{2+}]$, and $[\mathsf{H}^+]\}$ respectively as u_0, b_0, c_0, h_0. At the interface Γ_S, carbon dioxide gas is neither produced nor consumed, so there is a no-flux condition at this boundary

$$\frac{\partial u}{\partial \zeta} = 0, \qquad \left(\text{from} \quad \frac{\partial [\mathsf{CO}_2]}{\partial z} = 0 \right) \tag{4.43}$$

expressed in the dimensionless scaling. The actual value of u_0 remains undetermined at this point, as it will be chosen so that the condition at Γ_∞ is satisfied.

However, for any value of u_0 we can find using (4.36)–(4.40),

$$b_0 = \frac{[\mathsf{H}^+]_\infty}{[\mathsf{H}^+]_0}\frac{u_0}{h_0}, \qquad\qquad c_0 = \frac{[\mathsf{H}^+]_0^2}{[\mathsf{H}^+]_\infty^2}\frac{h_0^2}{u_0}, \tag{4.44}$$

with h_0 satisfying

$$\frac{2K_{\mathrm{sp}}[\mathsf{H}^+]_0^2}{K_2^c K_{\mathrm{P}}}\frac{h_0^4}{u_0^2} + \left([\mathsf{H}^+]_0 h_0^2 - [\mathsf{Cl}^-]h_0 - \frac{K_{\mathrm{W}}^c}{[\mathsf{H}^+]_0}\right)\frac{h_0}{u_0} - \frac{K_{\mathrm{P}}}{[\mathsf{H}^+]_0}\left(h_0 + \frac{2K_2^c}{[\mathsf{H}^+]_0}\right) = 0. \tag{4.45}$$

At Γ_∞, the boundary far away from the dissolution surface, we assume a state of equilibrium. Let u_∞, b_∞, c_∞, h_∞ denote the concentrations of the chemical species, in dimensionless coordinates at Γ_∞ with a similar correspondence so that

$$u_\infty = 1, \qquad\qquad b_\infty = \frac{[\mathsf{H}^+]_\infty}{[\mathsf{H}^+]_0}\frac{1}{h_\infty}. \tag{4.46}$$

The value of c_∞ depends on the amount of dissolved Ca^{2+}. Using (4.11),

$$c_\infty \simeq -\frac{c_s}{[\mathsf{Ca}^{2+}]_{\max}}\left(\frac{\nu}{\omega}\right)^{1/2}\frac{R_d^2\hat{S}(\hat{t})}{R_v^2 H_v}, \qquad \left(\lim_{\zeta\to\infty}[\mathsf{Ca}^{2+}](\zeta,t) \simeq \left(\frac{R_d}{R_v}\right)^2\frac{S(t)}{H_v}c_s\right). \tag{4.47}$$

Finally, h_∞ satisfies

$$h_\infty^3 + \left(\frac{2K_{\mathrm{sp}}[\mathsf{H}^+]_\infty^2}{K_2^c K_{\mathrm{P}}[\mathsf{H}^+]_0}c_\infty - \frac{[\mathsf{Cl}^-]}{[\mathsf{H}^+]_0}\right)h_\infty^2 - (K_{\mathrm{W}}^c + K_{\mathrm{P}})\frac{h_\infty}{[\mathsf{H}^+]_0^2} - \frac{2K_2^c K_{\mathrm{P}}}{[\mathsf{H}^+]_0^3} = 0. \tag{4.48}$$

In this chapter the formulation of the problem in radial and axial coordinates has been presented. It describes the dissolution of calcite in a closed environment with a swirling flow. The process described is faithful to the chemistry of the carbonate system and conserves mass through a Stefan condition at the dissolution interface. In the next chapter, the dissolution is assumed to occur at a flat interface, essentially neglecting any radial dependence.

CHAPTER 5

Radial independent problem

In the initial stages of an RDA experiment the dissolving interface remains flat, an observation that was used in Levich's initial analysis of the problem [23]. Following this precedent, we assume that there is no radial dependence, which ensures the surface dissolves uniformly. In the latter stages of an RDA experiment this assumption may not be justified. Collecting together the various results, the state equations (4.32)–(4.34) are

$$\frac{1}{\mathrm{Sc}}\frac{\partial u}{\partial \hat{t}} + H(\zeta)\frac{\partial u}{\partial \zeta} - \frac{1}{\mathrm{Sc}}\frac{\partial^2 u}{\partial \zeta^2} = \frac{k_1}{\omega}\frac{[\mathsf{H}^+]_0}{[\mathsf{H}^+]_\infty}\left(h + \frac{k_2 K_{\mathrm{W}}^c}{k_1[\mathsf{H}^+]_0}\right)\left(b - \frac{[\mathsf{H}^+]_\infty}{[\mathsf{H}^+]_0}\frac{u}{h}\right), \tag{5.1}$$

$$\frac{1}{\mathrm{Sc}}\frac{\partial b}{\partial \hat{t}} + H(\zeta)\frac{\partial b}{\partial \zeta} - \frac{1}{\mathrm{Sc}}\frac{\partial^2 b}{\partial \zeta^2} = \frac{k_{-2}}{\omega}\left(\frac{[\mathsf{H}^+]_\infty}{[\mathsf{H}^+]_0}\frac{u}{h} - b\right), \tag{5.2}$$

$$\frac{1}{\mathrm{Sc}}\frac{\partial c}{\partial \hat{t}} + H(\zeta)\frac{\partial c}{\partial \zeta} - \frac{1}{\mathrm{Sc}}\frac{\partial^2 c}{\partial \zeta^2} = 0, \tag{5.3}$$

for $\zeta > \hat{S}(\hat{t})$, $\hat{t} > 0$ where $H(\zeta)$ is a component of the von Kármán flow, and from (4.36)

$$h^2 + \left(\frac{2K_{\text{sp}}[\text{H}^+]_\infty^2}{K_2^c K_{\text{P}}[\text{H}^+]_0} c - \frac{K_{\text{P}}}{[\text{H}^+]_0[\text{H}^+]_\infty} b - \frac{[\text{Cl}^-]}{[\text{H}^+]_0} \right) h - \frac{K_{\text{W}}^c}{[\text{H}^+]_0^2} - \frac{2K_2^c K_{\text{P}}}{[\text{H}^+]_0^2[\text{H}^+]_\infty} b = 0. \quad (5.4)$$

For the boundary conditions at the dissolution interface, $\zeta = \hat{S}(\hat{t})$,

$$u(\hat{S}(\hat{t}), \hat{t}) = u_0(\hat{t}), \qquad b(\hat{S}(\hat{t}), \hat{t}) = b_0(\hat{t}), \qquad c(\hat{S}(\hat{t}), \hat{t}) = c_0(\hat{t}), \quad (5.5)$$

that satisfy

$$\frac{\partial u}{\partial \zeta} = 0, \qquad b_0(\hat{t}) = \frac{[\text{H}^+]_\infty}{[\text{H}^+]_0} \frac{u_0(\hat{t})}{h_0(\hat{t})}, \qquad c_0(\hat{t}) = \frac{[\text{H}^+]_0^2}{[\text{H}^+]_\infty^2} \frac{h_0(\hat{t})^2}{u_0(\hat{t})}. \quad (5.6)$$

The value of $u_0(\hat{t})$ is determined by the first condition of (5.6), and $h_0(\hat{t})$ is given by (4.45), repeated here

$$\frac{2K_{\text{sp}}[\text{H}^+]_0^2}{K_2^c K_{\text{P}}} h_0^4 + \left([\text{H}^+]_0 h_0^2 - [\text{Cl}^-] h_0 - \frac{K_{\text{W}}^c}{[\text{H}^+]_0} \right) h_0 u_0 - \frac{K_{\text{P}}}{[\text{H}^+]_0} \left(h_0 + \frac{2K_2^c}{[\text{H}^+]_0} \right) u_0^2 = 0. \quad (5.7)$$

In the bulk, far from the dissolution, and in the well mixed region as $\zeta \to \infty$,

$$\lim_{\zeta \to \infty} u(\zeta, \hat{t}) = u_\infty(\hat{t}), \qquad \lim_{\zeta \to \infty} b(\zeta, \hat{t}) = b_\infty(\hat{t}), \qquad \lim_{\zeta \to \infty} c(\zeta, \hat{t}) = c_\infty(\hat{t}), \quad (5.8)$$

that satisfy

$$u_\infty(\hat{t}) = 1, \quad b_\infty(\hat{t}) = \frac{[\text{H}^+]_\infty}{[\text{H}^+]_0} \frac{1}{h_\infty(\hat{t})}, \quad c_\infty(\hat{t}) = -\frac{K_2^c K_{\text{P}} c_s}{K_{\text{sp}}[\text{H}^+]_\infty^2} \left(\frac{R_d}{R_v} \right)^2 \frac{\hat{S}(\hat{t})}{\hat{H}_v}. \quad (5.9)$$

The expression for $c_\infty(\hat{t})$ is given by the dimensionless version of (4.11) and assuming radial independence. Here the value of h_∞ comes from (4.48), and repeated

here

$$h_\infty^3 + \left(\frac{2K_{\mathrm{sp}}[\mathsf{H}^+]_\infty^2}{K_2^c K_{\mathrm{P}}[\mathsf{H}^+]_0} c_\infty - \frac{[\mathsf{Cl}^-]}{[\mathsf{H}^+]_0} \right) h_\infty^2 - (K_{\mathrm{W}}^c + K_{\mathrm{P}}) \frac{h_\infty}{[\mathsf{H}^+]_0^2} - \frac{2K_2^c K_{\mathrm{P}}}{[\mathsf{H}^+]_0^3} = 0. \tag{5.10}$$

For any time $\hat{t} > 0$, the motion of the interface closes the system and is given by

$$\mathrm{St} \frac{\mathrm{d}\hat{S}}{\mathrm{d}\hat{t}} = \left. \frac{\partial c}{\partial \zeta} \right|_{\hat{S}}, \qquad \hat{S}(0) = 0. \tag{5.11}$$

5.1 Boundary Conditions

The large variation in the values of the chemical rate and equilibrium coefficients allow the expression for the hydrogen to be simplified. Beginning with h_0, the asymptotic form depends on $[\mathsf{Cl}^-]$. For the $[\mathsf{Cl}^-]$ dominant case, we choose $K_{\mathrm{P}} = 5.99 \times 10^{-12}$ M^2, corresponding to 400 ppm of CO_2(g), and to dominate the chemistry, $[\mathsf{Cl}^-] = 0.01$ M. Rewriting expression (5.7) as

$$h_0^4 + \gamma u_0 \left(a_0 h_0^3 - h_0^2 - a_1 u_0 h_0 \epsilon - a_1 h_0 \epsilon^{3/2} - a_2 u_0 \epsilon^2 \right) = 0, \tag{5.12}$$

with

$$\epsilon^{1/2} = \frac{K_{\mathrm{W}}^c}{K_{\mathrm{P}}} = 1.69 \times 10^{-3}, \qquad \gamma = \frac{K_2^c K_{\mathrm{P}}[\mathsf{Cl}^-]}{2K_{\mathrm{sp}}[\mathsf{H}^+]_0^2} = 3.14 \times 10^{-12} \sim 2.59\epsilon^2, \tag{5.13}$$

and

$$a_0 = \frac{[\mathsf{H}^+]_0}{[\mathsf{Cl}^-]}, \qquad a_1 = \frac{K_{\mathrm{P}}^3}{{K_{\mathrm{W}}^c}^2 [\mathsf{H}^+]_0 [\mathsf{Cl}^-]}, \qquad a_2 = \frac{2K_2^c K_{\mathrm{P}}^5}{{K_{\mathrm{W}}^c}^4 [\mathsf{H}^+]_0^2 [\mathsf{Cl}^-]}, \tag{5.14}$$

reveals a number of small parameters. In particular, $a_0 \simeq 1$, $a_1 \simeq 2.10 \times 10^{-2}$ and $a_2 \simeq 6.87 \times 10^{-5}$. With $\epsilon = \mathcal{O}(10^{-6})$, an expansion of h_0 in terms of γu_0 gives $h_0 = \pm(\gamma u_0)^{1/2} - \gamma u_0/2 + \mathcal{O}\left((\gamma u_0)^{3/2}\right)$ and is detailed in Appendix B. Choosing

the positive root, and using (5.6),

$$\begin{aligned} b_0(\hat{t}) &= \left(\frac{2K_{\text{sp}}[\text{H}^+]_\infty^2}{K_2^c K_{\text{P}}[\text{Cl}^-]}\right)^{1/2} u_0^{1/2} + \mathcal{O}(\gamma u_0)\,, \quad c_0(\hat{t}) = \frac{K_2^c K_{\text{P}}[\text{Cl}^-]}{2K_{\text{sp}}[\text{H}^+]_\infty^2} + \mathcal{O}(\gamma)\,, \\ h_0(\hat{t}) &= \left(\frac{K_2^c K_{\text{P}}[\text{Cl}^-]}{2K_{\text{sp}}[\text{H}^+]_0^2}\right)^{1/2} u_0^{1/2} + \mathcal{O}(\gamma u_0)\,. \end{aligned} \tag{5.15}$$

Moreover, from the approximate value of $[\text{H}^+]_\infty$ given by (3.65),

$$h_0(\hat{t}) \simeq \frac{[\text{H}^+]_\infty}{[\text{H}^+]_0} u_0^{1/2}, \qquad b_0(\hat{t}) \simeq u_0^{1/2}, \qquad c_0(\hat{t}) \simeq 1, \tag{5.16}$$

associated with the value of u_0, corresponding to the no-flux condition (4.43).

When there is no appreciable $[\text{Cl}^-]$, the analysis is slightly different. For $[\text{Cl}^-] = 0$, and K_{P} corresponding to 0.97 atm of CO_2(g), expression (5.7) can be rewritten as

$$h_0^4 + \gamma u_0 \epsilon \left(a_0 h_0^3 - a_1 h_0^2 - u_0 h_0 - \epsilon h - a_2 u_0 \epsilon\right) = 0, \tag{5.17}$$

with

$$\gamma = \frac{K_2^c K_{\text{P}}^3}{2K_{\text{W}}^c K_{\text{sp}}[\text{H}^+]_0^3} = 0.906, \qquad \epsilon = \frac{K_{\text{W}}^c}{K_{\text{P}}} = 6.97 \times 10^{-7}, \tag{5.18}$$

and

$$a_0 = \frac{[\text{H}^+]_0^2}{K_{\text{P}}}, \qquad a_1 = \frac{[\text{Cl}^-][\text{H}^+]_0}{K_{\text{P}}}, \qquad a_2 = \frac{2K_2^c K_{\text{P}}}{K_{\text{W}}^c [\text{H}^+]_0}, \tag{5.19}$$

reveals number of small parameters. In particular, $a_0 \simeq 1$, $a_1 = 0$ and $a_2 \simeq 1.11$. The asymptotic form of h_0 then becomes $h_0 = (\epsilon\gamma u_0^2)^{1/3} - \epsilon\gamma u_0/3 + \mathcal{O}\Big((\epsilon\gamma)^{5/3} u_0^{4/3}\Big)$. As a result,

$$\begin{aligned} b_0(\hat{t}) &= \left(\frac{2K_{\text{sp}}[\text{H}^+]_\infty^3}{K_2^c K_{\text{P}}^2}\right)^{1/3} u_0^{1/3} + \mathcal{O}(\gamma)\,, \qquad c_0(\hat{t}) = \left(\frac{K_2^c K_{\text{P}}^2}{2K_{\text{sp}}[\text{H}^+]_\infty^3}\right)^{2/3} u_0^{1/3} + \mathcal{O}(\gamma u_0)\,, \\ h_0(\hat{t}) &= \left(\frac{K_2^c K_{\text{P}}^2}{2K_{\text{sp}}[\text{H}^+]_0^3}\right)^{1/3} u_0^{2/3} + \mathcal{O}(\gamma u_0)\,. \end{aligned} \tag{5.20}$$

As with (5.16), from the approximate value of $[\mathsf{H}^+]_\infty$ given by (3.66),

$$h_0(\hat{t}) \simeq \frac{[\mathsf{H}^+]_\infty}{[\mathsf{H}^+]_0} u_0^{2/3}, \qquad b_0(\hat{t}) \simeq u_0^{1/3}, \qquad c_0(\hat{t}) \simeq u_0^{2/3}, \tag{5.21}$$

associated with the value of u_0 corresponding to the no-flux condition (4.43).

At Γ_∞, the boundary far away from the dissolution, the dimensionless charge balance equation is given by (5.10)

$$h_\infty^3 + \left(\frac{2K_{\mathsf{sp}}[\mathsf{H}^+]_\infty^2}{K_2^c K_{\mathrm{P}}[\mathsf{H}^+]_0} c_\infty - \frac{[\mathsf{Cl}^-]}{[\mathsf{H}^+]_0} \right) h_\infty^2 - (K_{\mathrm{W}}^c + K_{\mathrm{P}}) \frac{h_\infty}{[\mathsf{H}^+]_0^2} - \frac{2K_2^c K_{\mathrm{P}}}{[\mathsf{H}^+]_0^3} = 0. \tag{5.22}$$

For 400 ppm of $\mathsf{CO}_2(\mathsf{g})$ and $[\mathsf{Cl}^-] = 0.01$,

$$\begin{aligned} \frac{2K_{\mathsf{sp}}[\mathsf{H}^+]_\infty^2}{K_2^c K_{\mathrm{P}}[\mathsf{H}^+]_0} &= 1.0335, \qquad \frac{[\mathsf{Cl}^-]}{[\mathsf{H}^+]_0} = 1, \qquad \frac{K_{\mathrm{P}}}{[\mathsf{H}^+]_0^2} = 5.9932 \times 10^{-8}, \\ \frac{K_{\mathrm{W}}}{[\mathsf{H}^+]_0^2} &= 1.0132 \times 10^{-10}, \quad \frac{2K_2^c K_{\mathrm{P}}}{[\mathsf{H}^+]_0^3} = 5.6137 \times 10^{-16}. \end{aligned} \tag{5.23}$$

while for 0.97 atm of $\mathsf{CO}_2(\mathsf{g})$ and $[\mathsf{Cl}^-] = 0$,

$$\begin{aligned} \frac{2K_{\mathsf{sp}}[\mathsf{H}^+]_\infty^2}{K_2^c K_{\mathrm{P}}[\mathsf{H}^+]_0} &= 1.1656 \times 10^2, \quad \frac{[\mathsf{Cl}^-]}{[\mathsf{H}^+]_0} = 0, \qquad \frac{K_{\mathrm{P}}}{[\mathsf{H}^+]_0^2} = 1, \\ \frac{K_{\mathrm{W}}}{[\mathsf{H}^+]_0^2} &= 6.9713 \times 10^{-7}, \quad \frac{2K_2^c K_{\mathrm{P}}}{[\mathsf{H}^+]_0^3} = 7.7697 \times 10^{-7}. \end{aligned} \tag{5.24}$$

Corresponding to these choices, the value for $c_\infty(\hat{t})$ depends on the amount of dissolved $\mathsf{CaCO}_3(\mathsf{s})$ at any specific time. An approximate solution to (5.22)–(5.23) is given by

$$h_\infty(\hat{t}) = 1 - c_\infty(\hat{t}) + \mathcal{O}\left(\frac{K_{\mathrm{P}}}{[\mathsf{H}^+]_0^2} \right), \qquad b_\infty(\hat{t}) = \frac{[\mathsf{H}^+]_\infty}{[\mathsf{H}^+]_0} \frac{1}{h_\infty(\hat{t})}. \tag{5.25}$$

5.2 The Free Boundary

The free boundary condition (5.11) has been stated, but the details of how this condition is implemented have not been discussed. Much of the analytical techniques and numerical methods associated with free boundary problems can be found in the proceedings [29]. Application of a Stefan problem to a dissolution process is uncommon, but has been explored in the literature [9, 14, 45]. Of particular note is the general multiphase Stefan problem with unknown interface conditions described in [39]. A form of this transformation is described next.

5.2.1 Boundary transformation

The boundary transformation method changes the spatial variable so that the domain of the problem becomes fixed. However, doing this introduces nonlinear terms into the equations. In the case of the dissolution problem (5.1)–(5.11), the domain $\zeta \in [\hat{S}(\hat{t}), \zeta_0]$ can be transformed into the fixed domain $x \in [0, \zeta_0]$. This can be done with the transformation

$$x = \frac{\zeta - \hat{S}(\hat{t})}{\zeta_0 - \hat{S}(\hat{t})}\zeta_0, \tag{5.26}$$

with derivatives

$$\frac{\partial x}{\partial \zeta} = \frac{\zeta_0}{\zeta_0 - \hat{S}(\hat{t})}, \qquad \frac{\partial x}{\partial \hat{t}} = \frac{x - \zeta_0}{\zeta_0 - \hat{S}(\hat{t})}\frac{\mathrm{d}\hat{S}}{\mathrm{d}\hat{t}}. \tag{5.27}$$

From this transformation, where we denote $c(\zeta, \hat{t}) = c(\zeta(x, \hat{t}), \hat{t}) = \tilde{c}(x, \hat{t})$,

$$\frac{\partial c}{\partial \hat{t}} = \frac{\partial \tilde{c}}{\partial \hat{t}} + \frac{x - \zeta_0}{\zeta_0 - \hat{S}(\hat{t})}\frac{\mathrm{d}\hat{S}}{\mathrm{d}\hat{t}}\frac{\partial \tilde{c}}{\partial x}, \qquad \frac{\partial c}{\partial \zeta} = \frac{\zeta_0}{\zeta_0 - \hat{S}(\hat{t})}\frac{\partial \tilde{c}}{\partial x}, \tag{5.28}$$

and the state equation (5.3) becomes

$$\left(1-\frac{\hat{S}(\hat{t})}{\zeta_0}\right)^2\frac{\partial\tilde{c}}{\partial\hat{t}}+\left(\mathrm{Sc}\,H(\zeta)-\left(1-\frac{x}{\zeta_0}\right)\frac{\mathrm{d}\hat{S}}{\mathrm{d}\hat{t}}\right)\left(1-\frac{\hat{S}(\hat{t})}{\zeta_0}\right)\frac{\partial\tilde{c}}{\partial x}-\frac{\partial^2\tilde{c}}{\partial x^2}=0, \quad (5.29)$$

defined on the fixed domain $x\in[0,\zeta_0]$, $\hat{t}>0$, and the associated Stefan condition becomes

$$\mathrm{St}\,\frac{\mathrm{d}\hat{S}}{\mathrm{d}\hat{t}}=\left(1-\frac{\hat{S}(\hat{t})}{\zeta_0}\right)^{-1}\left.\frac{\partial\tilde{c}}{\partial x}\right|_0. \quad (5.30)$$

An extra complication with using this method, is that the equations that define the von Kármán flow assume that the dissolution surface does not move. A version of this method is used in [3] where the Stefan number is large. In this situation, an approximation to the solution can be computed by removing the time dependence in the state equations (5.1)–(5.3) while allowing $\hat{S}(\hat{t})$ to evolve according to the Stefan condition (5.11). The time scale is changed to where the interface is moving but slowly enough that the fluid flow is essentially steady state. This splitting of the time dependence is termed a quasi-steady solution.

5.2.2 Quasi-steady problem

Assuming a quasi-steady solution, the equations for $c(\zeta,\hat{t})$, restricted to $\zeta\geq 0$, and $\hat{S}(\hat{t})$ reduce to

$$H(\zeta)\frac{\partial c}{\partial\zeta}-\frac{1}{\mathrm{Sc}}\frac{\partial^2 c}{\partial\zeta^2}=0, \qquad c(0,\hat{t})=1, \qquad \lim_{\zeta\to\infty}c(\zeta,\hat{t})=-\gamma_1\hat{S}(\hat{t}), \quad (5.31)$$

$$\mathrm{St}\,\frac{\mathrm{d}\hat{S}}{\mathrm{d}\hat{t}}=\frac{\partial c}{\partial\zeta}(0,\hat{t}), \qquad \hat{S}(0)=0, \qquad \gamma_1=\frac{K_2^c K_{\mathrm{P}} c_s}{K_{\mathrm{sp}}[\mathsf{H}^+]_\infty^2}\left(\frac{\nu}{\omega}\right)^{1/2}\frac{R_d^2}{R_v^2 H_v}. \quad (5.32)$$

This is obtained by collecting (5.1), (5.9) with (3.56), (5.11), and (5.16). Using Table 4.1, and estimates (4.21)–(4.23), we have

$$\gamma_1 \simeq 1.907, \qquad \mathrm{Sc} \simeq 474, \qquad \mathrm{St} \simeq 5415. \tag{5.33}$$

5.3 Quasi-Steady Solution

The reduced quasi-steady problem has a closed form solution that is reminiscent of the solution of Levich [23]. Solving first for $c(\zeta, \hat{t})$,

$$c(\zeta, \hat{t}) = 1 + \left(\frac{\partial c}{\partial \zeta}(0, \hat{t})\right) \int_0^{\zeta} \exp\left(\int_0^{s_2} \mathrm{Sc}\, H(s_1)\, \mathrm{d}s_1\right) \mathrm{d}s_2. \tag{5.34}$$

Letting $\zeta \to \infty$ gives the condition

$$\frac{\partial c}{\partial \zeta}(0, \hat{t}) = -\left(1 + \gamma_1 S(\hat{t})\right) \underbrace{\left(\int_0^{\infty} \exp\left(\int_0^{s_2} \mathrm{Sc}\, H(s_1)\, \mathrm{d}s_1\right) \mathrm{d}s_2\right)^{-1}}_{\gamma_2}, \tag{5.35}$$

with $\gamma_2 \simeq 4.646708$ for $\mathrm{Sc} \simeq 474$. This reduces the Stefan condition to

$$\frac{\mathrm{d}\hat{S}}{\mathrm{d}\hat{t}} = -\frac{\gamma_2}{\mathrm{St}}\left(1 + \gamma_1 \hat{S}(\hat{t})\right), \qquad \hat{S}(0) = 0, \tag{5.36}$$

with solution

$$\hat{S}(\hat{t}) = \frac{1}{\gamma_1}\left(\mathrm{e}^{-\gamma_1 \gamma_2 \hat{t}/\,\mathrm{St}} - 1\right) \tag{5.37}$$

so that $\lim_{\hat{t}\to\infty} \hat{S}(\hat{t}) = -\gamma_1^{-1}$ corresponding to $\lim_{\hat{t}\to\infty} c(\zeta\hat{t}) = 1$ for any $\hat{t}$. For expression (5.37, it is important to realize that $\hat{t} \sim \mathcal{O}(\mathrm{St})$.[1]

[1] Based on the experiments in [34], an experiment of $t = 1000$ minutes, with a rotation rate of $\omega = 100$ rpm, and $\mathrm{Sc} \simeq 474$, we find that $\hat{t} = \omega t/\,\mathrm{Sc} \simeq 10^3 \sim \mathcal{O}(\mathrm{St})$.

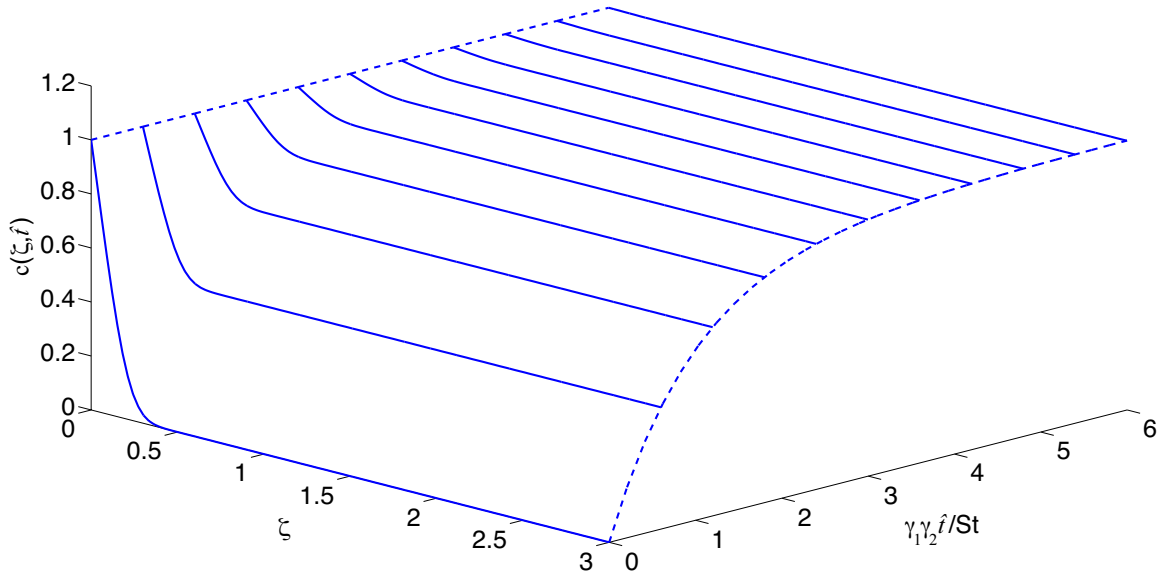

Figure 5.1: The time evolution of the scaled concentration of calcium $c(\zeta, \hat{t})$ for the quasi-steady case.

Putting all these pieces together gives the concentration profile

$$c(\zeta, \hat{t}) = 1 - \mathrm{e}^{-\gamma_1\gamma_2\hat{t}/\,\mathrm{St}} \frac{\displaystyle\int_0^{\zeta} \exp\left(\int_0^{s_2} \mathrm{Sc}\, H(s_1)\, \mathrm{d}s_1\right) \mathrm{d}s_2}{\displaystyle\int_0^{\infty} \exp\left(\int_0^{s_2} \mathrm{Sc}\, H(s_1)\, \mathrm{d}s_1\right) \mathrm{d}s_2}. \tag{5.38}$$

Far away from the dissolving interface, With $\zeta \to \infty$,

$$c_\infty(\hat{t}) = \lim_{\zeta\to\infty} c(\zeta, \hat{t}) = 1 - \mathrm{e}^{-\gamma_1\gamma_2\hat{t}/\,\mathrm{St}} \tag{5.39}$$

defines the calcium concentration in the bulk. Beyond the boundary layer, the concentrations do approach their limiting values for a homogeneous, well mixed solution. A plot of the time evolution of the scaled calcium concentration is shown in Figure 5.1. Note that the boundary layer structure disappears as the calcium reaches its saturation limit.

The behaviour of c_∞ gives some insight into the rate of dissolution of the calcite

at the dissolving interface. In particular, we see that from (5.38),

$$\frac{\partial c}{\partial t} = \frac{\gamma_1\gamma_2}{\mathrm{St}}\mathrm{e}^{-\gamma_1\gamma_2\hat{t}/\,\mathrm{St}}\frac{\displaystyle\int_0^{\zeta}\exp\left(\int_0^{s_2}\mathrm{Sc}\,H(s_1)\;\mathrm{d}s_1\right)\mathrm{d}s_2}{\displaystyle\int_0^{\infty}\exp\left(\int_0^{s_2}\mathrm{Sc}\,H(s_1)\;\mathrm{d}s_1\right)\mathrm{d}s_2} \tag{5.40}$$

and that taking the spatial derivative,

$$\frac{\partial c}{\partial \zeta} = -\mathrm{e}^{-\gamma_1\gamma_2\hat{t}/\,\mathrm{St}}\frac{\displaystyle\exp\left(\int_0^{\zeta}\mathrm{Sc}\,H(s_1)\;\mathrm{d}s_1\right)}{\displaystyle\int_0^{\infty}\exp\left(\int_0^{s_2}\mathrm{Sc}\,H(s_1)\;\mathrm{d}s_1\right)\mathrm{d}s_2}. \tag{5.41}$$

With respect to the dimensionless quantities,

$$-\frac{1}{\mathrm{St}}\frac{\partial c}{\partial \zeta}(0,\hat{t}) = \frac{\gamma_2}{\mathrm{St}}\mathrm{e}^{-\gamma_1\gamma_2\hat{t}/\,\mathrm{St}} = \frac{1}{\gamma_1}\frac{\mathrm{d}c_\infty}{\mathrm{d}\hat{t}}(\hat{t}). \tag{5.42}$$

Therefore, the flux of material at the dissolving interface is a constant multiple of the time rate of change of the concentration far from the interface. Returning to dimensional coordinates, equation (5.42) becomes

$$J = -D\frac{\partial[\mathsf{Ca}^{2+}]}{\partial z}(0,t) = \frac{c_s - [\mathsf{Ca}^{2+}]_{\max}}{c_s}\left(\frac{R_v}{R_s}\right)^2 H_v \lim_{z\to\infty}\frac{\mathrm{d}[\mathsf{Ca}^{2+}]}{\mathrm{d}t}(z,t). \tag{5.43}$$

Expression (5.41) leads to a new dimensional expression for the flux of

$$J = D\nu^{-1/2}\omega^{1/2}\gamma_2[\mathsf{Ca}^{2+}]_{\max}\exp\left(-\frac{\gamma_1\gamma_2}{\mathrm{St}\,\mathrm{Sc}}\omega t\right), \tag{5.44}$$

which can be compared to either (1.1), or its correction (1.2). The γ_2 factor is a dimensional version of (5.35), with an approximation given by (2.25). It is this term that is responsible for the correction in (1.2). Levich introduced a generic concentration factor, and by including the actual chemistry in this process of dissolution, we see that it should be replaced by $[\mathsf{Ca}^{2+}]_{\max}$. This means that the initial rate of

dissolution is governed by the chemical environment that determines $[\mathsf{Ca}^{2+}]_{\max}$. Finally, there is an exponential behaviour that reduces the overall flux as the dissolution process reaches saturation. There is a natural time scale over which the flux is essentially in steady state. This condition is

$$t \ll \frac{\mathrm{Sc}\,\mathrm{St}}{\omega\gamma_1\gamma_2} \sim D^{-2/3}\nu^{1/6}\omega^{-1/2}\left(1-\frac{[\mathsf{Ca}^{2+}]_{\max}}{c_s}\right)\left(\frac{R_v}{R_d}\right)^2 H_v \sim 10^5\ \mathsf{s} \tag{5.45}$$

using the parameters for the RDA experiment. After this point, the flux begins to slow due to the build up of the dissolving material in the bulk.

At the beginning of this work, the question was posed as to why there is so much variation seen from one laboratory to the next. The dependence on $[\mathsf{Ca}^{2+}]_{\max}$ suggests that a possible explanation is due to the different chemical environments. Another possibility is the violation of laminar flow which would modify the dissolution rate. These effects need to be validated through a new set of experiments. Another point of clarification is provided by comparing (5.44) and (5.45). The factor γ_1, which contains the geometric effects, only plays a role in the time scale where the flux begins to decrease due to chemical saturation of the environment.

Now that we developed an expression for predicting the calcium profile and rate of dissolution, it should be validated by experimental data. It would not be possible to validate the chemical boundary layer structure at the dissolution surface because of the experimental limitations. The boundary layer is too thin for such experiments, so the existing data applies to the concentrations in the bulk of the solution.

CHAPTER 6

Model Validation

Having developed this model, it can be validated by returning to the original experiments that lead to the development of the PWP model. The first of these is the 1976 work of Plummer and Wigley [34] where they study the dissolution of calcite in a saturated CO_2(g) atmosphere of 0.97 atm at standard temperature with $[Cl^-] = 0$. The second set of experimental data comes from the seminal work of Plummer, Wigley, and Parkhurt [35], where the kinetics of calcite dissolution was studied over a wider temperature and pressure range. This extensive work, consisting of over one hundered separate experimental runs, resulted in the development of the contemporary PWP model, named after its founders. Each experiment was conducted with fixed value of P_{CO_2}, anywhere from 0 to 1 atm, and a fixed temperature that could lie in the range of $5°C$ to $60°C$, and a variety of acidic environments ($[Cl^-] \neq 0$).

6.1 Plummer and Wigley, 1976

The experimental data list of [34], and reproduced in Appendix D, is obtained by first bubbling $CO_2(g)$ through distilled water until equilibrium is established. A weight of calcite (5 to 20 times in excess of the solubility limit) is added to the continuously stirred solution. During this process the pH is measured as a function of time. The dissolution rate changes from one experiment to the next. The reason for this is that for each run, the amount and average size of the calcite particles varies, which changes the effective surface area from one experiment to the next. To compare the results of these experiments with this thesis, the calcium concentration takes on the form of (5.38) where the samples are taken far away from any dissolving boundary, so $\zeta \to \infty$. This means that the dimensionless version of the calcium concentration, as a function of time, is taken as

$$c_\infty(t) = 1 - \mathrm{e}^{-\lambda t} \tag{6.1}$$

where $\lambda > 0$ is a single fitting parameter. This exponential behaviour is ubiquitous throughout the physical chemistry literature, where it is known as the Kolmogorov-Avrami model, and may be found in any standard reference book [43]. Recall that this functional dependence of c_∞ comes about as a direct result of the consistency of applying mass conservation to the dissolving interface (5.39), and assuming that this interface motion does not affect the hydrodynamics. The value of λ encapsulates the Stefan number, the rates of reaction, and the hydrodynamics. The dissolution rate at the dissolving surface was shown in the previous chapter to be proportional to the time rate of change of c_∞. For this reason, we prescribe that the modelling rate of dissolution be given as

$$J_{\mathrm{mod}}(t) = \frac{\mathrm{d}c_\infty}{\mathrm{d}t} = \lambda \mathrm{e}^{-\lambda t}, \tag{6.2}$$

where the proportionality constant is taken as one.

To choose λ, the pH corresponding to c_∞ given by (4.48) is computed and compared to the experimental data in the sense of $\ell^2(\mathbb{R}^N)$ for N data points. In particular, we find

$$\lambda = \arg\min_{\alpha>0} \| \mathrm{pH}_{\text{mod}} - \mathrm{pH}_{\text{obs}} \|_{\ell^2(\mathbb{R}^N)} \tag{6.3}$$

where α enters through $c_\infty(t) = 1 - \mathrm{e}^{-\alpha t}$, $\mathrm{pH}_{\text{mod}} = -\log_{10} h_\infty$, and h_∞ satisfies equation (5.22), repeated here for convenience

$$h_\infty^3 + \left(\frac{2K_{\text{sp}}[\mathsf{H}^+]_\infty^2}{K_2^c K_{\text{P}}[\mathsf{H}^+]_0} c_\infty - \frac{[\mathsf{Cl}^-]}{[\mathsf{H}^+]_0} \right) h_\infty^2 - (K_{\text{W}}^c + K_{\text{P}}) \frac{h_\infty}{[\mathsf{H}^+]_0^2} - \frac{2K_2^c K_{\text{P}}}{[\mathsf{H}^+]_0^3} = 0. \tag{6.4}$$

The experiments are broken into two series. Runs 7–11, and runs 12–14, corresponding to the two different samples of Icelandic spar as a source of the calcite. The authors in [34] note that the rock sample used in runs 12–14 was not as transparent as the sample used in runs 7–11. No further detail is provided. Table 6.1 lists the optimal value of λ for each of the experimental runs and the corresponding minimal relative percent error, while Figures 6.1 and 6.2 show the corresponding optimal fits to the data points.

Being able to effectively fit to this data, as evidenced in Table 6.1, establishes that the Stefan model in a closed system is capable of reproducing the time evolution of the dissolution process using only the bulk chemistry. It also illustrates that this new model can provide insight into the chemical environment at the interface, and information on how the environment changes in a closed system as it nears saturation.

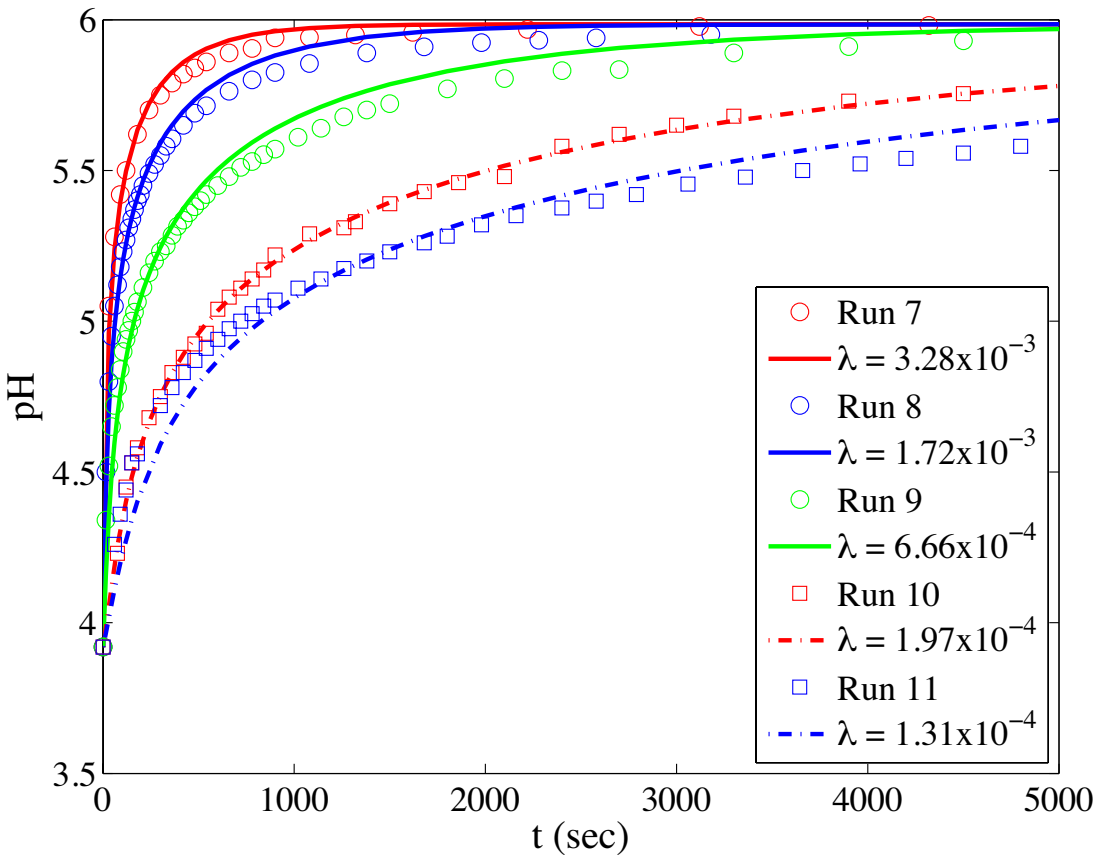

Figure 6.1: Runs 7–11 of [34] compared to the current model. The markers denote the experimental data points and the lines correspond to the model predictions.

6.2 The PWP Model

The work in [35] develops the PWP model, which we describe next, so that its predictions can be compared to the new model. The PWP model presumes that the net rate of calcite dissolution, denoted as J_{PWP}, depends on three forward rates, and one backward reaction. The specific form proposed in [35] is

$$J_{\text{PWP}} = \kappa_1[H^+] + \kappa_2([H_2CO_3{}^0] + [CO_2]) + \kappa_3[H_2O] - \kappa_4[Ca^{2+}][HCO_3^-]. \tag{6.5}$$

This model has been extended to larger pressure and temperature ranges but has not changed significantly since its introduction. The dependence of all four con-

Table 6.1: Relative percent error in the comparison of [34] with the current model.

Run	λ	$100\frac{\|\,\mathrm{pH}_{\mathrm{mod}}-\mathrm{pH}_{\mathrm{obs}}\,\|}{\|\,\mathrm{pH}_{\mathrm{obs}}\,\|}$	Run	λ	$100\frac{\|\,\mathrm{pH}_{\mathrm{mod}}-\mathrm{pH}_{\mathrm{obs}}\,\|}{\|\,\mathrm{pH}_{\mathrm{obs}}\,\|}$
7	3.28×10^{-3}	0.578%	12	7.98×10^{-5}	0.475%
8	1.72×10^{-3}	0.816%	13	4.02×10^{-5}	1.26%
9	6.66×10^{-4}	1.22%	14	1.14×10^{-4}	0.849%
10	1.97×10^{-4}	0.788%			
11	1.31×10^{-4}	1.61%			

stants was estimated in [35] using statistical methods from over a set of one hundred separate experiments. For example, the value of κ_1 is obtained from the slope of a plot of the dissolution rate versus the activity of H^+ in solutions that are far from equilibrium (low pH). The experimentally inspired expression (6.5) can be interpreted as a set of surface reactions of $CaCO_3(s)$ that depends on the acidity. In detail, the respective processes are with a strong acid

$$CaCO_3(s) + H^+ \xrightarrow{\kappa_1} Ca^{2+} + HCO_3^-, \tag{6.6}$$

a weak acid

$$CaCO_3(s) + {H_2CO_3}^0 \xrightarrow{\kappa_2} Ca^{2+} + 2HCO_3^-, \tag{6.7}$$

and water

$$CaCO_3(s) + H_2O \underset{\kappa_4}{\overset{\kappa_3}{\rightleftharpoons}} Ca^{2+} + HCO_3^- + OH^-. \tag{6.8}$$

The backward reaction, governed by κ_4, is proposed to be the result of Ca^{2+} and HCO_3^- ions interacting with the surface. The rates given by κ_1, κ_2, κ_3, and κ_4 all depend on the temperature, and this behaviour, as presented in [35], is given by

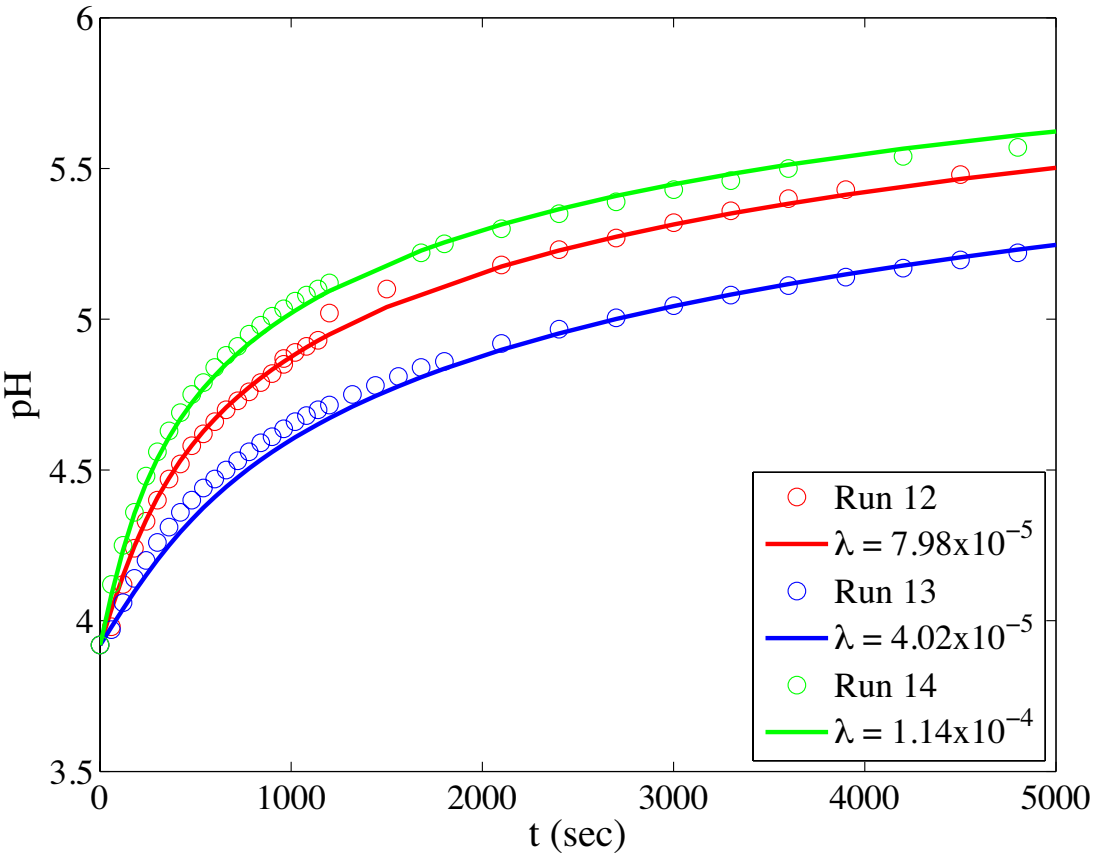

Figure 6.2: Runs 12–14 of [34] compared to the current model. The markers denote the experimental data points and the lines correspond to the model predictions.

the Arrhenius relationships

$$\kappa_1 = A_{\kappa_1} \mathrm{e}^{-E_1/T}, \quad \kappa_2 = A_{\kappa_2} \mathrm{e}^{-E_2/T}, \quad \kappa_3 = \begin{cases} A_{\kappa_{3a}} \mathrm{e}^{-E_{3a}/T}, & 278 \leq T \leq 298, \\ A_{\kappa_{3b}} \mathrm{e}^{-E_{3b}/T}, & 298 \leq T \leq 321, \end{cases} \tag{6.9}$$

with $A_{\kappa_1} = 1.58$, $E_1 = 1022$, $A_{\kappa_2} = 692$, $E_2 = 5013$, $A_{\kappa_{3a}} = 1.38 \times 10^{-6}$, $E_{3a} = 730$, $A_{\kappa_{3b}} = 7.93 \times 10^{-2}$, $E_{3b} = 4000$ from [35]. Only κ_4 is affected by changes in the partial pressure of CO_2(g).

Rather than comparing the new model with the predictions given by J_{PWP}, we fit to the original experimental results. Tables E.1 and E.2 of Appendix E list a sub-collection of experimental results for a variety of pressures and temperatures re-

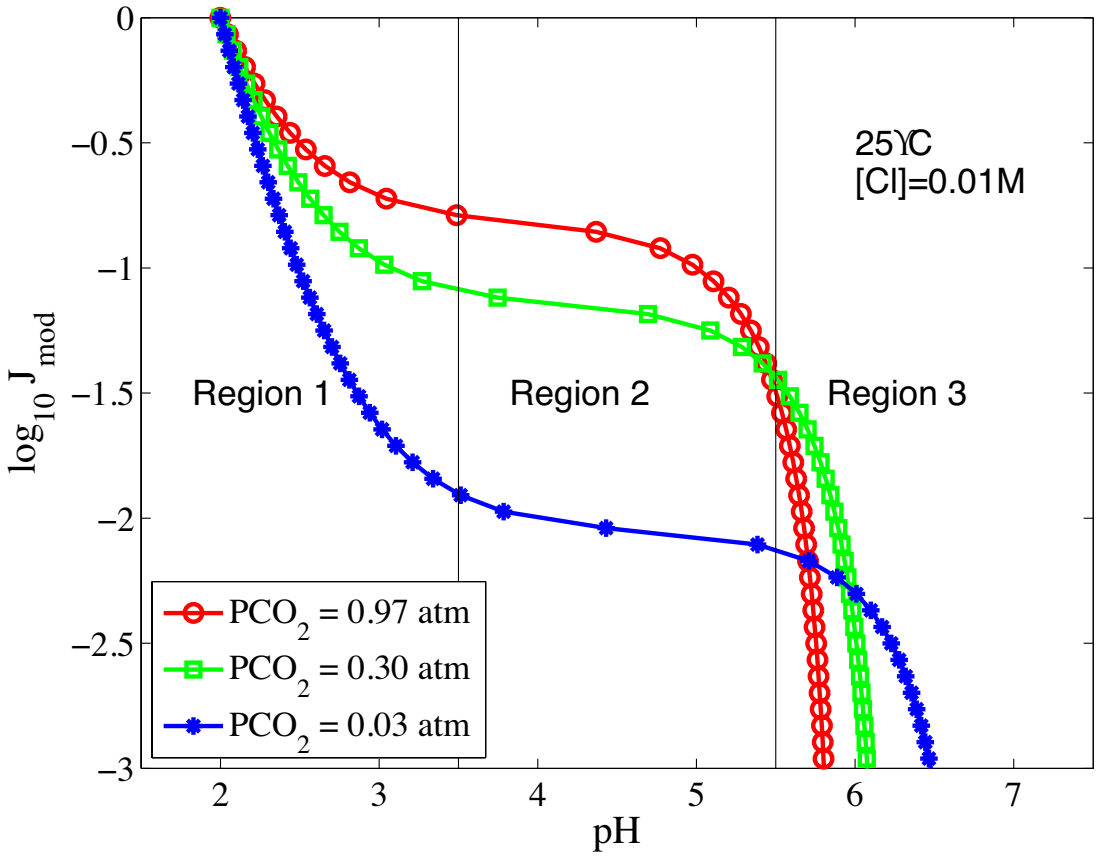

Figure 6.3: Logarithm of the rate of calcite dissolution, J_{mod} with $\lambda = 1$, as a function of pH for a variety of partial pressures of $CO_2(g)$. The initial $\mathrm{pH} = 2$ is set with $[Cl^-] = 0.01$ M. This plot has comparable features to Figure 1 of [35].

produced from [35]. This data will be used to validate the new model.

In developing the PWP equation, three separate regions were identified. These same region are indicated in Figure 6.3 which shows the model prediction for $25°C$ and $[Cl^-] = 0.01$, extended to the full pH range. The trends are the same as indicated in Figure 1 of [35], with the change in inflection confined to region 3. One difference between the model behaviour and the experimental data is that the predictive curves separate at high acidity. This is a result of the high concentration of Cl^- and artificially setting the activity coefficient to one for all pH levels. It is in the region of low pH where the pH dependence of the activity coefficient dominates. The current model assumes that the activity coefficient is always one, and this assumption will

modify the resulting curves within the highly acidic region.

6.3 Plummer, Wigley, and Parkhurt, 1978

In their 1978 paper, Plummer, Wigley, and Parkhurt used both 'pH-stat' and 'free-drift' methods to estimate the dissolution rate of the calcite for a variety of temperatures and pressures of CO_2(g). In the pH-stat method, a standardized HCl solution is added so as to maintain a constant specified pH in solution at fixed P_{CO_2} and temperature. For every mole of CO_3^{2-} that is released by the calcite, two moles of H^+ are consumed. As a result, the rate of calcite dissolution is one-half the rate of the H^+ addition in a pH-stat experiment. This assumes both the P_{CO_2} and temperature are fixed. This particular method was found to be effective when the system is far from equilibrium. For comparison, Figure 6.4 shows the logarithm of the dissolution rate J_{PWP}, as given by (6.5), where it is assumed that $\kappa_4 = 0$. The plot was generated using experimental runs 63, 77, 89, 92, and 100 in Table E.1.

For the situation when the reaction is in the vicinity of equilibrium, the pH is measured as a function of time without the addition of HCl as in [34]. Using this technique, known as 'free-drift', the pH and P_{CO_2} determine the composition of the bulk solution, and from this information, the dissolution rate of the calcite is inferred. Figure 6.5 shows a selection of 'free-drift' runs from Table E.2 reproduced from [35]. The behaviour in the higher pH environment is similar to that predicted by the new model, with the end point determined by P_{CO_2}. For lower pH there is a discrepancy that may be due to the activity coefficients being set to one.

6.4 Stefan Model Predictions

Figure 6.6 illustrates the model prediction by assuming $c_\infty(t)$ is given by (6.1). To specify λ, the knee of the blue curve $(25°\text{C}, 0.956\ \text{atm})$ is matched. This gives a value

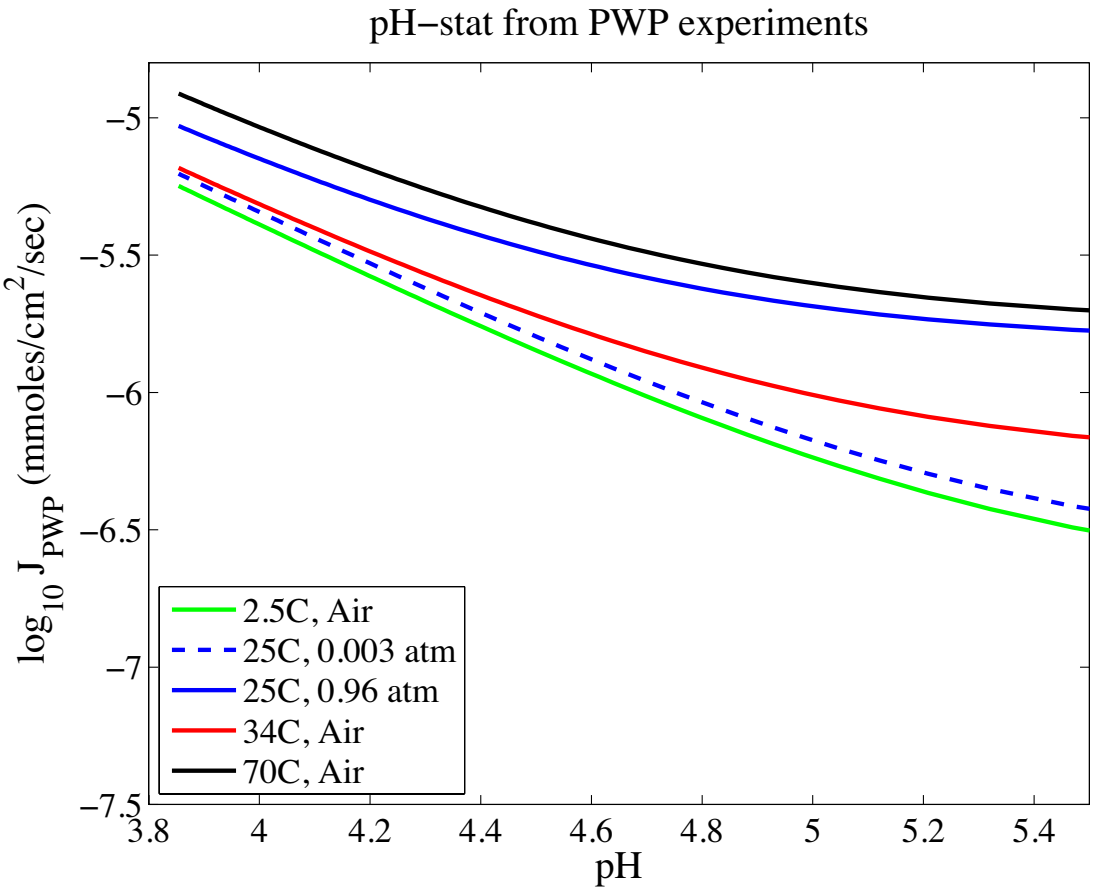

Figure 6.4: Logarithm of the rate of calcite dissolution, J_{PWP}, as given by (6.5), with $\kappa_4 = 0$, as a function of pH for a variety of partial pressure of CO_2(g) and temperatures. This corresponds to experimental runs 63, 77, 89, 92, and 100 of Table E.1.

of $\lambda = 2.415 \times 10^{-4}$. The temperatures and pressures are chosen to be consistent with Figure 6.4, and the value of λ is chosen to match the dissolution rate of experimental run 38 ($25°$C, $P_{CO_2} = 0.96$ atm). The experimental runs are in reasonable agreement, indicating that using the Stefan condition, the model correctly predicts the experimental dissolution rate as a function of P_{CO_2} for standard temperature, and for temperatures below $25°$C.

One of the difficulties in comparing the current model with the PWP predictions, given by (6.5), is that without the addition of HCl or another reagent, the P_{CO_2} level places a restriction on the pH range. For the utilized experimental runs, Table 6.2 shows the corresponding pH range.

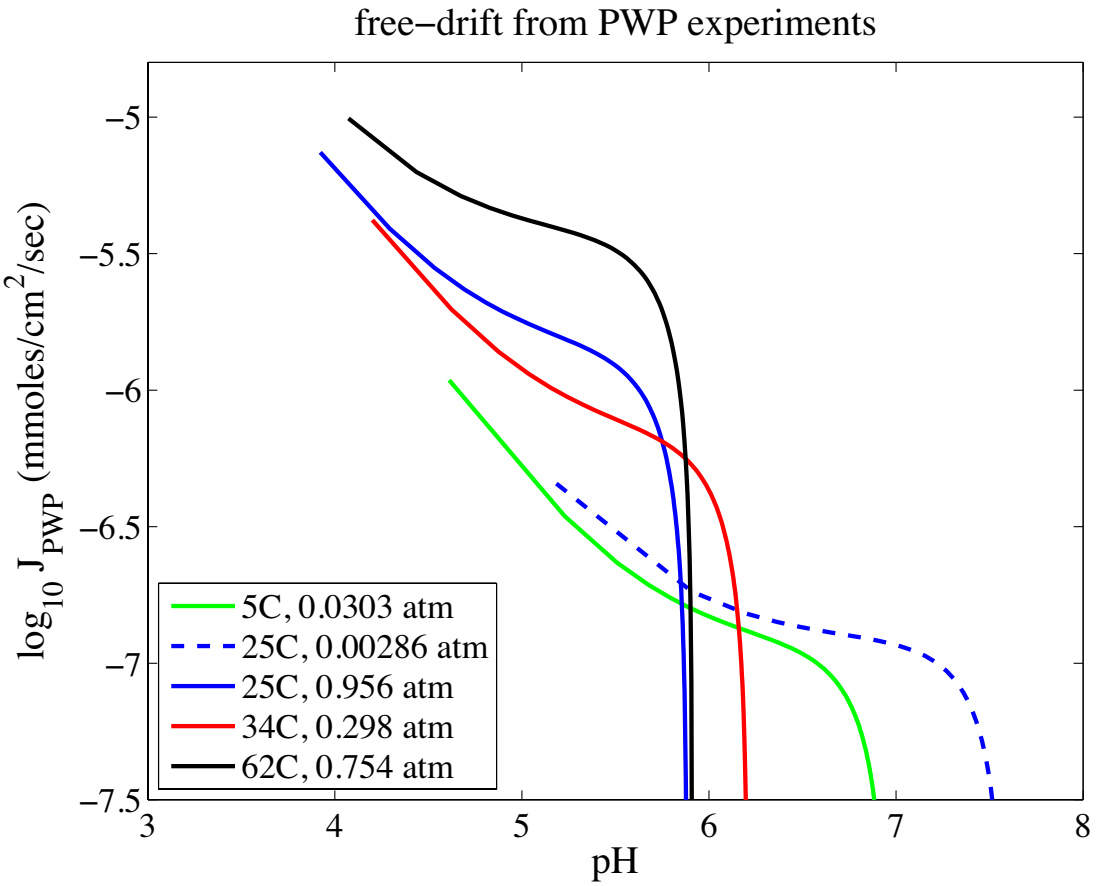

Figure 6.5: Logarithm of the rate of calcite dissolution, J_{PWP}, given by the free-drift method as a function of pH for a variety of partial pressure of CO_2(g) and temperatures. This corresponds to experimental runs 14, 29, 32, 38, and B7 of Table E.2.

Table 6.2: pH range of the experimental runs without the addition of HCl.

Run No.	Temp. (°C)	Pressure (atm)	Lower $-\log_{10}[H^+]_0$	Upper $-\log_{10}[H^+]_\infty$
29	5.0	3.03×10^{-2}	4.611	6.985
14	25	2.86×10^{-3}	5.184	7.672
38	25	9.57×10^{-1}	3.922	5.989
32	34	2.98×10^{-1}	4.200	6.337
B7	62	7.54×10^{-1}	4.072	6.127

Another way to compare the new model predictions with J_{PWP} is to compare the maximum amount of dissolved calcium. The experimental results of [35] include this value for a number of the experimental runs. This prediction is listed

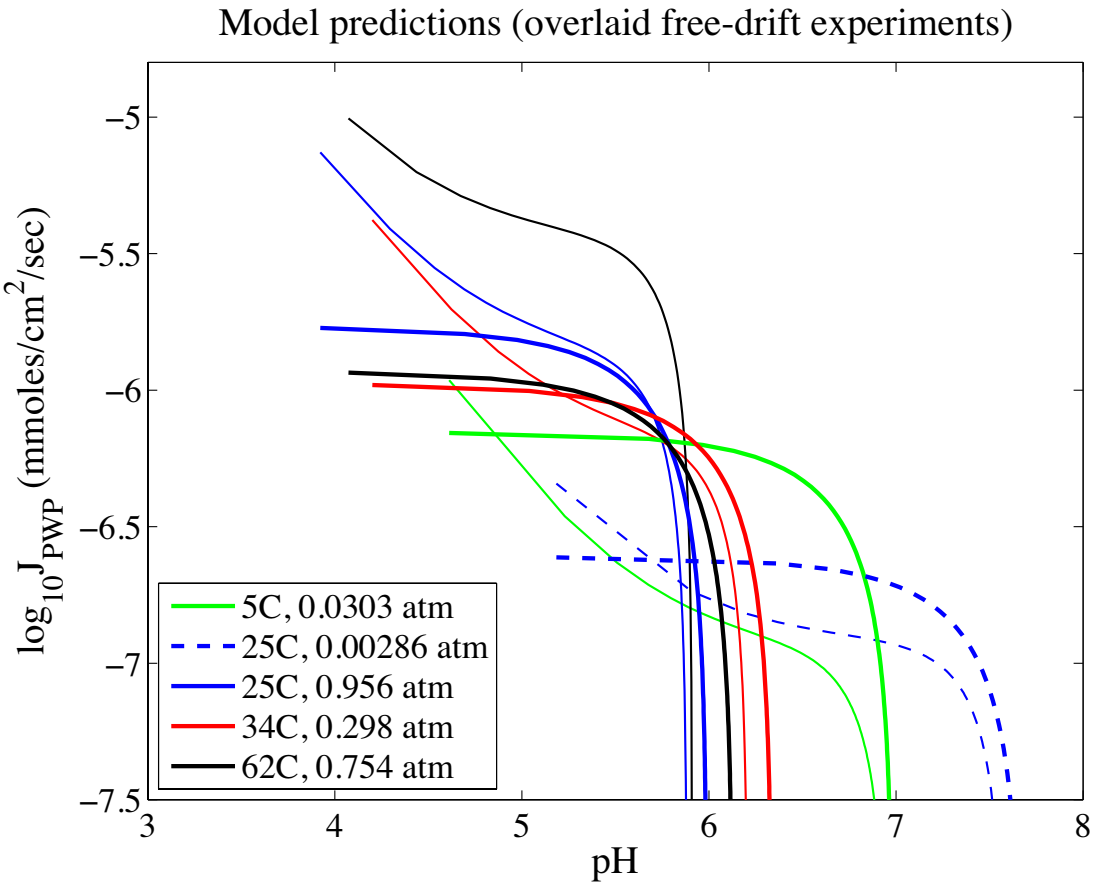

Figure 6.6: Logarithm of the rate of calcite dissolution given by the model prediction, J_{mod} (6.2), as a function of pH for a variety of partial pressure of CO_2(g) and temperatures. The choices are consistent with Figure 6.5.

alongside the predictions of the new Stefan model in Table 6.3. For each of experimental runs, Table E.2 lists the temperature and $P_{\text{CO}_2(\text{g})}$. From these parameters the values of $[\text{H}^+]_0$ and $[\text{H}^+]_\infty$ dictate the range in pH for that experiment and $\text{pH}_\infty = -\log_{10}[\text{H}^+]_\infty$ is compared to the observed end run value of pH_{obs}. The maximum amount of calcium that can be dissolved into a given solution is related to $[\text{H}^+]_\infty$ through the relationship

$$[\text{Ca}^{2+}]_{\max} = \frac{K_{\text{sp}}[\text{H}^+]_\infty^2}{K_2^c K_{\text{P}}} \simeq \left(\frac{K_{\text{sp}} K_{\text{P}}}{4K_2^c}\right)^{1/3}, \tag{6.10}$$

assuming $[\text{Cl}^-] = 0$. Figure 6.7 illustrates the comparison between $[\text{Ca}^{2+}]_{\max}$ and

Table 6.3: End of run values for pH and total calcium dissolved. Portions of this table are reproduced from Table 6 of [35]. For the purposes of this table, $\mathrm{pH}_0 = -\log_{10}[\mathrm{H}^+]_0$, $\mathrm{pH}_\infty = -\log_{10}[\mathrm{H}^+]_\infty$, $|\Delta\,\mathrm{pH}| = |\,\mathrm{pH}_\infty - \mathrm{pH}_{\mathrm{obs}}\,|$, and $|\Delta[\mathrm{Ca}^{2+}]| = |[\mathrm{Ca}^{2+}]_{\max} - [\mathrm{Ca}^{2+}]_{\mathrm{obs}}|$. $[\mathrm{Ca}^{2+}]_{\max}$ is determined using $K_{\mathrm{sp}} = 4.47 \times 10^{-9}\ \mathrm{M}^2$.

Run no.	pH_0	pH_∞	$\mathrm{pH}_{\mathrm{obs}}$	$\lvert\Delta\,\mathrm{pH}\rvert$	$[\mathrm{Ca}^{2+}]_{\max}$ (mmol/L)	$[\mathrm{Ca}^{2+}]_{\mathrm{obs}}$ (mmol/L)	$\lvert\Delta[\mathrm{Ca}^{2+}]\rvert$ (mmol/L)
29	4.611	6.984	6.952	0.032	2.89	2.62	0.27
27	4.125	6.336	6.333	0.003	6.09	6.56	0.47
5	3.861	5.984	6.041	0.057	9.12	11.13	2.01
3	3.859	5.981	6.059	0.078	9.15	11.28	2.13
6	3.859	5.980	6.066	0.086	9.16	12.08	2.92
4	3.858	5.979	6.028	0.049	9.18	11.48	2.30
26	5.152	7.662	7.714	0.052	1.15	1.34	0.19
21	4.645	6.987	6.942	0.045	2.49	2.56	0.07
19	4.159	6.339	6.243	0.096	5.24	5.44	0.20
8	3.890	5.981	6.029	0.048	7.92	10.53	2.61
9	3.888	5.977	6.030	0.053	7.95	10.18	2.23
17	5.189	7.678	7.644	0.034	1.00	1.17	0.17
14	5.184	7.672	7.623	0.049	1.01	1.13	0.12
13	4.677	6.997	6.976	0.021	2.19	2.45	0.26
16	4.677	6.997	6.951	0.046	2.19	2.57	0.38
12	4.191	6.348	6.312	0.036	4.63	5.39	0.76
10	3.922	5.990	6.017	0.027	6.99	9.18	2.19
B2	3.932	5.995	5.979	0.016	6.78	8.60	1.82
31	4.705	7.010	6.964	0.046	1.99	2.02	0.03
32	4.200	6.337	6.260	0.077	4.32	4.52	0.20
30	3.949	6.003	5.959	0.044	6.35	7.34	0.99
B4	3.956	6.010	5.986	0.024	6.26	7.70	1.44
36	4.756	7.052	6.998	0.054	1.74	1.56	0.18
35	4.250	6.379	6.297	0.082	3.77	3.58	0.19
37	4.001	6.047	5.999	0.048	5.53	5.52	0.01
B5	4.009	6.056	6.021	0.035	5.45	5.40	0.05
B8	4.077	6.133	6.047	0.086	4.76	4.00	0.76

$[\mathrm{Ca}^{2+}]_{\mathrm{obs}}$ and shows a remarkable agreement for low solubility. For larger solubility, the new model underestimates $[\mathrm{Ca}^{2+}]_{\max}$, which indicates either an inaccuracy in K_{sp} or a breakdown in the validity of expression (6.10).

Ideally, the temperature dependence of K_{sp} should be inferred from the literature, but this is not readily available. Instead, an approximation of just the temperature dependence of K_{sp} can be estimated by the data itself. Inverting (6.10) gives

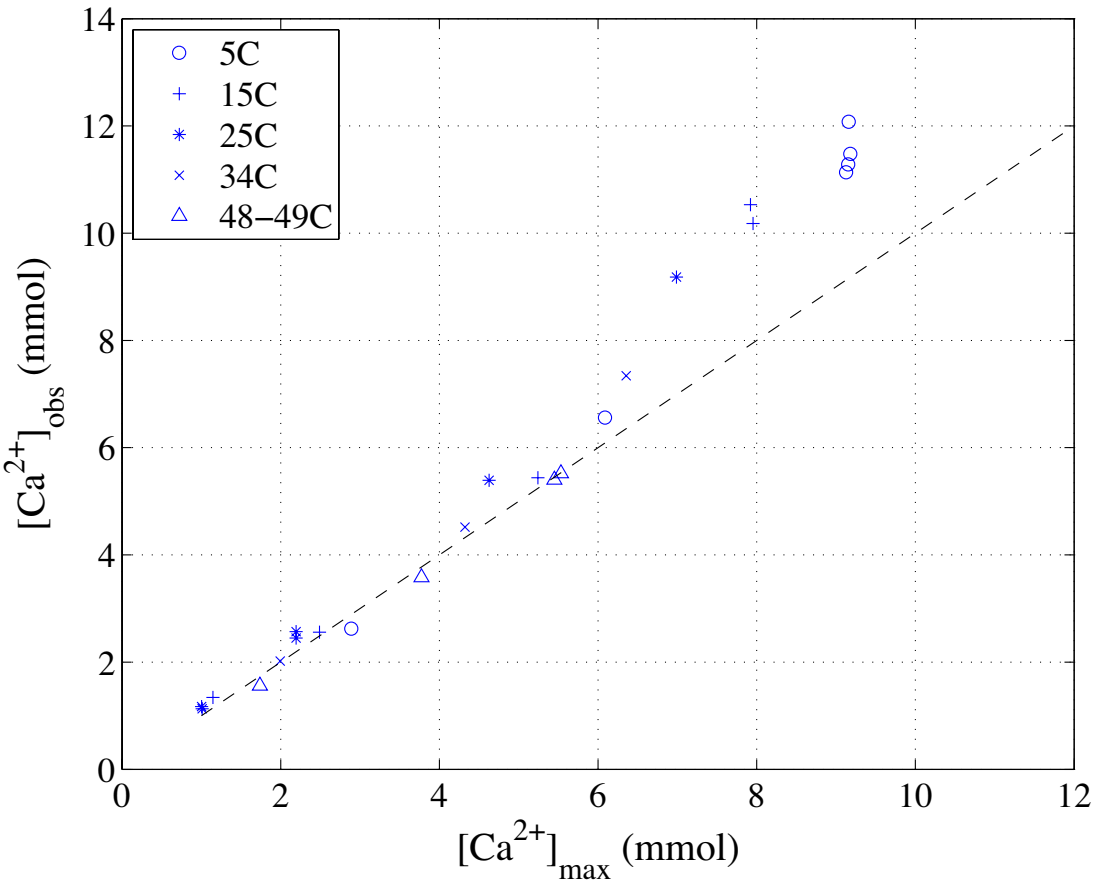

Figure 6.7: Predicted versus observed $[\mathsf{Ca}^{2+}]$ solubility using $K_{\text{sp}} = 4.47 \times 10^{-9}\ \mathsf{M}^2$. There is a noticeable discrepancy for lower temperatures.

the estimate

$$K_{\text{sp}} \simeq \frac{4K_2^c[\mathsf{Ca}^{2+}]_{\text{obs}}^3}{K_{\text{P}}}, \tag{6.11}$$

and from these values an Arrhenius relationship is assumed. Fitting the data to this assumed K_{sp} temperature behaviour and minimizing the ℓ^2 error results in the expression

$$K_{\text{sp}}(T) = A_{\text{sp}}\mathrm{e}^{E_{\text{sp}}/T}, \qquad A_{\text{sp}} = 1.097 \times 10^{-10}, \qquad E_{\text{sp}} = 1199. \tag{6.12}$$

The corrected predictions can be seen in Figure 6.8. With the proposed temperature

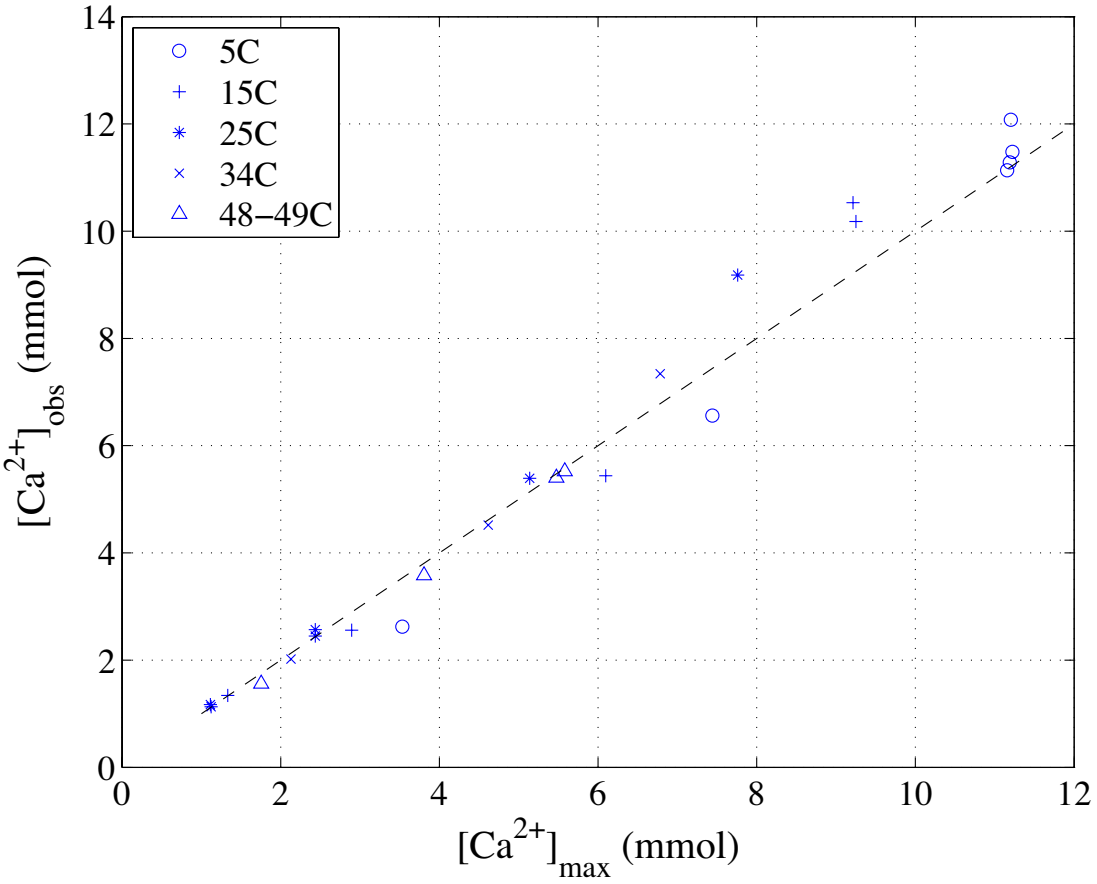

Figure 6.8: Predicted versus observed $[Ca^{2+}]$ solubility using K_{sp} given by expression (6.11). The discrepancy at lower temperatures is reduced.

dependence of K_{sp}, the new Stefan model is capable of reproducing the observed maximum dissolved calcium.

This chapter has illustrated that the Stefan model is capable of reproducing the observed dissolution rate of calcite across a wide range of temperatures and pressures. The difference in the chemical environment at the dissolution interface and far from the interface drives the rate of dissolution. This naturally gives rise to three separate regions of pH corresponding to $[H^+]_0$ where no appreciable amount of calcium has been dissolved, a rapid transition range, and an end of run value of $[H^+]_\infty$ as the solution becomes saturated. The final chapter will recap the results of this new model of dissolution for the calcium carbonate system and the work that still needs to be done.

CHAPTER 7

Conclusions and Future Work

The experimental investigation of calcite dissolution has a long history over the last century with interest across a wide range of scientific disciplines [6, 8, 12, 16, 18, 22, 27, 31, 37]. Much of this research was the result of the exploration and mapping of karst landscapes, and the bodies of natural waters contained within them. When studying natural waters, it was noticed that many carbonate reservoirs were undersaturated with respect to calcite [34]. These observations led to the development the PWP expression which was determined through a systematic set of experiments at a variety of temperatures, pressures, and acidity levels [35].

The thesis begins with a discussion of the origins of the problem of calcite dissolution. The pertinent question is why are the simplified classical expressions of mass flux, given by (1.1), inconsistent from one experimental study to the next? Why is the correction given by (1.2) insufficient? To begin answering these questions, a derivation of the classical Levich problem appears in Chapter 2. This work reveals that a number of assumptions are required to reach the Levich expression, including the need for a uniform dissolving surface, and the need for a laminar fluid

flow over this surface. These assumptions are typically violated with the economic pressure to provide results quickly. Another shortcoming of the classical Levich problem is that it disregards the actual chemical reactions involved in the dissolution in favour of a generic behaviour. This last point becomes particularly important for dissolution in highly acidic chemical environments. Chapter 2 also points out the equivalency between the rotating disc reaction vessel and the rotating disc electrode method of electrochemistry with expression (2.31).

Part of the derivation of Chapter 2 includes an analysis of the von Kármán equations. Because of the need to solve these equations on a finite domain, an expansion of the solution about infinity was computed. This high-order asymptotic expansion is consistent, and exceeds the current literature on this topic. In addition, a high-order expansion at the dissolving interface was also computed. The details of these expansions are compared to the numerical solutions in Appendix A. This material, although exceeding the current literature, did not significantly contribute to the dissolution problem, and was collected in the Appendix.

Chapter 3 examines the carbonate system with the presence of dissolving calcite, and the possible addition of HCl to change the pH level. It is shown that there are always two extreme points of chemical equilibrium. When no calcium is in solution, the equilibrium is determined by the balance of HCl, and the amount of $\mathsf{CO_2}$ in solution. If there is enough HCl it will be the determining factor. The other equilibrium point is when $\mathsf{Ca^{2+}}$ is saturated. In this saturated situation there are two possibilities. If there is a lot of HCl in solution then $[\mathsf{Ca^{2+}}]_{\max} \sim \frac{1}{2}[\mathsf{Cl^-}]$. If there is no HCl, as in natural waters, then $[\mathsf{Ca^{2+}}]_{\max} \sim \frac{1}{2}[\mathsf{HCO_3^-}]$. Details of the asymptotic analysis are summarized in (3.65)–(3.66), and for the maximum amount of dissolved calcium, see (3.67). To simplify the analysis, an activity coefficient is taken as one but can easily be compensated with the use of expression (3.43).

A detailed model of the carbonate system, coupled to a dissolving calcite sur-

face, is presented in Chapter 4. This model includes a generalized fluid flow, and a Stefan condition imposed at the dissolving interface. This complex model is then systematically simplified by assuming an axial flow, given by the von Kármán flow, and that the dissolution is quasi-steady. What this means is that the dissolving surface changes very slowly when compared to the speed of the fluid passing over the calcite as it dissolves. In Chapter 5, it is shown that in this limit, the expression for Ca^{2+} decouples. In a closed system, the concentration of calcium has a boundary layer structure in space that saturates over time according to a simple exponential relationship. It also illustrates that the mass flux from the surface at any given time is a constant multiple of the time rate of change of the calcium concentration infinitely far from the dissolving interface. This illuminating insight gives access to the boundary layer structure that is very difficult to experimentally validate.

Finally, with Chapter 6, the simplified Stefan model is shown to be consistent with the experimental results obtained in [34] and [35]. This implies that it is compatible with the PWP model that is routinely used to close dissolution problems that involve calcite. What this work has shown is that the inclusion of the a mass conserving Stefan condition at the dissolving surface is essential in understanding the changing chemical environment of a dissolving species within a closed environment. The relatively simple behaviours that are seen experimentally are a result of a sophisticated interplay between the ions. The ions find a balance between the saturated calcium environment near the surface, and the bulk concentration that is typically much lower. The tension between these two chemical extremes is what ultimately drives the mass flux.

This new model of dissolution, that incorporates a Stefan condition to conserve mass at the dissolving interface, has shown that it can predict the dissolution rate of calcite over a broad range of temperatures and pressures. This can be accomplished using the time dependence of the calcium concentration far from the dissolving in-

terface, and is therefore independent of the nature of the fluid flow. The effective behaviour in the modelled closed system is the result of a combination of dimensionless parameters that characterize the fluid flow, and the exact chemical environment. A set of experiments that can validate this dependence and verify how the fluid and chemical behaviours interact is a natural first step towards future work. Connected with this is a mathematical validation of the pH-stat predictions, and how they can be interpreted in a manner consistent with free-drift experiments.

From the research presented, it is clear that the highly acidic region is particularly challenging in an experimental setting. Inclusion of a nontrivial activity coefficient for all of the ionic species is a first step towards resolving this. Although prosaic, it may provide some useful insight to the underlying chemistry. In addition, completely solving the system of PDEs to extract the boundary layer structure would be quite useful and add to other research in this direction [3]. This would lead to a full solution that depicts the dynamic profile for each of the chemical constituents. Important in this process is the realization that $[Cl^-]$ forms a boundary layer, and this will affect the boundary layer of $[CO_2]$.

One curious point that remains is the initial question that began this research. We have shown in this work that the fluid flow is not particularly critical when extracting the flux at the dissolving surface. In fact, the model is based on von Kármán flow, yet is capable of modelling the dissolution of granulated calcite pellets that are manually stirred. This thesis has shown that the exact nature of the chemistry in the bulk plays a significant role in determining the surface flux as a material dissolves. The intricacies of the fluid flow and the Stefan number combine to determine the overall scale of the dissolution rate. Details of this complex question will have to remain unsolved until we are able verify these results through further experimentation.

Bibliography

[1] M.A. Abdou. New analytic solution of von Kármán swirling viscous flow. *Acta Applicandae Mathematicae*, 111(1):7–13, 2010.

[2] E.R. Benton. On the flow due to a rotating disk. *Journal of Fluid Mechanics*, 24(7):781–800, 1966.

[3] C.S. Bohun. A Stefan model for mass transfer in a rotating disk reaction vessel. *European Journal of Applied Mathematics*, 26(4):453–475, 2015.

[4] D. Buhmann and W. Dreybrodt. The kinetics of calcite dissolution and precipitation in geologically relevant situations of karst areas: 1. Open system. *Chemical Geology*, 48(1-4):189–211, 1985.

[5] D. Buhmann and W. Dreybrodt. The kinetics of calcite dissolution and precipitation in geologically relevant situations of karst areas: 2. Closed system. *Chemical Geology*, 53(1):109–124, 1985.

[6] A.V. Carozzi. La formation des concrétions d'après un savant du XVIIIe siècle. *Revue Polytechnique*, pages 1–4, 1944.

[7] W.G. Cochran. The flow due to a rotating disc. *Proceedings of the Cambridge Philosophical Society*, 30(03):365–375, 1934.

[8] G.A.J. Cole and O.H. Little. I.-The mineral condition of the calcium carbonate in fossil shells. *Geological Magazine*, 8(2):49–55, 1911.

[9] J.R. Crank. Finite difference methods. In *Moving boundary problems in heat flow and diffusion*, pages 192–207. Clarendon Press, Oxford, England, 1975.

[10] C.W. Davies. *Ion association*. Butterworth, London, 1962.

[11] A.G. Dickson and J.P. Riley. The estimation of acid dissociation constants in seawater media from potentionmetric titrations with strong base. I. The ionic product of water—Kw. *Marine Chemistry*, 7(2):89–99, 1979.

[12] H.W. Douglas and R.A. Walker. The electrokinetic behaviour of Iceland spar against aqueous electrolyte solutions. *Transactions of the Faraday Society*, 46:559–568, 1950.

[13] R.A. Feely, S.C. Doney, and S.R. Cooley. Ocean acidification: Present conditions and future changes in a high-CO_2 world. *Oceanography*, 22(4):36–47, 2009.

[14] D.H. Ferris. Fixation of a moving boundary by means of a change of independent variable. In *Moving boundary problems in heat flow and diffusion*, pages 251–255. Clarendon Press, Oxford, England, 1975.

[15] H.E. Fettis. On the integration of a class of differential equations occurring in boundary layer and other hydrodynamic problems. *Proceedings of the 4th Midwestern Conference on Fluid Mechanics*, 1955.

[16] P. Gaubert. On the dissolution faces of calcite and on the corrosion figures of rhomboédrique carbonates. *Bulletin de Minérealogy*, 24(5):326–351, 1901.

[17] H.S. Harned and W.J. Hamer. The ionization constant of water and the dissociation of water in potassium chloride solutions from electromotive forces

of cells without liquid junction. *Journal of the American Chemical Society*, 55(6):2194–2206, 1933.

[18] E.S. Hedges. CXIII.-Liquid-line corrosion. *Journal of the Chemical Society (Resumed)*, 129:831–833, 1926.

[19] G. Kaufmann and W. Dreybrodt. Calcite dissolution kinetics in the system $CaCO_3$-H_2O-CO_2 at high undersaturation. *Geochimica et Cosmochimica Acta*, 71(6):1398–1410, 2007.

[20] D.M. Kern. The hydration of carbon dioxide. *Journal of Chemical Education*, 37(1):14, 1960.

[21] J. Keslin. Viscosity of liquid water in the range - 8°C to 150°C. *Journal of Physical and Chemical Reference Data*, 7(3):941–948, 1978.

[22] D. Langmuir. Stability of calcite based on aqueous solubility measurements. *Geochimica et Cosmochimica Acta*, 32(8):835–851, 1968.

[23] V.G. Levich and D.B. Spalding. *Physicochemical hydrodynamics*, volume 689. Prentice-Hall Englewood Cliffs, NJ, 1962.

[24] G.N. Lewis and M. Randall. *Thermodynamics, revised by K.S. Pitzer and L. Brewer*. McGraw-Hill, New York, 1961.

[25] S. Liao. *Beyond perturbation: introduction to homotopy analysis method*. CRC Press, 2004.

[26] M.J. Mitchell, O.E. Jensen, K.A. Cliffe, and M.M. Maroto-Valer. A model of carbon dioxide dissolution and mineral carbonation kinetics. *Proceedings of the Royal Society A: Mathematical, Physical and Engineering Science*, 466(2117):1265–1290, 2010.

[27] R.C. Murray. Origin of porosity in carbonate rocks. *Journal of Sedimentary Research*, 30(1):59–84, 1960.

[28] J. Newman. Schmidt number correction for the rotating disk. *The Journal of Physical Chemistry*, 70(4):1327–1328, 1966.

[29] J.R. Ockendon and W.R. Hodgkins, editors. *Moving boundary problems in heat flow and diffusion*. Clarendon Press, Oxford, England, 1975.

[30] P. Patnaik. *Handbook of Inorganic Chemicals*, volume 28. McGraw-Hill New York, 2003.

[31] M.N.A. Peterson. Calcite: rates of dissolution in a vertical profile in the central Pacific. *Science*, 154(3756):1542–1544, 1966.

[32] K.S. Pitzer. Characteristics of very concentrated aqueous solutions. *Physics and Chemistry of the Earth*, 13:249–272, 1981.

[33] L.N. Plummer and E. Busenberg. The solubilities of calcite, aragonite and vaterite in CO_2-H_2O solutions between 0 and $90°C$, and an evaluation of the aqueous model for the system $CaCO_3$-CO_2-H_2O. *Geochimica et Cosmochimica Acta*, 46(6):1011–1040, 1982.

[34] L.N. Plummer and T.M.L. Wigley. The dissolution of calcite in CO_2-saturated solutions at 25 C and 1 atmosphere total pressure. *Geochimica et Cosmochimica Acta*, 40(2):191–202, 1976.

[35] L.N. Plummer, T.M.L. Wigley, and D.L. Parkhurst. The kinetics of calcite dissolution in CO_2-water systems at 5–$60°C$ and 0.0–1.0 atm CO_2. *American Journal of Science*, 278:179–216, 1978.

[36] R. Sander. Modeling atmospheric chemistry: Interactions between gas-phase species and liquid cloud/aerosol particles. *Surveys in Geophysics*, 20(1):1–31, 1999.

[37] W. Spring. On the dissolution rate of Iceland spar in hydrochloric acid. *Bulletin de la Société Chimique de Paris*, 3:177–184, 1890.

[38] P. Tans. NOAA ESRL data, 2020.

[39] A.B. Taylor. The mathematical formulation of Stefan problems. In *Moving boundary problems in heat flow and diffusion*, pages 120–137. Clarendon Press, Oxford, England, 1975.

[40] K. Taylor and H.A. Nasr-El-Din. Measurement of acid reaction rates with the rotating disk apparatus. *Journal of Canadian Petroleum Technology*, 48(6):66–70, 2009.

[41] E. Usdowski. Reactions and equilibria in the systems CO_2-H_2O and $CaCO_3$-CO_2-H_2O (0–50°C). *Neues Jahrbuch für Mineralogie. Abhandlungen*, 144(2):148–171, 1982.

[42] T. von Kármán. Über laminare und turbulente Reibung. *ZAMM-Journal of Applied Mathematics and Mechanics/Zeitschrift für Angewandte Mathematik und Mechanik*, 1(4):233–252, 1921.

[43] B. Wunderlich. *Macromolecular Physics, vol 2: Crystal Nucleation, Growth, Annealing*. Academic Press Inc., San Diego, 1976.

[44] C. Yang and S. Liao. On the explicit, purely analytic solution of von Kármán swirling viscous flow. *Communications in Nonlinear Science and Numerical Simulation*, 11(1):83–93, 2006.

[45] J. Yao, W. Liu, and Z. Chen. Numerical solution of a moving boundary problem of one-dimensional flow in semi-infinite long porous media with threshold pressure gradient. *Mathematical Problems in Engineering*, 2013, 2013.

[46] L. Yuan-Hui and S. Gregory. Diffusion of ions in sea water and in deep-sea sediments. *Geochimica et Cosmochimica Acta*, 38(5):703–714, 1974.

[47] P.J. Zandbergen and D. Dijkstra. Von Kármán swirling flows. *Annual Review of Fluid Mechanics*, 19(1):465–491, 1987.

[48] R.E. Zeebee. On the molecular diffusion coefficients of dissolved CO_2, HCO_3^-, and CO_3^{2-} and their dependence on isotopic mass. *Geochimica et Cosmochimica Acta*, 75:2483–2498, 2011.

APPENDIX A

von Kármán flow

A.1 Preliminaries

This discussion assuming an incompressible viscous fluid that satisfies the Navier-Stokes equations. These equations with an incompressiblity condition are

$$\frac{\partial \vec{u}}{\partial t} + (\vec{u} \cdot \nabla)\vec{u} = -\frac{1}{\rho}\nabla p + \nu \nabla^2 \vec{u}, \qquad \nabla \cdot \vec{u} = 0, \tag{A.1}$$

where both the density ρ and dynamic viscosity μ with ($\nu = \mu/\rho$ is the kinematic viscosity) are assumed to be constant. Considering the geometrical setting of the swirling flow, we use cylindrical coordinates (r, θ, z), and assume the solution is independent of the angular coordinate. Furthermore, let the surface of the disc be the plane $z = 0$, with z increasing with depth within the fluid, and the rotation axis coincident with $r = 0$. The velocity field for the swirling flow, $\vec{u} = \langle u_r, u_\theta, u_z \rangle$, with the convention that an upwelling flow corresponds to $u_z < 0$, reduces the steady

state equations (A.1) to

$$u_r\frac{\partial u_r}{\partial r}+u_z\frac{\partial u_r}{\partial z}-\frac{u_\theta^2}{r}=\nu\left(\frac{\partial^2 u_r}{\partial r^2}+\frac{1}{r}\frac{\partial u_r}{\partial r}-\frac{u_r}{r^2}+\frac{\partial^2 u_r}{\partial z^2}\right), \tag{A.2}$$

$$u_r\frac{\partial u_\theta}{\partial r}+u_z\frac{\partial u_\theta}{\partial z}+\frac{u_r u_\theta}{r}=\nu\left(\frac{\partial^2 u_\theta}{\partial r^2}+\frac{1}{r}\frac{\partial u_\theta}{\partial r}-\frac{u_\theta}{r^2}+\frac{\partial^2 u_\theta}{\partial z^2}\right), \tag{A.3}$$

$$u_r\frac{\partial u_z}{\partial r}+u_z\frac{\partial u_z}{\partial z}=-\frac{1}{\rho}\frac{\partial p}{\partial z}+\nu\left(\frac{\partial^2 u_z}{\partial r^2}+\frac{1}{r}\frac{\partial u_z}{\partial r}+\frac{\partial^2 u_z}{\partial z^2}\right), \tag{A.4}$$

$$\frac{\partial u_r}{\partial r}+\frac{u_r}{r}+\frac{\partial u_z}{\partial z}=0, \tag{A.5}$$

expressed in cylindrical coordinates. The quantity p denotes the pressure, which is considered to be a function of depth z alone.

In this model, the disc is of infinite extent and is rotating at a constant angular velocity of $\omega \geq 0$, and the bottom of the vessel is assumed to be infinitely far away.[1] Applying a no-slip condition on the fluid in contact with the disc gives the boundary conditions

$$u_r(r,0)=0, \qquad u_\theta(r,0)=\omega r, \qquad u_z(r,0)=0. \tag{A.6}$$

Due to the rotation of the disc, fluid close to this surface fans out over the rotating disc towards the outer edge of the cylinder (reaction vessel). Since the amount of fluid is conserved, this outward flow at the disc surface induces an upwelling of fluid from the bottom. In the limit of increasing depth, all fluid velocities must vanish, aside from the induced axial component, $\lim_{z\to\infty} u_z(r,z) = -U_0$. This implies additional boundary conditions of the form

$$\lim_{z\to\infty} u_r(r,z)=0, \qquad \lim_{z\to\infty} u_\theta(r,z)=0. \tag{A.7}$$

By setting this problem up as a boundary value problem, although inconvenient,

[1] Having a finite disc radius and a finite depth will introduce significant differences in the fluid flow. The connection with a finite disc is discussed in [47].

that one boundary is at $z \to \infty$, we are searching for a solution with vanishing radial and tangential velocities as the depth increases. This leaves only axial flow with a steady value of U_0 toward the disc.

In this idealized geometry, there is only one physical boundary located at $z = 0$, and the flow is allowed to develop according to the symmetry of the governing PDEs, without the influence of any other boundaries. To pick up these geometric aspects, a similarity solution is attempted. In particular, a similarity variable ζ is identified, and the equations (A.2)–(A.7) are nondimensionalized by applying the transformation

$$z = \sqrt{\frac{\nu}{\omega}}\zeta, \quad u_r = r\omega F(\zeta), \quad u_\theta = r\omega G(\zeta), \quad u_z = \sqrt{\nu\omega}H(\zeta), \quad p = -\rho\nu\omega P(\zeta). \tag{A.8}$$

This reduces the system (A.2)–(A.5) to a system of non-linear coupled ordinary differential equations

$$F'' = F^2 - G^2 + F'H, \tag{A.9}$$

$$G'' = 2FG + G'H, \tag{A.10}$$

$$H'' = HH' - P', \tag{A.11}$$

$$H' = -2F, \tag{A.12}$$

where the primes denote derivatives with respect to ζ. This set of equations is subject to the following associated boundary conditions

$$F(0) = 0, \quad G(0) = 1, \quad H(0) = 0, \quad \lim_{\zeta\to\infty} F(\zeta) = 0, \quad \lim_{\zeta\to\infty} G(\zeta) = 0. \tag{A.13}$$

Using (A.11) and (A.12), $P' = HH' + 2F'$ so that (F, G, H) decouples from the

system (A.9)–(A.12). Furthermore,

$$P(\zeta) = P(0) + \frac{1}{2}H^2(\zeta) + 2F(\zeta). \tag{A.14}$$

Considering (A.8), we see that U_0 is determined by finding $\lim_{\zeta\to\infty} H(\zeta)$ after imposing the other five conditions. The system of equations can be further reduced by eliminating F, giving the tightly coupled system

$$H''' = -\frac{1}{2}H'^2 + 2G^2 + H''H, \qquad H(0) = 0, H'(0) = 0, \lim_{\zeta\to\infty} H'(\zeta) = 0, \tag{A.15}$$

$$G'' = -H'G + G'H, \qquad G(0) = 1, \lim_{\zeta\to\infty} G(\zeta) = 0. \tag{A.16}$$

Equations (A.15)–(A.16) were solved approximately by von Kármán [42], and subsequently improved upon by Cochran [7]. They were adapted by Levich [23] to develop his classical solution of the rotating disc dissolution problem. More accurate approximations [2, 15] and different techniques [1, 25, 44] can be found elsewhere. A review of the history of this problem can be found in [47].

A.2 Numerical Solution

An inconvenience of the von Kármán system is that it is framed as a boundary value problem with one of the boundaries at $\zeta \to \infty$. Consider instead the related initial value problem

$$H''' = -\frac{1}{2}H'^2 + 2G^2 + H''H, \qquad H(0) = 0, H'(0) = 0, H''(0) = -2a_1, \tag{A.17}$$

$$G'' = -H'G + G'H, \qquad G(0) = 1, G'(0) = b_1, \tag{A.18}$$

where a_1 and b_1 are chosen so that both G and H' tend to zero as $\zeta \to \infty$. Letting $\vec{y} = (H, H', H'', G, G')$, the system (A.17)–(A.18) can be written as

$$\begin{pmatrix} y_1' \\ y_2' \\ y_3' \\ y_4' \\ y_5' \end{pmatrix} = \begin{pmatrix} y_2 \\ y_3 \\ -\frac{1}{2}y_2^2 + 2y_4^2 + y_1 y_3 \\ y_5 \\ -y_2 y_4 + y_1 y_5 \end{pmatrix}, \qquad \begin{pmatrix} y_1(0) \\ y_2(0) \\ y_3(0) \\ y_4(0) \\ y_5(0) \end{pmatrix} = \begin{pmatrix} 0 \\ 0 \\ -2a_1 \\ 1 \\ b_1 \end{pmatrix}. \tag{A.19}$$

The solution of the system with $a_1 \simeq 0.510232618867$ and $b_1 \simeq -0.615922014399$ is displayed in Figure A.1.

Due to the axisymmetry, all three velocity components $\langle u_r, u_\theta, u_z \rangle$ only depend on r and z, and not on the azimuthal angle θ. Visualization of this axisymmetrical flow is aided by plotting the streamlines that correspond to curves of constant stream function Ψ. In this situation, the azimuthal velocity component u_θ does not depend on the stream function, whereas the radial and axial components satisfy

$$u_r = \frac{1}{r}\frac{\partial \Psi}{\partial z} = r\omega F(\zeta), \qquad u_z = -\frac{1}{r}\frac{\partial \Psi}{\partial r} = \sqrt{\nu\omega} H(\zeta), \qquad \zeta = \sqrt{\frac{\omega}{\nu}} z, \tag{A.20}$$

so that $\vec{u} \cdot \nabla \Psi = 0$. Since $\nabla \Psi$ is perpendicular to the level curves of $\Psi(r, z)$, the streamlines are parallel to the flow velocity $\vec{u}$. Up to an arbitrary constant,[2]

$$\Psi(r, z) = -\frac{\sqrt{\nu\omega}}{2} r^2 H\left(\sqrt{\frac{\omega}{\nu}} z\right). \tag{A.21}$$

A plot of the streamlines is displayed in Figure A.2.

In the remaining portion of the Appendix we present the asymptotic expansion of the von Kármán solution both near the plate at $\zeta = 0$ and in the vicinity of $\zeta \to \infty$.

[2]Integrating (A.20b) gives $\Psi(r, \zeta) = -\sqrt{\nu\omega} r^2 H(\zeta)/2 + g(\zeta)$ for an arbitrary $g(\zeta)$. From (A.20a) $r^{-1}\partial\Psi/\partial z = -r\omega H'(\zeta)/2 + g'(\zeta)\omega^{1/2}/\nu^{-1/2} = r\omega F(\zeta)$ provided $g(\zeta) =$ constant.

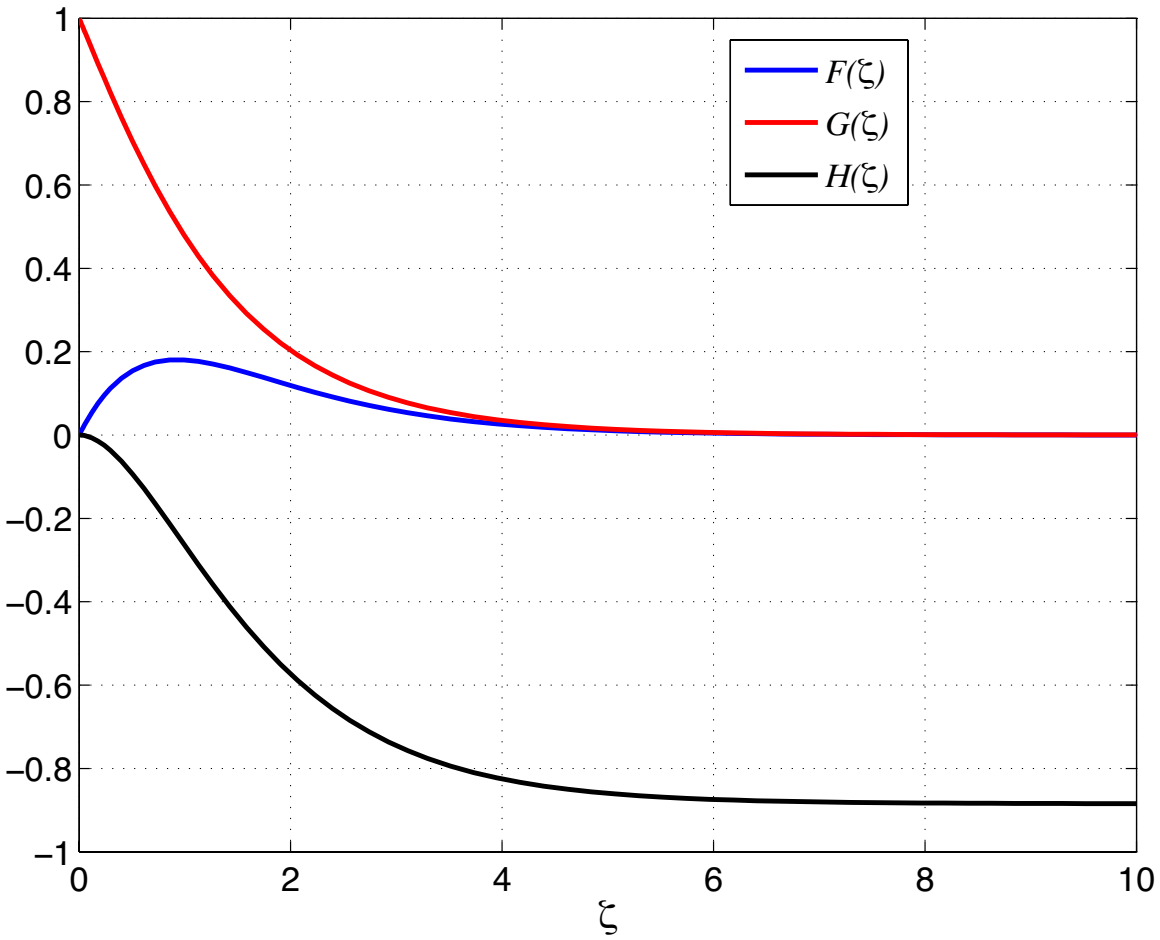

Figure A.1: Components $F(\zeta), G(\zeta)$ and $H(\zeta)$ of the system (A.19) with values of $a_1 \simeq 0.510232618867$, and $b_1 \simeq -0.615922014399$. This results in the asymptotic value of $\lim_{\zeta\to\infty} H(\zeta) = -\alpha \simeq 0.884919$.

The former expansion is useful inside the hydrodynamic boundary layer thickness where $\zeta < 1$ and is a polynomial expansion in the coordinate ζ. For large ζ, the expansion is in terms of exponential functions and extends the result of Cochran [7].

A.3 Expansion about $\zeta = 0$

To find a solution valid near the rotating disc, $\zeta \to 0$, we suppose that

$$F = \sum_{j=0}^{\infty} a_j \zeta^j, \qquad G = \sum_{j=0}^{\infty} b_j \zeta^j, \qquad H = \sum_{j=0}^{\infty} c_j \zeta^j, \qquad P = \sum_{j=0}^{\infty} p_j \zeta^j. \tag{A.22}$$

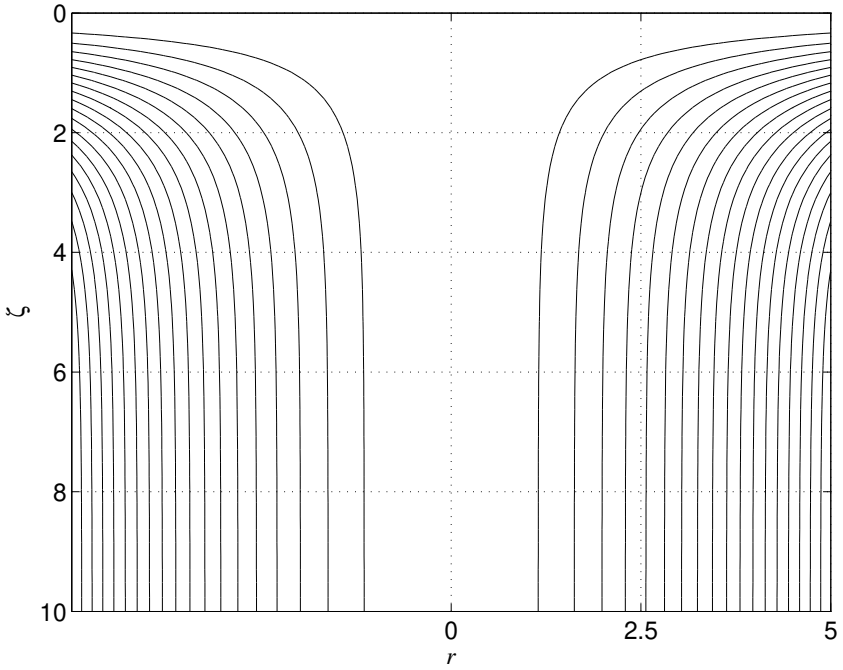

Figure A.2: Streamlines of the von Kármán flow for the rotating disc showing the upwelling of fluid near $r = 0$ which subsequently fans out over the disc located at $\zeta = 0$. Notice that $\zeta = 1$ corresponds to a dimensional boundary layer thickness of $z = \sqrt{\nu/\omega}$.

In order to satisfy the boundary conditions at $\zeta = 0$. $a_0 = c_0 = 0$, and $b_0 = 1$. From the fourth equation $H' = -2F$ one finds that

$$H = -a_1\zeta^2 - \frac{2a_2}{3}\zeta^3 - \frac{a_3}{2}\zeta^4 - \frac{2a_4}{5}\zeta^5 + \cdots . \tag{A.23}$$

Inserting (A.22) into (A.9)–(A.12), expanding and collecting like powers of ζ, gives for $\zeta \to 0$

$$F(\zeta) = a_1\zeta - \frac{1}{2}\zeta^2 - \frac{b_1}{3}\zeta^3 - \frac{b_1^2}{12}\zeta^4 - \frac{a_1}{60}\zeta^5 + \mathcal{O}\left(\zeta^6\right), \tag{A.24}$$

$$G(\zeta) = 1 + b_1\zeta + \frac{a_1}{3}\zeta^3 + \frac{1}{12}(a_1b_1 - 1)\zeta^4 - \frac{b_1}{15}\zeta^5 + \mathcal{O}\left(\zeta^6\right), \tag{A.25}$$

$$H(\zeta) = -a_1\zeta^2 + \frac{1}{3}\zeta^3 + \frac{b_1}{6}\zeta^4 + \frac{b_1^2}{30}\zeta^5 + \mathcal{O}\left(\zeta^6\right), \tag{A.26}$$

where as stated earlier,

$$(a_1, b_1) = (F'(0), G'(0)) \simeq (0.510232618867, -0.615922014399) \tag{A.27}$$

are chosen to ensure that

$$\lim_{\zeta\to\infty} (F(\zeta), G(\zeta)) = (0, 0). \tag{A.28}$$

For completeness, we also find with (A.14) that

$$P(\zeta) = P(0) + 2a_1\zeta - \zeta^2 - \frac{2b_1}{3}\zeta^3 - \frac{1}{6}(b_1^2 - 3a_1^2)\zeta^4 - \frac{11a_1}{30}\zeta^5 + \mathcal{O}\left(\zeta^6\right) \tag{A.29}$$

where $P(0)$ is an arbitrary pressure level at $\zeta = 0$. Plots of the asymptotic expansions (A.24)–(A.29) compared to the numerical solution can be found in Figures A.3–A.5.

A.4 Expansion for $\zeta \to \infty$

Far away from the rotating surface, we expect that the flow will become primarily axial so that as $\zeta \to \infty$, $H(\zeta) \to -\alpha$ whereas $F(\zeta) \to 0$ and $G(\zeta) \to 0$. In this limit, one can argue that (A.9)–(A.10) effectively become

$$F'' + \alpha F' \sim 0, \qquad\qquad G'' + \alpha G' \sim 0, \tag{A.30}$$

implying that an expansion in terms of exponential functions may be possible. With this in mind, we assume for $\zeta \to \infty$,

$$F = \sum_{n=0}^{\infty} A_n \mathrm{e}^{-n\alpha\zeta}, \qquad G = \sum_{n=0}^{\infty} B_n \mathrm{e}^{-n\alpha\zeta}, \qquad H = \sum_{n=0}^{\infty} C_n \mathrm{e}^{-n\alpha\zeta}, \tag{A.31}$$

with $A_0 = B_0 = 0$ and $C_0 = -\alpha$ to satisfy the boundary conditions. Once again, continuing the analysis, one finds consistent with [7], and letting $C^2 = A_1^2 + B_1^2$, that

$$F(\zeta) = A_1 \mathrm{e}^{-\alpha\zeta} - \frac{C^2}{2\alpha^2}\mathrm{e}^{-2\alpha\zeta} + \frac{A_1 C^2}{4\alpha^4}\mathrm{e}^{-3\alpha\zeta} - \frac{C^2}{144\alpha^6}(17A_1^2 + B_1^2)\mathrm{e}^{-4\alpha\zeta} + \frac{A_1 C^2}{1152\alpha^8}(61A_1^2 + 13B_1^2)\mathrm{e}^{-5\alpha\zeta} + \mathcal{O}\left(\mathrm{e}^{-6\alpha\zeta}\right), \tag{A.32}$$

$$G(\zeta) = B_1 \mathrm{e}^{-\alpha\zeta} - \frac{B_1 C^2}{12\alpha^4}\mathrm{e}^{-3\alpha\zeta} + \frac{A_1 B_1 C^2}{18\alpha^6}\mathrm{e}^{-4\alpha\zeta} - \frac{B_1 C^2}{1920\alpha^8}(53A_1^2 + 5B_1^2)\mathrm{e}^{-5\alpha\zeta} + \mathcal{O}\left(\mathrm{e}^{-6\alpha\zeta}\right), \tag{A.33}$$

$$H(\zeta) = -\alpha + \frac{2A_1}{\alpha}\mathrm{e}^{-\alpha\zeta} - \frac{C^2}{2\alpha^3}\mathrm{e}^{-2\alpha\zeta} + \frac{A_1 C^2}{6\alpha^5}\mathrm{e}^{-3\alpha\zeta} - \frac{C^2}{288\alpha^7}(17A_1^2 + B_1^2)\mathrm{e}^{-4\alpha\zeta} + \frac{A_1 C^2}{2880\alpha^9}(61A_1^2 + 13B_1^2)\mathrm{e}^{-5\alpha\zeta} + \mathcal{O}\left(\mathrm{e}^{-6\alpha\zeta}\right). \tag{A.34}$$

In this limit, we identify $\alpha = 0.884919$ and

$$(A_1, B_1) = \lim_{\zeta\to\infty} \mathrm{e}^{\alpha\zeta}(F(\zeta), G(\zeta)) \simeq (0.93344, 1.21046), \tag{A.35}$$

and from (A.14)

$$P(\zeta) = P(0) + \frac{\alpha^2}{2} + \frac{1}{2\alpha^2}(3A_1^2 - B_1^2)\mathrm{e}^{-2\alpha\zeta} - \frac{2A_1 C^2}{3\alpha^4}\mathrm{e}^{-3\alpha\zeta} + \frac{C^2}{96\alpha^6}(27A_1^2 + 11B_1^2)\mathrm{e}^{-4\alpha\zeta} - \frac{A_1 C^2}{180\alpha^8}(21A_1^2 + 13B_1^2)\mathrm{e}^{-5\alpha\zeta} + \mathcal{O}\left(\mathrm{e}^{-6\alpha\zeta}\right). \tag{A.36}$$

A comparison of these asymptotic expansions for the various components of the velocity are plotted in Figures A.3–A.5.

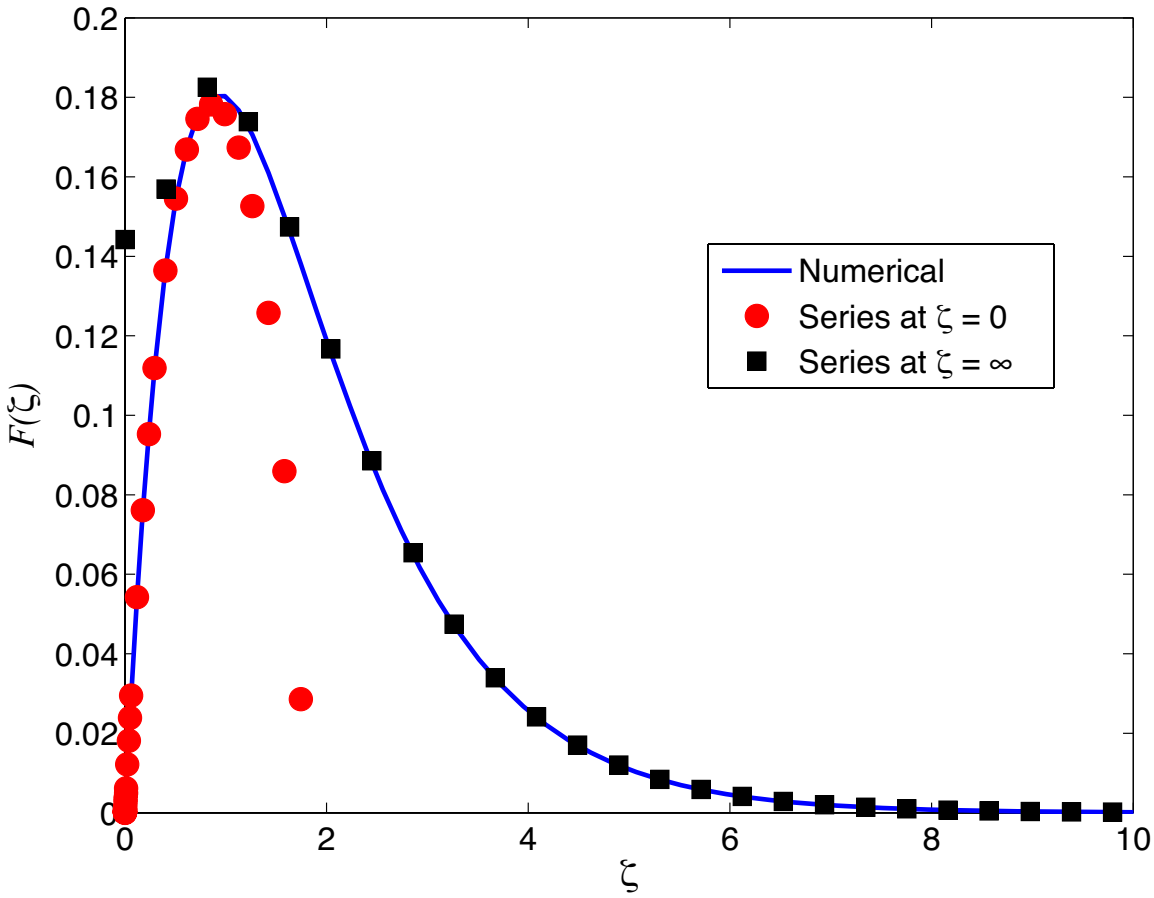

Figure A.3: The $F(\zeta)$ component of the system (A.9)–(A.12) together with the asymptotic expansions (A.24) and (A.32).

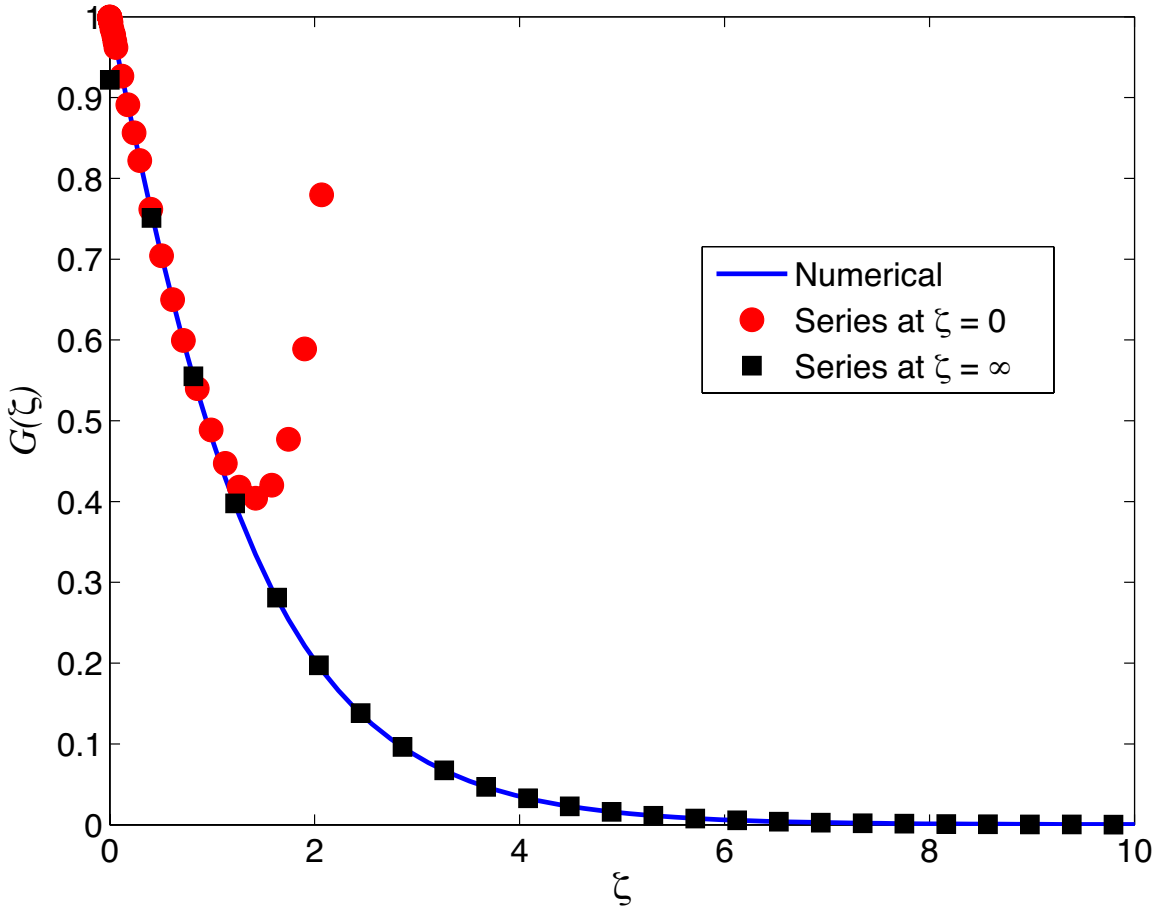

Figure A.4: The $G(\zeta)$ component of the system (A.9)–(A.12) together with the asymptotic expansions (A.25) and (A.33).

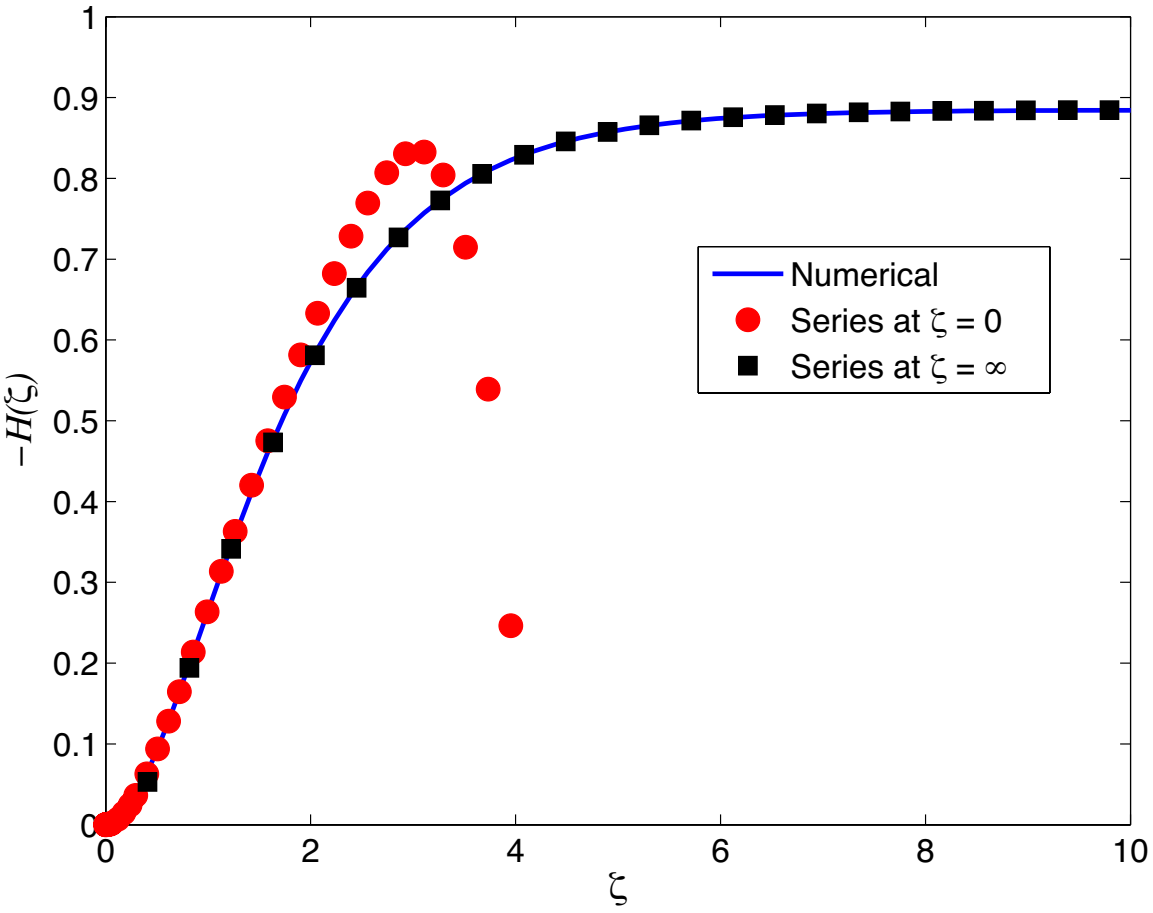

Figure A.5: The $-H(\zeta)$ component of the system (A.9)–(A.12) together with the asymptotic expansions (A.26) and (A.34).

APPENDIX B

Extra Results

The following analysis is taken from Appendix A of [3] and referenced in Section 5.1, and is used with the permission of the author. It assumes that there is a significant amount of $[Cl^-]$ in solution to drive the reaction.

As stated in Section 5.1, both $[H^+]_0$ and $[H^+]_\infty$ satisfy algebraic relations that can be solved explicitly for a given set of parameters. As noticed by Mitchell et al. [26], the variability of the parameters over many orders of magnitude decouples the carbonic acid system into effectively disjoint regions. Their accessibility is governed by the partial pressure of carbon dioxide and the amount of chlorine in solution. For $[H^+]_0$ this results in the asymptotic expansion

$$[H^+]_0 \sim \begin{cases} K_{P0}^{1/2}\left(1+\frac{1}{2}\frac{1+2\kappa_2}{1-\kappa_1}\left(\frac{K_P}{K_{P0}}\right)+\mathcal{O}\left(\frac{K_P^2}{K_{P0}^2}\right)\right), & K_P \ll K_{P0}, \\ K_P^{1/2}\left(1+(\kappa_1+\kappa_2)\left(\frac{K_{P0}^{1/2}}{K_P^{1/2}}\right)+\mathcal{O}\left(\frac{K_{P0}}{K_P}\right)\right), & K_P \gg K_{P0}, \end{cases} \tag{B.1}$$

with

$$K_{\mathrm{P0}}^{1/2} = \frac{[\mathsf{Cl}^-]}{2} + \left(\frac{[\mathsf{Cl}^-]^2}{4} + K_{\mathrm{W}}^c\right)^{1/2}, \qquad \kappa_1 = \frac{[\mathsf{Cl}^-]}{2K_{\mathrm{P0}}^{1/2}}, \qquad \kappa_2 = \frac{K_2^c}{K_{\mathrm{P0}}^{1/2}}, \tag{B.2}$$

so that $0 \leq \kappa_1 < \frac{1}{2}$ and using the data in Table 3.1, $0 < \kappa_2 \leq K_2^c {K_{\mathrm{W}}^c}^{-1/2} \sim 4.66 \times 10^{-4}$ as $[\mathsf{Cl}^-]$ takes on all possible nonzero values. In the region where[1] $K_{\mathrm{P}} \ll K_{\mathrm{P0}}$, $[\mathsf{H}^+]_0 \simeq [\mathsf{Cl}^-]$ and that the concentration of bicarbonate increases with K_{P} until $[\mathsf{H}^+]_0 \simeq [\mathsf{HCO}_3^-]$ for $K_{\mathrm{P}} \gg K_{\mathrm{P0}}$.

When calcium is present none of the equilibrium constraints can be neglected. From (3.38), at equilibrium, $[\mathsf{CO}_2] = \mathcal{O}(K_{\mathrm{P}})$ and $[\mathsf{H}_2\mathsf{CO}_3\mathsf{0}] = \mathcal{O}(K_{\mathrm{P}})$ so if $[\mathsf{H}^+] = \mathcal{O}(K_{\mathrm{P}}^s)$ for a given s then[2] from the equilibrium conditions (3.33), $[\mathsf{HCO}_3^-] = \mathcal{O}\left(K_{\mathrm{P}}^{1-s}\right)$, $[\mathsf{OH}^-] = \mathcal{O}\left(K_{\mathrm{P}}^{-s}\right)$ and $[\mathsf{CO}_3^{2-}] = \mathcal{O}\left(K_{\mathrm{P}}^{1-2s}\right)$ whereas (3.46) implies that $[\mathsf{Ca}^{2+}]_{\max} = \mathcal{O}\left(K_{\mathrm{P}}^{2s-1}\right)$.

It is relatively straightforward to show that $[\mathsf{H}^+]_\infty$ is monotonic with K_{P} through differentiation, and substitution, giving

$$\begin{aligned}\frac{\mathrm{d}[\mathsf{H}^+]_\infty}{\mathrm{d}K_{\mathrm{P}}} &= \frac{\frac{1}{\lambda K_{\mathrm{P}}^2}[\mathsf{H}^+]_\infty^4 + [\mathsf{H}^+]_\infty + 2K_2^c}{\frac{4}{\lambda K_{\mathrm{P}}}[\mathsf{H}^+]_\infty^3 + 3[\mathsf{H}^+]_\infty^2 - 2[\mathsf{Cl}^-][\mathsf{H}^+]_\infty - K_{\mathrm{W}}^c - K_{\mathrm{P}}} \\ &= \frac{\left(\frac{1}{\lambda K_{\mathrm{P}}^2}[\mathsf{H}^+]_\infty^4 + [\mathsf{H}^+]_\infty + 2K_2^c\right)[\mathsf{H}^+]_\infty}{\frac{1}{\lambda K_{\mathrm{P}}}[\mathsf{H}^+]_\infty^4 + [\mathsf{Cl}^-][\mathsf{H}^+]_\infty^2 + 2\left(K_{\mathrm{W}}^c + K_{\mathrm{P}}\right)[\mathsf{H}^+]_\infty + 6K_2^c K_{\mathrm{P}}} > 0\end{aligned} \tag{B.3}$$

with

$$\lambda = \frac{K_2^c}{2K_{\mathrm{sp}}}. \tag{B.4}$$

For small K_{P}, the dominant *positive* term is $[\mathsf{H}^+]_\infty^4/\lambda K_{\mathrm{P}}$, eventually becoming $[\mathsf{H}^+]_\infty^3$ as K_{P} increases. Physically this corresponds to an exchange of the dominant positively charged ionic species from calcium to hydrogen with an increase in partial

[1] For very low to vanishing levels of $[\mathsf{Cl}^-]$, $[\mathsf{H}^+] \simeq [\mathsf{OH}^-]$ in the $K_{\mathrm{P}} \ll K_{\mathrm{P0}}$ region.
[2] In expressions (B.1), (B.5), (B.9), $s \in \{0, \frac{1}{2}, \frac{1}{3}, \frac{2}{3}\}$.

pressure of carbon dioxide. The dominant *negative* term is more complicated moving from the $K_{\mathrm{W}}^{c}[\mathsf{H}^+]_\infty$ term to $[\mathsf{Cl}^-][\mathsf{H}^+]_\infty^2$, provided $[\mathsf{Cl}^-]$ is large enough. Finally to $K_{\mathrm{P}}[\mathsf{H}^+]_\infty$ as K_{P} increases, reflecting exchanges in the dominant negative ionic species from hydroxide to chlorine, and to bicarbonate ions. A detailed discussion of the equilibrium chemistry can now be revealed.

Referring to the right panel of Figure 3.2, in region I K_{P} is sufficiently small so that $[\mathsf{H}^+]_\infty^4/\lambda K_{\mathrm{P}} \simeq K_{\mathrm{W}}^{c}[\mathsf{H}^+]_\infty$, corresponding to $2[\mathsf{Ca}^{2+}]_{\max} \simeq [\mathsf{OH}^-]$. In this region, the very low partial pressure drives dissolved CO_2 from solution, reducing the amount of HCO_3^- and $\mathsf{H}_2\mathsf{CO}_3 0$, which in turn drives down $[\mathsf{H}^+]$. As $[\mathsf{H}^+]_\infty = \mathcal{O}\left(K_{\mathrm{P}}^{1/3}\right)$ in this region, $[\mathsf{HCO}_3^-] = \mathcal{O}\left(K_{\mathrm{P}}^{2/3}\right)$ and $[\mathsf{CO}_3^{2-}] = \mathcal{O}\left(K_{\mathrm{P}}^{1/3}\right)$ are both increasing and $[\mathsf{Ca}^{2+}]_{\max} = \mathcal{O}\left(K_{\mathrm{P}}^{-1/3}\right), [\mathsf{OH}^-] = \mathcal{O}\left(K_{\mathrm{P}}^{-1/3}\right)$ both decrease with K_{P}.

For appreciable levels of chlorine, $\lambda[\mathsf{Cl}^-]^3 > K_{\mathrm{W}}^{c}$ ($[\mathsf{Cl}^-] \gtrsim 1.25 \times 10^{-4}$ M) the dominant balance becomes $[\mathsf{H}^+]_\infty^4/\lambda K_{\mathrm{P}} \simeq [\mathsf{Cl}^-][\mathsf{H}^+]_\infty^2$ corresponding to $2[\mathsf{Ca}^{2+}]_{\max} \simeq [\mathsf{Cl}^-]$ and indicated as region II on the figure. Because $[\mathsf{OH}^-] < [\mathsf{Cl}^-] < [\mathsf{HCO}_3^-]$, the chlorine ions rather than the hydroxide ions balance the calcium. Noting that from the dominant balance, $[\mathsf{H}^+]_\infty = \mathcal{O}\left(K_{\mathrm{P}}^{1/2}\right)$, one has $[\mathsf{HCO}_3^-] = \mathcal{O}\left(K_{\mathrm{P}}^{1/2}\right)$, $[\mathsf{OH}^-] = \mathcal{O}\left(K_{\mathrm{P}}^{-1/2}\right)$, $[\mathsf{CO}_3^{2-}] = \mathcal{O}(1)$ and the maximum amount of dissolved calcium becomes independent of K_{P} with $[\mathsf{Ca}^{2+}]_{\max} = \mathcal{O}(1)$.

Increasing K_{P} further, the bicarbonate level increases until it exceeds $[\mathsf{Cl}^-]$ resulting in the formation of region III with a dominant balance of $2[\mathsf{Ca}^{2+}]_{\max} \simeq [\mathsf{HCO}_3^-]$ ($[\mathsf{H}^+]_\infty^4/\lambda K_{\mathrm{P}} \simeq K_{\mathrm{P}}[\mathsf{H}^+]_\infty$). Because $[\mathsf{H}^+]_\infty = \mathcal{O}\left(K_{\mathrm{P}}^{2/3}\right)$, the remaining dependencies are $[\mathsf{HCO}_3^-] = \mathcal{O}\left(K_{\mathrm{P}}^{1/3}\right)$, $[\mathsf{OH}^-] = \mathcal{O}\left(K_{\mathrm{P}}^{-2/3}\right)$, $[\mathsf{CO}_3^{2-}] = \mathcal{O}\left(K_{\mathrm{P}}^{-1/3}\right)$ and $[\mathsf{Ca}^{2+}]_{\max} = \mathcal{O}\left(K_{\mathrm{P}}^{1/3}\right)$. Finally, region IV corresponds to a switch in the dominant positive ionic species to hydrogen ions giving the dominant balance of $[\mathsf{H}^+]_\infty^3 \simeq K_{\mathrm{P}}[\mathsf{H}^+]_\infty$ yielding $[\mathsf{H}^+]_\infty = \mathcal{O}\left(K_{\mathrm{P}}^{1/2}\right)$ as in region II.

For each of these regions one can expand $[\mathsf{H}^+]_\infty$ in powers of K_{P} and build a composite expression for the whole domain. Summarizing the results to the first

two nontrivial terms in each branch, when $\lambda[\mathsf{Cl}^-]^3 > K_{\mathrm{W}}^c$, gives

$$[\mathsf{H}^+]_\infty \sim \begin{cases} [\mathsf{H}^+]_{\mathrm{I}} = K_{\mathrm{P}}^{1/3}\left((\lambda K_{\mathrm{W}}^c)^{1/3} + \frac{[\mathsf{Cl}^-]\lambda^{2/3}}{3{K_{\mathrm{W}}^c}^{1/3}} K_{\mathrm{P}}^{1/3}\right), & K_{\mathrm{P}} \ll K_{\mathrm{P}}^{(12)}, \\ [\mathsf{H}^+]_{\mathrm{IIa}} = K_{\mathrm{P}}^{1/2}\left((\lambda[\mathsf{Cl}^-])^{1/2} + \frac{K_{\mathrm{W}}^c}{2[\mathsf{Cl}^-]} K_{\mathrm{P}}^{-1/2}\right), & K_{\mathrm{P}}^{(12)} \ll K_{\mathrm{P}} \ll K_{\mathrm{P}}^{(22)}, \\ [\mathsf{H}^+]_{\mathrm{IIb}} = K_{\mathrm{P}}^{1/2}\left((\lambda[\mathsf{Cl}^-])^{1/2} + \frac{1}{2[\mathsf{Cl}^-]} K_{\mathrm{P}}^{1/2}\right), & K_{\mathrm{P}}^{(22)} \ll K_{\mathrm{P}} \ll K_{\mathrm{P}}^{(23)}, \\ [\mathsf{H}^+]_{\mathrm{IIIa}} = K_{\mathrm{P}}^{2/3}\left(\lambda^{1/3} + \frac{[\mathsf{Cl}^-]\lambda^{2/3}}{3} K_{\mathrm{P}}^{-1/3}\right), & K_{\mathrm{P}}^{(23)} \ll K_{\mathrm{P}} \ll K_{\mathrm{P}}^{(33)}, \\ [\mathsf{H}^+]_{\mathrm{IIIb}} = K_{\mathrm{P}}^{2/3}\left(\lambda^{1/3} - \frac{\lambda}{3} K_{\mathrm{P}}^{1/3}\right), & K_{\mathrm{P}}^{(33)} \ll K_{\mathrm{P}} \ll K_{\mathrm{P}}^{(34)}, \\ [\mathsf{H}^+]_{\mathrm{IV}} = K_{\mathrm{P}}^{1/2}\left(1 - \frac{1}{2\lambda} K_{\mathrm{P}}^{-1/2}\right), & K_{\mathrm{P}} \gg K_{\mathrm{P}}^{(34)}, \end{cases} \tag{B.5}$$

with

$$K_{\mathrm{P}}^{(12)} = \frac{{K_{\mathrm{W}}^c}^2 f^{(12)}}{\lambda[\mathsf{Cl}^-]^3}, \qquad f^{(12)} \simeq 7.723, \qquad K_{\mathrm{P}}^{(22)} = K_{\mathrm{W}}^c, \tag{B.6}$$

$$K_{\mathrm{P}}^{(23)} = \lambda[\mathsf{Cl}^-]^3 f^{(23)}, \qquad f^{(23)} \simeq 0.1295, \qquad K_{\mathrm{P}}^{(33)} = \frac{[\mathsf{Cl}^-]^{3/2}}{\lambda^{1/2}}, \tag{B.7}$$

$$K_{\mathrm{P}}^{(34)} = \frac{f^{(34)}}{\lambda^2}, \qquad f^{(34)} \simeq 2.041, \tag{B.8}$$

determined by enforcing continuity at the transition points. In detail for $K_{\mathrm{P}}^{(12)}$, matching the lower order terms gives the condition $(\lambda K_{\mathrm{W}}^c K_{\mathrm{P}})^{1/3} \simeq (\lambda[\mathsf{Cl}^-]K_{\mathrm{P}})^{1/2}$ implying that $K_{\mathrm{P}}^{(12)}$ has the form ${K_{\mathrm{W}}^c}^2/(\lambda[\mathsf{Cl}^-]^3)$. By letting $K_{\mathrm{P}}^{(12)} = {K_{\mathrm{W}}^c}^2 f^{(12)}/(\lambda[\mathsf{Cl}^-]^3)$ one finds that to enforce continuity at $K_{\mathrm{P}}^{(12)}$, $f^{(12)}$ satisfies $6f^{1/3} + 2f^{2/3} = 6f^{1/2} + 3$ with solution $f^{(12)} \simeq 7.723$. The other values are obtained in a similar fashion. In detail, $f^{(23)} \simeq 0.1295$ satisfies $6f^{1/6} + 3f^{2/3} = 6f^{1/3} + 2$ and $f^{(34)} \simeq 2.041$ satisfies $6f^{2/3} - 2f = 6f^{1/2} - 3$.

The effect of changing $[\mathsf{Cl}^-]$ only changes the domain of region II and at low enough concentrations, $\lambda[\mathsf{Cl}^-]^3 < K_{\mathrm{W}}^c$, branch II is removed and we have the sim-

plified ($[\mathsf{H}^+]_{\text{I}}$ and $[\mathsf{H}^+]_{\text{IIIa}}$ modified) result

$$[\mathsf{H}^+]_\infty \sim \begin{cases} [\mathsf{H}^+]_{\text{I}} = K_{\text{P}}^{1/3}\left((\lambda K_{\text{W}}^c)^{1/3} + \frac{\lambda^{1/3}}{3K_{\text{W}}^{c\,2/3}}K_{\text{P}}\right), & K_{\text{P}} \ll K_{\text{W}}^c, \\ [\mathsf{H}^+]_{\text{IIIa}} = K_{\text{P}}^{2/3}\left(\lambda^{1/3} + \frac{\lambda^{1/3}K_{\text{W}}^c}{3}K_{\text{P}}^{-1}\right), & K_{\text{W}}^c \ll K_{\text{P}} \ll \frac{K_{\text{W}}^{c\,3/4}}{\lambda^{1/2}}, \\ [\mathsf{H}^+]_{\text{IIIb}} = K_{\text{P}}^{2/3}\left(\lambda^{1/3} - \frac{\lambda}{3}K_{\text{P}}^{1/3}\right), & \frac{K_{\text{W}}^{c\,3/4}}{\lambda^{1/2}} \ll K_{\text{P}} \ll K_{\text{P}}^{(34)}, \\ [\mathsf{H}^+]_{\text{IV}} = K_{\text{P}}^{1/2}\left(1 - \frac{1}{2\lambda}K_{\text{P}}^{-1/2}\right), & K_{\text{P}} \gg K_{\text{P}}^{(34)}. \end{cases} \tag{B.9}$$

Algebraically, the $[\mathsf{H}^+]_{\text{IIIa,b}}$ branches could be lost if region II extended into region IV which would require a chlorine concentration in excess of $\lambda^{-1} \sim 191$ M which is not physically possible.

APPENDIX C

Temperature Dependent Rate Coefficients

The rate and equilibrium coefficients for the carbonate system at 298.15 K are described in Table 3.1. In this appendix the temperature dependence of these reactions are given as a continuous function chosen to fit observed experimental data.

Table C.1: Temperature dependent rate and equilibrium constants associated with the carbonic acid system.

Q	Units	$\log_{10} Q(T)$	Ref.
k_1	s^{-1}	$329.850 - 17265.4T^{-1} - 110.54 \log_{10} T$	[41]
k_{-1}	s^{-1}	$13.558 - 3617.1T^{-1}$	[41]
k_2	$\mathsf{M}^{-1}\mathsf{s}^{-1}$	$13.635 - 2895T^{-1}$	[41]
k_{-2}	s^{-1}	$14.09 - 5308T^{-1}$	[41]
K_1	M	$-252.046 + 10047T^{-1} + 86.888 \log_{10} T$	$\frac{k_{-1}k_2}{k_1k_{-2}} K_{\mathrm{W}}^c$
K_2	M	$-107.8871 + 5151.79T^{-1} - 0.03252849T$ $+38.92561 \log_{10} T - 563713.9T^{-2}$	[33]
K_{W}	M^2	$64.7013 - 6013.79T^{-1} - 23.6521 \log_{10} T$	[11]
K_{H}	$\mathsf{M\,atm}^{-1}$	$108.3865 - 6919.53T^{-1} + 0.01985076T$ $-40.45154 \log_{10} T + 669365T^{-2}$	[33]
K_{sp}	M^2	—	[30]

APPENDIX D

Plummer and Wigley, 1976 Data

Table D.1: pH versus time minutes for the dissolution of Icelandic spar in CO_2(g) saturated at 0.97 atm and 25°C. Runs 7–11 reproduced from [34].

Run #7		Run #8		Run #9		Run #10		Run #11		Run #11 (cont)	
min	pH	min	pH	min	pH	min	pH	min	pH	min	pH
0.00	3.919	0.00	3.919	0.00	3.919	0.00	3.919	0.00	3.919	224.00	5.815
0.50	5.050	0.25	4.500	0.25	4.340	1.25	4.230	1.00	4.260	233.00	5.820
1.00	5.280	0.50	4.800	0.50	4.520	2.00	4.450	1.50	4.360	245.00	5.825
1.50	5.420	0.75	4.950	0.75	4.650	2.50	4.530	2.00	4.440	259.00	5.830
2.00	5.500	1.00	5.050	1.00	4.720	3.00	4.580	2.50	4.530	269.00	5.835
3.00	5.620	1.25	5.120	1.25	4.780	4.00	4.680	3.00	4.560	291.00	5.840
4.00	5.700	1.50	5.180	1.50	4.840	5.00	4.750	5.00	4.720	311.00	5.845
5.00	5.750	1.75	5.230	1.75	4.900	6.00	4.830	6.00	4.780	344.00	5.850
6.00	5.790	2.00	5.270	2.00	4.940	7.00	4.880	7.00	4.830	367.00	5.855
7.00	5.820	2.25	5.310	2.25	4.970	8.00	4.925	8.00	4.870	425.00	5.860
8.00	5.840	2.50	5.340	2.50	5.000	9.00	4.960	9.00	4.910	510.00	5.865
9.00	5.860	2.75	5.370	2.75	5.030	10.00	5.040	10.00	4.940	747.00	5.870
11.00	5.890	3.00	5.400	3.00	5.065	11.00	5.080	11.00	4.975	877.00	5.875
13.00	5.905	3.25	5.420	3.50	5.112	12.00	5.110	12.00	5.000	917.00	5.880
15.00	5.940	3.50	5.450	4.00	5.160	13.00	5.140	13.00	5.025	1027.00	5.885
18.00	5.942	4.00	5.490	4.50	5.200	14.00	5.170	14.00	5.050	1087.00	5.890
22.00	5.950	4.50	5.520	5.00	5.230	15.00	5.220	15.00	5.070	1260.00	5.895
27.00	5.958	5.00	5.550	5.50	5.250	18.00	5.290	17.00	5.110	1440.00	5.900
37.00	5.968	5.50	5.580	6.00	5.285	21.00	5.310	19.00	5.140		
52.00	5.978	6.00	5.605	6.50	5.315	22.00	5.330	21.00	5.175		
72.00	5.981	7.00	5.650	7.00	5.335	25.00	5.390	23.00	5.200		
102.00	5.987	8.00	5.690	7.50	5.360	28.00	5.430	25.00	5.230		
152.00	5.989	9.00	5.715	8.00	5.380	31.00	5.460	28.00	5.260		
677.00	5.999	11.00	5.763	8.50	5.400	35.00	5.480	30.00	5.282		
		13.00	5.800	9.00	5.420	40.00	5.580	33.00	5.320		
		15.00	5.825	10.00	5.450	45.00	5.620	36.00	5.350		
		18.00	5.855	11.00	5.480	50.00	5.650	40.00	5.376		
		23.00	5.890	12.00	5.510	55.00	5.680	43.00	5.398		
		28.00	5.910	13.00	5.530	65.00	5.730	46.50	5.420		
		33.00	5.924	14.00	5.552	75.00	5.755	51.00	5.455		
		38.00	5.932	15.00	5.571	91.00	5.780	56.00	5.478		
		43.00	5.940	17.00	5.610	175.00	5.820	61.00	5.500		
		53.00	5.951	19.00	5.640	205.00	5.838	66.00	5.522		
		94.00	5.969	21.00	5.678	355.00	5.872	70.00	5.540		
		169.00	5.980	23.00	5.700	475.00	5.896	75.00	5.558		
		964.00	6.020	25.00	5.722	1210.00	5.902	80.00	5.580		
				30.00	5.770			85.00	5.595		
				35.00	5.805			92.00	5.620		
				40.00	5.831			98.00	5.632		
				45.00	5.835			104.00	5.658		
				55.00	5.890			115.00	5.695		
				65.00	5.911			126.00	5.715		
				75.00	5.930			139.00	5.735		
				85.00	5.942			147.00	5.745		
				115.00	5.969			161.00	5.765		
				145.00	5.982			176.00	5.780		
				175.00	5.990			189.00	5.790		
				205.00	5.991			195.00	5.795		
				475.00	6.000			210.00	5.805		

Table D.2: pH versus time minutes for the dissolution of Icelandic spar in CO_2(g) saturated at 0.97 atm and $25°$C. Runs 12–14 reproduced from [34].

Run #12		Run #12 (cont)		Run #13		Run #13 (cont)		Run #14		Run #14 (cont)	
min	pH	min	pH	min	pH	min	pH	min	pH	min	pH
0.00	3.919	115.00	5.630	0.00	3.919	75.00	5.197	0.00	3.919	130.00	5.700
1.00	3.980	135.00	5.665	1.00	3.970	80.00	5.220	1.00	4.120	160.00	5.755
2.00	4.120	165.00	5.715	2.00	4.060	85.00	5.240	2.00	4.250	190.00	5.780
3.00	4.240	195.00	5.755	3.00	4.140	90.00	5.260	3.00	4.360	210.00	5.800
4.00	4.330	225.00	5.788	4.00	4.200	100.00	5.300	4.00	4.480	250.00	5.810
5.00	4.400	255.00	5.812	5.00	4.260	110.00	5.330	5.00	4.560	290.00	5.820
6.00	4.470	285.00	5.835	6.00	4.310	120.00	5.360	6.00	4.630	356.00	5.837
7.00	4.520	315.00	5.855	7.00	4.360	130.00	5.385	7.00	4.690	965.00	5.872
8.00	4.580	345.00	5.865	8.00	4.400	140.00	5.406	8.00	4.750		
9.00	4.620	375.00	5.872	9.00	4.440	150.00	5.420	9.00	4.790		
10.00	4.660	405.00	5.880	10.00	4.470	180.00	5.479	10.00	4.840		
11.00	4.700	435.00	5.886	11.00	4.500	210.00	5.522	11.00	4.880		
12.00	4.730	720.00	5.920	12.00	4.530	240.00	5.560	12.00	4.910		
13.00	4.760	1295.00	5.930	13.00	4.560	270.00	5.592	13.00	4.950		
14.00	4.790	2375.00	5.950	14.00	4.590	300.00	5.620	14.00	4.980		
15.00	4.820			15.00	4.610	330.00	5.645	15.00	5.010		
16.00	4.850			16.00	4.636	360.00	5.668	16.00	5.035		
16.00	4.870			17.00	4.660	390.00	5.685	17.00	5.060		
17.00	4.890			18.00	4.680	420.00	5.700	18.00	5.080		
18.00	4.910			19.00	4.700	450.00	5.710	19.00	5.100		
19.00	4.930			20.00	4.715	490.00	5.730	20.00	5.120		
20.00	5.020			22.00	4.750	515.00	5.735	28.00	5.220		
25.00	5.100			24.00	4.780	715.00	5.780	30.00	5.250		
35.00	5.180			26.00	4.810	945.00	5.810	35.00	5.300		
40.00	5.230			28.00	4.840	1155.00	5.825	40.00	5.350		
45.00	5.270			30.00	4.860	1350.00	5.840	45.00	5.390		
50.00	5.320			35.00	4.920	1710.00	5.850	50.00	5.430		
55.00	5.360			40.00	4.967	1950.00	5.865	55.00	5.460		
60.00	5.400			45.00	5.005	2175.00	5.870	60.00	5.500		
65.00	5.430			50.00	5.045	2925.00	5.885	70.00	5.540		
75.00	5.480			55.00	5.080			80.00	5.570		
85.00	5.520			60.00	5.112			90.00	5.600		
95.00	5.560			65.00	5.140			100.00	5.635		
105.00	5.595			70.00	5.170			107.00	5.660		

APPENDIX E

Plummer, Wigley, and Parkhurt, 1978

Data

Table E.1: pH-stat results in the range $3.8 < \mathrm{pH} < 5.5$. Data is reproduced from Table 1 of [35]. 'Air' denotes $P_{\mathsf{CO}_2} = 10^{-3.5}$ atm $\simeq 316$ ppm.

Run no.	Temp (°C)	P_{CO_2} (atm)	Stirring rate (rpm)	κ_1 ($\mathrm{cm\,s^{-1}}$)	$\log_{10}(\kappa_2([H_2CO_3{}^0]+$ $+[CO_2]) + \kappa_3)$
100	2.5	Air	1800	0.039	-6.721
90	11.5	Air	1800	0.043	-6.699
63	25.0	0.003	800	0.043	-6.620
70	25.0	0.003	800	0.046	-6.699
75	25.0	0.003	1800	0.051	-6.585
62	25.0	0.10	800	0.049	-6.523
72	25.0	0.10	800	0.049	-6.523
81	25.0	0.10	1300	0.049	-6.523
61	25.0	0.30	800	0.059	-6.260
71	25.0	0.30	800	0.059	-6.260
79	25.0	0.48	1300	0.052	-6.125
80	25.0	0.48	1300	0.052	-6.125
78	25.0	0.67	1300	0.052	-5.979
69	25.0	0.97	1300	0.049	–
77	25.0	0.96	1100	0.056	-5.824
85	34.0	Air	800	0.068	-6.301
85	34.0	Air	1800	0.077	-6.301
85	34.0	Air	2300	0.082	-6.301
91	34.0	Air	1800	0.050	-6.260
92	34.0	Air	800	0.043	-6.260
93	34.0	Air	1300	0.053	-6.284
94	34.0	Air	1800	0.057	-6.301
95	34.0	Air	2300	0.064	-6.456
96	34.0	Air	800	0.054	-6.398
97	34.0	Air	1300	0.060	-6.301
98	34.0	Air	1800	0.064	-6.569
99	34.0	Air	1800	0.056	-6.161
87	45.0	Air	2300	0.068	-6.022
88	55.0	Air	2300	0.071	-6.027
89	70.0	Air	2300	0.075	-5.757

Table E.2: free-drift results reproduced from Table 2 of [35].

Run no.	Temp (°C)	P_{CO_2} (atm)	κ_1 ($cm\,s^{-1}$)	$\log_{10}(\kappa_2([H_2CO_3^0]+$ $+[CO_2])+\kappa_3)$	$\log_{10}\kappa_4$
29	5.0	0.03030	0.03997	-6.959	-2.101
27	5.0	0.28400	0.03997	-6.502	-2.238
5	5.0	0.95700	0.03997	-6.195	-2.277
3	5.0	0.96600	0.03997	-6.040	-2.199
6	5.0	0.96900	0.03997	-6.064	-2.204
4	5.0	0.97400	0.03997	-6.162	-2.259
26	15.0	0.00290	0.04541	-6.879	-1.255
21	15.0	0.02990	0.04541	-6.914	-1.832
19	15.0	0.28000	0.04541	-6.783	-2.268
8	15.0	0.96600	0.04541	-6.045	-2.017
9	15.0	0.97800	0.04541	-6.025	-2.032
17	25.0	0.00280	0.05115	-6.896	-1.031
14	25.0	0.00286	0.05115	-6.921	-1.040
13	25.0	0.02950	0.05115	-6.775	-1.604
16	25.0	0.02950	0.05115	-6.796	-1.577
12	25.0	0.27700	0.05115	-6.406	-1.826
10	25.0	0.95500	0.05115	-5.932	-1.754
11	25.0	0.95500	0.05115	-5.995	-1.739
15	25.0	0.96200	0.05115	-5.979	-1.650
38	25.0	0.95700	0.05115	-5.884	-1.638
B1	27.0	0.94500	0.05233	-5.924	-1.673
B2	27.5	0.94500	0.05263	-5.903	-1.638
31	34.0	0.02920	0.05655	-6.666	-1.358
32	34.0	0.29800	0.05655	-6.201	-1.490
30	34.0	0.94600	0.05655	-5.847	-1.460
B3	34.0	0.92800	0.05655	-5.831	-1.419
B4	34.9	0.92800	0.05711	-5.809	-1.415
36	48.0	0.02740	0.06538	-6.400	-0.893
35	48.0	0.28100	0.06538	-6.001	-1.079
34	48.0	0.28000	0.06538	-5.984	-1.059
37	48.0	0.88500	0.06538	-5.601	-1.060
B5	49.0	0.86400	0.06603	-5.586	-1.044
B6	49.0	0.86400	0.06603	-5.600	-1.032
B7	62.0	0.75400	0.07468	-5.448	-0.669
B8	62.8	0.74500	0.07523	-5.460	-0.642

APPENDIX F

Computer Code

F.1 Model Code

```
function bvp_vonKarman_cub_new_2020

clc
clear all
close all

ZL = 5; % Maximum distance over which to solve the PDE
Cl = 1e-2; % [Cl-] concentration to set the pH of the fluid
PCO2inPPM = 400e-6; % PCO2 = 400 ppm in
P0 = 1; % 1 atm of air
Tc = 25; % T = 25 Celcius
rpm = 100; % Rotation rate in rpm
PCO2 = PCO2inPPM*P0; % The actual partial pressure of CO2

flags_newton = 1; % Flag to show [H0] and [Hinf] details (Newton solvers)
flags_rundata = 1; % Show parameters of the run
flags_kvals = 1; % Flag to show k values
flags_consistency = 1; % Consistency checks
% A) KP, 2*Ksp/K2/KP, KW, 2*K2*KP with values reports in section 3.3.3
% B) H0, KW/H0, KP/H0, K2*KP/H0^2 with approximate values using [Cl]
% C) Hinf, KW/Hinf, KP/Hinf, K2*KP/Hinf^2, Ksp*Hinf^2/K2/KP
flags_showh0 = 1; % Dumps out the calculation of h0
flags_showhinf = 1; % Dumps out the calculation of hinf
flags_init = 0;% Diagnostic flag to show initial guesses for the fcns
```

```
%-------------------------------------------------------------------------
% State the run parameters
%-------------------------------------------------------------------------
if flags_rundata == 1
    fprintf('Dynamic code solving on ZL = %5.3f at a temperature of Tc = %5.3f\n',ZL,Tc)
    fprintf('Chlorine concentration of %5.3e (pH = %5.3f)\n',Cl,-log10(Cl))
    fprintf('PCO2 pressure of %7.3f ppm in %5.3f atm\n',PCO2inPPM*1e6,P0)
    fprintf('Rotation rate of %7.3f rpm\n',rpm)
    if flags_kvals == 1
        fprintf('TRUE: Show k values\n')
    else
        fprintf('FALSE: Show k values\n')
    end
    if flags_newton == 1
        fprintf('TRUE: Show [H0], [Hinf] details\n')
    else
        fprintf('FALSE: Show [H0], [Hinf] details\n')
    end
    if flags_init == 1
        fprintf('TRUE: Show initial functions\n')
    else
        fprintf('FALSE: Show initial functions\n\n')
    end
end
%-------------------------------------------------------------------------
% Get the rates and the equilibrium values
%-------------------------------------------------------------------------
set1 = rock_kcarbonatevals(Tc);
k1 = set1(1); km1 = set1(2); k2 = set1(3); km2 = set1(4);
KW=set1(5); K2=set1(6); K1=set1(7); KH=set1(8); K1prime=K1*k1/(k1+km1);
Ksp=set1(9);
KP = k2/km2*KW*KH*PCO2;
if flags_kvals == 1
    fprintf('Chemical parameters at T = %5.2fK (%5.2fC)\n',Tc + 273.16,Tc);
    fprintf('k+1 = %6.3e  ',k1)
    fprintf('k-1 = %6.3e  \n',km1)
    fprintf('k+2 = %6.3e  ',k2)
    fprintf('k-2 = %6.3e\n',km2)
    fprintf('K1  = %6.3e  ',K1)
    fprintf('K1'' = %6.3e  \n',K1prime)
    fprintf('K2  = %6.3e  \n',K2)
    fprintf('KW  = %6.3e  ',KW)
    fprintf('KH  = %6.3e\n',KH)
    fprintf('Ksp = %6.3e\n',Ksp)
end
```

```
if flags_consistency == 1
    fprintf('\nTest of consistency (K values).\n')
    fprintf('These two lines should be the same at 25C\n')
    fprintf('[KP=%6.3e 2*Ksp/K2/KP=%6.3e KW=%6.3e 2*K2*KP=%6.3e] (Calculated)\n',.
        KP,2*Ksp/K2/KP,KW,2*K2*KP)
    fprintf('[KP=%6.3e 2*Ksp/K2/KP=%6.3e KW=%6.3e 2*K2*KP=%6.3e] (Thesis section 3
        5.99e-12,3.19e13,1.01e-14,5.61e-22)
end
%-------------------------------------------------------------------------
% Find the value of [HO] (Hydrogen level when [Ca] = 0 and [CO2] = 1)
%-------------------------------------------------------------------------
% [HO] satisfies f = HO^3 - Cl*HO^2 - (KW+KP)*HO - 2*K2*KP = 0 and we
% choose [HO] = lam*[Cl] with lam = 1 initially.
% Interate to find lam with f = lam^3 - lam^2 - (KW+KP)/Cl^2*lam - 2*K2*KP/Cl^3 =
lam = 1;j = 1;f = 1;
if flags_newton == 1, fprintf('Newton iterations to compute HO\n'), end
while (j < 20 && abs(f) > eps)
    if flags_newton == 1, fprintf('j = %3i lam = %16.13e err = %5.3e\n',j,lam,f),
    f = lam^3 - lam^2 - (KW+KP)/Cl^2*lam - 2*K2*KP/Cl^3;
    fp = 3*lam^2 - 2*lam - (KW+KP)/Cl^2;
    lam = lam - f/fp;
    j = j + 1;
end
HO = lam*Cl;
if abs(f) > eps
    fprintf('ERROR: HO DID NOT CONVERGE\n')
else
    fprintf('j = %3i lam = %16.13e err = %5.3e\n',j,lam,f)
end
fprintf('Computed HO = %16.13e\n',HO)
if flags_consistency == 1
    fprintf('\nTest of consistency (HO values).\n')
    fprintf('(Calculated)                (Thesis section 3.3.3)\n')
    fprintf('(H)   =%16.13e (H)   =%16.13e\n',HO,Cl)
    fprintf('(OH)  =%16.13e (OH)  =%16.13e\n',KW/HO,KW/Cl)
    fprintf('(HCO3)=%16.13e (HCO3)=%16.13e\n',KP/HO,KP/Cl)
    fprintf('(CO3) =%16.13e (CO3) =%16.13e\n\n',K2*KP/HO^2,K2*KP/Cl^2)
end
%-------------------------------------------------------------------------
% Find the value of [Hinf] (Hydrogen level when [Ca] = [Ca]_{max} and [CO2] = 1)
%-------------------------------------------------------------------------
% [Hinf] satisfies f = 2*KP/K2KP*Hinf^4 + Hinf^3 - Cl*Hinf^2 - (KW+KP)*Hinf - 2*
% choose [Hinf] = lam*sqrt(K2*KP*Cl/2/Ksp) with lam = 1 initially.
% Interate to find lam with
% f = lam^4 + gam/Cl*lam^3 - lam^2 - (KW+KP)/Cl/gam*lam - 2*K2*KP/Cl/gam^2 = 0
```

```
% and gam = sqrt(K2*KP*Cl/2/Ksp)
lam = 1;j = 1;f = 1;
gam = sqrt(K2*KP*Cl/2/Ksp);
if flags_newton == 1, fprintf('Newton iterations to compute Hinf\n'), end
while (j < 20 && abs(f) > eps)
    if flags_newton == 1, fprintf('j = %3i lam = %16.13e err = %5.3e\n',j,lam,f), end
    f = lam^4 + lam^3*gam/Cl - lam^2 - (KW+KP)/Cl/gam*lam - 2*K2*KP/Cl/gam^2;
    fp = 4*lam^3 + 3*lam^2*gam/Cl - 2*lam - (KW+KP)/Cl/gam;
    lam = lam - f/fp;
    j = j + 1;
end
Hinf = lam*gam;
if abs(f) > eps
    fprintf('ERROR: Hinf DID NOT CONVERGE\n')
else
    fprintf('j = %3i lam = %16.13e err = %5.3e\n',j,lam,f)
end
fprintf('Computed Hinf = %16.13e\n',Hinf)
if flags_consistency == 1
    fprintf('\nTest of consistency ([Hinf] values).\n')
    fprintf('(Calculated)                (Thesis section 3.3.3)\n')
    fprintf('(H)   =%16.13e (H)   =%16.13e\n',Hinf,gam)
    fprintf('(OH)  =%16.13e (OH)  =%16.13e\n',KW/Hinf,KW/gam)
    fprintf('(HCO3)=%16.13e (HCO3)=%16.13e\n',KP/Hinf,KP/gam)
    fprintf('(CO3) =%16.13e (CO3) =%16.13e\n',K2*KP/Hinf^2,K2*KP/gam^2)
    fprintf('(Ca)  =%16.13e (Ca)  =%16.13e\n\n',Ksp*Hinf^2/K2/KP,Ksp*gam^2/K2/KP)
end
cmax = Ksp*Hinf^2/K2/KP;
%-------------------------------------------------------------------------
% Returns the physical parameters of the experiment
%-------------------------------------------------------------------------
% 1A: DCO2 (Diffusion coefficient of dissolved CO2: Zeebe, 2011)
% 1B: nu (Viscosity of water: Kreslin, 1978)
% 1: Sc (Schmidt number)
% 2: Re (Reynolds number)
% 3: omega (Rotation rate in rad/sec)
% 4: cs (Molarity of calcium in a calcite crystal)
% 5: Rd (Radius of sample)
% 6: Ru (Radius of container)
set2 = rock_carbonatedissnparams(Tc,rpm);
Sc = set2(1); Re = set2(2);
omega = set2(3);
cs = set2(4);
%Rd = set2(5); Ru = set2(6);
St = (cs-cmax)/cmax;
```

```
if flags_rundata == 1
    fprintf('Reynolds number: %10.6f\n',Re)
    fprintf('Schmidt number: %10.6f\n',Sc)
    fprintf('Rotation rate: %10.6f rad/sec\n',omega)
    fprintf('[Ca2+] in calcite = %10.6f mol/l\n',cs)
    fprintf('Stefan number: %10.6e (exact) %10.6e (approx)\n',St,(cs-Cl/2)/(Cl/2))
    fprintf('[Ca2+] maximal value: %10.6e (exact) %10.6e (approx)\n\n',cmax,Cl/2)
end
%-------------------------------------------------------------------------
% Details of the system of equations
%-------------------------------------------------------------------------
% This code solves the fluid transition (von Karman) flow along with the
% concentration equations with zero order u,b,c.  Solving this bvp
% consisting of a higher-order ODEs using bvp4c built in routine
%
%      y^(n) = f(x,y,y',...,y^(n-1)) with  BV: y(a)=ya, y(b)=yb, ...
%
% Rewritten as a system of 1st order ODEs Y'=F(x,Y) with BC: Y(b)=[y0;y1;...]
% with the differential equations are: (the indepenent variable is z)
%
%      F'' = F^2 - G^2 + F'*H,
%      G'' = 2*F*G + G'*H,
%      2*F +H' = 0.
%
% In the von Karman Fluid flow H is the vertical component, G is the flow
% theta direction and F is the radial component direction and F is the
% subject to the following boundary conditions
%
%      F(0) = 0, G(0) = 1, H(0) = 0,
%      F(infinity) = 0, G(infinity) = 0.
%
% For the Ca2+, HCO2-
%
%      H*c' - c''/Sc = 0,
%      c(0) = (H0/Hinf)^2*h0^2/u0, c(infinity) = 0,
%
% From the third equation H'= -2F, by subsituting for F and its derivatives
% with H we reduce to two variables
%
% a) -0.5*H''' = (-0.5*H')^2 - (G)^2 + (-0.5H'')*H or
%    H''' = -0.5*(H')^2 + 2*(G)^2 + H''*H,       (A.7a)
% b) G'' = 2*(-0.5*H')*G + G'*H or
%    G'' = -H'*G + G'*H.                         (A.7b)
%
% with boundary conditions
```

```
%
% H(0) = 0, H'(0) = 0, H'(infinity) = 0,
% G(0) = 1, G(infinity) = 0.
%
% Start with letting y1 = H, y2 = H', y3 = H'', y4 = G, y5 = G'
%
% y1' = y2, y1(0) = 0,
% y2' = y3, y2(0) = 0, y2(infinity) = 0,
% y3' = -0.5*y2^2 + 2*y4^2 + y1*y3, y3(0) = ? (H''(0) = -2*a1)
% y4' = y5, y4(0) = 1, y4(infinity) = 0,
% y5' = -y2*y4 + y1*y5, y5(0) = ? (G'(0) = b1)
%
% Taking y6 = c, y7 = c'
%
% y6' = y7, y6(0) = (H0/Hinf)^2*h0^2/u0
% y7' = Sc*y1*y7, y6(infinity) = 0.
%-------------------------------------------------------------------------
%-------------------------------------------------------------------------
% Verify that h0 with u0 = 1 gives back Hinf
%-------------------------------------------------------------------------
if flags_showh0 == 1
    temp = geth0(1,0,0);
    fprintf('Verify that h0 with u0 = 1 gives back Hinf\n')
    fprintf('h0 with u0 = 1 is %16.13e, Hinf = %16.13e\n\n',temp(1)*H0,Hinf)
end
%-------------------------------------------------------------------------
% Verify that hinf with cinf = 0 gives back H0
%-------------------------------------------------------------------------
if flags_showhinf == 1
    temp = gethinf(0,0,0);
    fprintf('Verify that hinf with cinf = 0 gives back H0\n')
    fprintf('hinf with cinf = 0 is %16.13e, H0 = %16.13e\n\n',temp(1)*H0,H0)
end
%-------------------------------------------------------------------------
% Verify that hinf bridges H0 to Hinf as 0 \le cinf \le 1
%-------------------------------------------------------------------------
if (flags_showhinf == 1) || (flags_showh0 == 1)
    cvals = linspace(0,1);
    for jjj = 1:length(cvals)
        temp = gethinf(cvals(jjj),0,0);
        hinfvals(jjj) = temp(1);
        fprintf('j=%5i c=%16.13e h=%16.13e\n',jjj,cvals(jjj),temp(1))
    end
    figure(20)
    semilogy(cvals,hinfvals,'b-o'), hold on
```

```
    plot([0.945 0.945],[1e-8 2.835131840451e3],'r-')
end

%u0vals = logspace(-8,-6,60); ROUGH 1
%u0vals = linspace(1.3e-7,1.6e-7,30); REFINED 1

% Summary of the solutions that have been extracted
% cinf Bound(left) Bound(right) ZL RelTol AbsTol
% Default RelTol = 1e-3 Default AbsTol = 1e-6
SOLS = [...
    0.99  9.0e-1 1.0e0 9.9936242587e-1 5 1e-3 1e-6;...
    0.98  9.0e-1 1.0e0 9.9666246710e-1 5 1e-3 1e-6;...
    0.97  9.0e-1 1.0e0 9.93645085210e-1 5 1e-3 1e-6;...
    0.969 9.0e-1 1.0e0 9.985452182044e-1 5 1e-3 1e-6;...
    0.968 9.0e-1 1.0e0 1.047413945080e0 5 1e-3 1e-6;...
    0.967 1.0e0  4.0e0 3.53407650362e0 5 1e-3 1e-6;...
    0.966 2.0e1  2.5e1 2.080169670e1 5 1e-3 1e-6;...
    0.965 5.0e1  6.0e1 5.60779170952e1 5 1e-3 1e-6;...
    0.964 1.0e2  1.1e2 1.068107576783e2 5 1e-3 1e-6;...
    0.963 1.6e2  1.8e2 1.710279514449e2 5 1e-3 1e-6;...
    0.962 2.4e2  2.5e2 2.473265159132e2 5 1e-3 1e-6;...
    0.961 3.3e2  3.4e2 3.34658969038e2 5 1e-3 1e-6;...
    0.960 4.3e2  4.4e2 4.3220863434727e2 5 1e-3 1e-6;...
    0.955 1.0e3  1.1e3 1.0535671553495e3 5 1e-3 1e-6;...
    0.950 1.8e3  1.9e3 1.864222196518e3 5 1e-3 1e-6;...
    0.945 2.8e3  2.9e3 2.835131840451e3 5 1e-3 1e-6;...
    0.940 3.4e3  3.5e3 2.835131840451e3 5 1e-3 1e-6];

myrow = 15;
%myrow = 17;
semilogy(SOLS(:,1),SOLS(:,4),'ro')

% Z = 5,
%u0vals = linspace(0.9993625,0.9993626,2); %cinf = 0.99
%u0vals = linspace(0.9966629,0.9966630,2); %cinf = 0.98
%u0vals = linspace(0.9936459,0.9936460,2); %cinf = 0.97
%u0vals = linspace(0.9985453,0.9985454,2); %cinf = 0.969
%u0vals = linspace(1.04740633,1.04740634,2); %cinf = 0.968
%u0vals = linspace(3.53347531,3.53347533,2); %cinf = 0.967
%u0vals = linspace(2.07963447e1,2.07963448e1,2); %cinf = 0.966
%u0vals = linspace(5.60632461e1,5.60632462e1,2); %cinf = 0.965
%u0vals = linspace(1.06783053e2,1.06783054e2,2); %cinf = 0.964
%u0vals = linspace(1.70984203e2,1.70984204e2,2); %cinf = 0.963
%u0vals = linspace(2.47263844e2,2.47263845e2,2); %cinf = 0.962
%u0vals = linspace(3.34574965e2,3.34574965e2,2); %cinf = 0.961
```

```
%u0vals = linspace(4.32101011e2,4.32101012e2,2); %cinf = 0.96
%u0vals = linspace(1.86377779e3,1.86377780e3,2); %cinf = 0.95
%u0vals = linspace(1.86377779e3,1.86377780e3,2); %cinf = 0.95 Z = 3

% %u0vals = linspace(1.8684281010333,1.8684281010335,2); %cinf = 0.95 Z = 2
% Left value input = 1.8642221696932e+03
% New           u0 = 1.8642221965180e+03
%                    1.8642222591002e+03
% Results:  49: u0 1.86422217e+03 up0 7.52680772e-05
% Left value output = 7.5268077246503e-05
% Right value input = 1.8642222591002e+03
% Results:  50: u0 1.86422226e+03 up0 -1.75596884e-04
% Right value output = -1.7559688440612e-04
% New u0 = 1.8642221965183e+03


% myc = [0.99 0.98 0.97...
%     0.969 0.968 0.967...
%     0.966 0.965 0.964...
%     0.963 0.962 0.961...
%     0.96  0.95];
% myu0 = [0.9993625 0.9966629 0.9936459...
%     0.9985453 1.04740633 3.53347531...
%     2.07963447e1 5.60632461e1 1.06783053e2...
%     1.70984203e2 2.47263844e2 3.34574965e2...
%     4.32101011e2 1.86377779e3];
% figure(50)
% semilogy(myc,myu0,'b-o')

u0valsL = SOLS(myrow,2);
u0valsR = SOLS(myrow,3);
ZL = SOLS(myrow,5);

%-------------------------------------------------------------------------
% There are three mode of operating:
% Single solution
%   Given a u0, cinf value compute the curves (u, b, c, and h)
%   and display the curves
% Bounds
% Given two values of u0 and a single cinf, determine the the these
%   u0 values bracket a solution where u0'(0) = 0
% Interation
method = 'Solution';
%method = 'Bounds';
%method = 'Search';
```

```
340
341 switch lower(method)
342     case 'solution'
343         NUMITERS = 1;
344         fprintf('\nSolving for a single solution\n')
345     case 'bounds'
346         NUMITERS = 2;
347         fprintf('\nDetermining if a solution is bounded\n')
348     case 'search'
349         NUMITERS = 15;
350         fprintf('\nIterating to optimize the solution\n')
351     otherwise
352         NUMITERS = 0;
353         fprintf('\nUnknown method\n')
354 end
355
356 for loop = 1:NUMITERS
357     %-------------------------------------------------------------------------
358     % For a give u0 determine h0 and then b0, c0
359     %-------------------------------------------------------------------------
360     if NUMITERS > 1
361         if mod(loop,2)==1
362             u0 = u0valsL;
363 %             fprintf('Left value input = %16.13e\n',u0)
364         else
365             u0 = u0valsR;
366 %             fprintf('Right value input = %16.13e\n',u0)
367         end
368     end
369     if NUMITERS == 1, u0 = SOLS(myrow,4); end
370     temp = geth0(u0,0,0);
371     h0 = temp(1);
372     b0 = temp(2);
373     c0 = temp(3);
374     %-------------------------------------------------------------------------
375     % For a give cinf determine hinf and then binf
376     %-------------------------------------------------------------------------
377     cinf = SOLS(myrow,1);
378     uinf = 1;
379     temp = gethinf(cinf,0,0);
380     hinf = temp(1);
381     binf = temp(2);
382     %cinf = temp(3);
383     %-------------------------------------------------------------------------
384     % Show the initial guesses for the various quantities
```

```
%-------------------------------------------------------------------------
temp = show_inits(flags_init);
%-------------------------------------------------------------------------
% Solve the higher-order ODE as a system of first-order ODEs
%-------------------------------------------------------------------------
%  solver = 'bvp4c';
solver = 'bvp5c';
bvpsolver = fcnchk(solver);
if flags_rundata == 1, options = bvpset('stats','on'); end
options = bvpset('RelTol',SOLS(myrow,6),'AbsTol',SOLS(myrow,7));
solinit = bvpinit([0,ZL],@fcnsinit);
sol = bvpsolver(@fcnsSolns,@fcnsBC,solinit,options);
%sol = bvpsolver(@fcnsSolns,@fcnsBC,solinit);
%-------------------------------------------------------------------------
% Extract the solution
% y1 = H, y2 = H', y3 = H'', y4 = G, y5 = G'
% y6 = c, y7 = c', y8 = b, y9 = b', y10 = u, y11 = u'
%-------------------------------------------------------------------------
xfin = linspace(0,ZL);
yfin = deval(sol,xfin);
%H = yfin(1,:);
%Hp = yfin(2,:):
%Hpp = yfin(3,:);
%G = yfin(4,:);
%Gp = yfin(5,:);
%F = -0.5*yfin(2,:);
c = yfin(6,:);
%cp = yfin(7,:);
b = yfin(8,:);
%bp = yfin(9,:);
u = yfin(10,:);
up = yfin(11,:);
%-------------------------------------------------------------------------
% Extract the h from the c and b values for charge balance
%-------------------------------------------------------------------------
AA = 1;
BB = 2*Ksp*Hinf^2*c/K2/KP/H0 - KP*b/Hinf/H0 - Cl/H0;
CC = -KW/H0^2 - 2*K2*KP/H0^2/Hinf*b;
hp = -BB/2 + sqrt(BB.^2 - 4*AA.*CC)/2;
hn = -BB/2 - sqrt(BB.^2 - 4*AA.*CC)/2;
%-------------------------------------------------------------------------
brhsplot = Hinf*u./H0./hp - b;
urhsplot = -k1/omega*H0/Hinf*(hp+k2*KW/k1/H0).*(Hinf*u./H0./hp-b);
%-------------------------------------------------------------------------
% If there is a single solution then dump out the curves
```

```
430     %-------------------------------------------------------------------------
431     if NUMITERS == 1
432         %         if toggle == 0
433         %             figure1 = figure(1);
434         %             axes1 = axes('Parent',figure1,'FontSize',16);
435         %             hold(axes1,'all');
436         %             title('Velocity components','FontSize',18)
437         %             xlabel('\zeta','FontSize',16);
438         %         end
439         %             plot(xfin,F,'b-','LineWidth',2,'Parent',axes1)
440         %             plot(xfin,G,'g-','LineWidth',2,'Parent',axes1)
441         %             plot(xfin,H,'r-','LineWidth',2,'Parent',axes1)
442         %             legend(axes1,'show','F','G','H')
443
444         %         if toggle == 0
445         %             figure2 = figure(2);
446         %             axes2 = axes('Parent',figure2,'FontSize',16);
447         %             hold(axes2,'all');
448         %             title('[Ca2+](\zeta)','FontSize',18)
449         %             xlabel('\zeta','FontSize',16);
450         %         end
451         figure(1)
452         plot(xfin,c,'b-','LineWidth',2), hold on
453         title('[Ca2+](\zeta)','FontSize',18)
454
455         %         figure(1)
456         %         plot(xfin,u,'b-','LineWidth',2), hold on
457         %         figure(2)
458         %         plot(xfin,c,'b-','LineWidth',2), hold on
459         %            ylim([0 1])
460         %         if toggle == 0
461         %             figure3 = figure(3);
462         %             axes3 = axes('Parent',figure3,'FontSize',16);
463         %             hold(axes3,'all');
464         %             title('[HCO3-](\zeta)','FontSize',18)
465         %             xlabel('\zeta','FontSize',16);
466         %         end
467         figure(2)
468         plot(xfin,b,'b-','LineWidth',2), hold on
469         title('[HCO3-](\zeta)','FontSize',18)
470
471         %         if toggle == 0
472         %             figure4 = figure(4);
473         %             axes4 = axes('Parent',figure4,'FontSize',16);
474         %             hold(axes4,'all');
```

```
475         %             title('[CO2](\zeta)','FontSize',18)
476         %             xlabel('\zeta','FontSize',16);
477         %         end
478         figure(3)
479         plot(xfin,u,'b-','LineWidth',2), hold on
480         title('[CO2](\zeta)','FontSize',18)
481
482         %         if toggle == 0
483         %             figure5 = figure(5);
484         %             axes5 = axes('Parent',figure5,'FontSize',16);
485         %             hold(axes5,'all');
486         %             title('[H+](\zeta)','FontSize',18)
487         %             xlabel('\zeta','FontSize',16);
488         %         end
489         figure(4)
490         plot(xfin,hp,'b-','LineWidth',2), hold on
491         title('[H+](\zeta)','FontSize',18)
492         figure(5)
493         plot(xfin,brhsplot,'bo','LineWidth',2), hold on
494         title('brhs','FontSize',18)
495         figure(6)
496         plot(xfin,urhsplot,'bo','LineWidth',2), hold on
497         title('urhs','FontSize',18)
498     end
499     fprintf('Loop = %3i\n',loop)
500     u0vals(loop) = u0;
501     upvals(loop) = up(1);
502     %-------------------------------------------------------------------------
503     % Every two iterations update to a new estimate of u0 such that
504     % u0'(0) = 0
505     %-------------------------------------------------------------------------
506     if mod(loop,2)==1
507         fLEFT = up(1);
508         fprintf('L: %16.13e f(L) = %16.13e\n',u(1),up(1))
509     else
510         fRIGHT = up(1);
511         fprintf('R: %16.13e f(L) = %16.13e\n',u(1),up(1))
512         u0new = u0valsL - fLEFT*(u0valsR-u0valsL)/(fRIGHT-fLEFT);
513         fprintf('N: %16.13e\n',u0new)
514         if abs(fLEFT) < abs(fRIGHT)
515             u0valsR = u0new;
516         else
517             u0valsL = u0new;
518         end
519         if NUMITERS == 2
```

```
            figure
            plot(u0vals,upvals,'bo-')
        end
    end
end


%-------------------------------------------------------------------------
% EMBEDDED FUNCTIONS
%-------------------------------------------------------------------------

    function dydx = fcnsSolns(x,y)
        % Start with letting y1 = H, y2 = H', y3 = H'', y4 = G, y5 = G'
        %
        % y1' = y2, y1(0) = 0,
        % y2' = y3, y2(0) = 0, y2(infinity) = 0,
        % y3' = -0.5*y2^2 + 2*y4^2 + y1*y3, y3(0) = ? (H''(0) = -2*a1)
        % y4' = y5, y4(0) = 1, y4(infinity) = 0,
        % y5' = -y2*y4 + y1*y5, y5(0) = ? (G'(0) = b1)
        %
        % y6 = c, y7 = c'
        % y8 = b, y9 = b'
        % y10= u, y11= u'
        %
        % y6' = y7, y6(0) = (H0/Hinf)^2*h0^2/u0,
        % y7' = Sc*y1*y7, y6(infinity) = 0,
        % y8' = y9,
        % y9' = Sc*y1*y9 - Sc*km2/omega/h*(Hinf*u/H0-b*h)
        % y10'= y11,
        % y11'= Sc*y1*y11 - Sc*k1/omega*H0/Hinf*(h+k2*KW/k1/H0)*(Hinf*u/H0-b*h)
        A = 1;
        B = 2*Ksp*Hinf^2*y(6)/K2/KP/H0 - KP*y(8)/Hinf/H0 - Cl/H0;
        C = -KW/H0^2 - 2*K2*KP/H0^2/Hinf*y(8);
        hh = -B/2 + sqrt(B.^2 - 4*A.*C)/2;
        %hh = 1-y(6);
        %    if x==ZL
        %        fprintf('x=%5.3e h (exact)=%5.3e h (approx)=%5.3f\n',x,hh,1-y(6)
        %    end
        brhs = km2/omega                                *(Hinf*y(10)/H0./hh-y(8));
        urhs = -k1/omega*H0/Hinf*(hh+k2*KW/k1/H0).*(Hinf*y(10)/H0./hh-y(8));
        %        if x==0
        %            fprintf('Hinf*y(10)/H0/hh-y(8) = %16.13e\n',Hinf*y(10)/H0/hh
        %        end
        dydx =[y(2)
            y(3)
```

```
            -0.5*y(2)^2 + 2*y(4)^2 + y(1)*y(3)
            y(5)
            -y(2)*y(4) + y(1)*y(5)
            y(7)
            Sc*y(1)*y(7)
            y(9)
            Sc*y(1)*y(9) - Sc*brhs
            y(11)
            Sc*y(1)*y(11) - Sc*urhs];
    end


    function res = fcnsBC(ya,yb)
        % Boundary conditions for the system on the boundaries [a,b]
        % The initial functions for all of the solutions
        % y1 = H, y2 = H', y3 = H'',
        % y4 = G, y5 = G'
        %
        % H(0) = 0, H'(0) = 0, H'(infinity) = 0,
        % G(0) = 1, G(infinity) = 0
        %
        % y6 = c, y7 = c'
        % y8 = b, y9 = b'
        % y10= u, y11= u'
        %
        % c(0) = (H0/Hinf)^2*h0^2/u0, c(infinity) = const*S(t)
        % b(0) = (Hinf/H0)*u0/h0, b(infinity) = (Hinf/H0)*1/hinf
        % u'(0) = 0, u(infinity) = 1;
        %Hp00 = -2*a1;
        %Gp0 = b1;
        temp = fcnsinit(ZL);
        GZL = temp(4);
        HpZL = temp(2);
        %         u0 = ya(10);
        %         temp = geth0(u0,0,0);
        %         b0 = temp(2);
        %         c0 = temp(3);
        res = [ya(1) %H(0) = 0
            ya(2) %H'(0) = 0
            yb(2)-HpZL %H'(ZL) = HpZL
            ya(4)-1 %G(0) = 1
            yb(4)-GZL %G(ZL) = GZL
            ya(6)-c0 %c(0) = (H0/Hinf)^2*h0^2/u0
            yb(6)-cinf %c(ZL) = cinf
            ya(8)-b0 %b(0) = b0
```

```
            yb(8)-binf %b(ZL) = binf
            ya(10)-u0
            %ya(11) %u'(0) = 0
            yb(10)-uinf]; %u(ZL) = uinf
    end


    function y = show_inits(flag)
        y = 0;
        if flag == 1
            r = linspace(0,ZL);
            yinit = fcnsinit(r);
            figure
            subplot(3,4,1)
            plot(r,yinit(1,:))
            title('Initial H(\zeta)');
            subplot(3,4,2)
            plot(r,yinit(2,:))
            title('Initial H''(\zeta)');
            subplot(3,4,3)
            plot(r,yinit(3,:))
            title('Initial H''''(\zeta)');
            subplot(3,4,4)
            plot(r,yinit(4,:))
            title('Initial G(\zeta)');
            subplot(3,4,5)
            plot(r,yinit(5,:))
            title('Initial G''(\zeta)');
            subplot(3,4,6)
            plot(r,yinit(6,:))
            title('Initial c(\zeta)');
            subplot(3,4,7)
            plot(r,yinit(7,:))
            title('Initial c''(\zeta)');
            subplot(3,4,8)
            plot(r,yinit(8,:))
            title('Initial b(\zeta)');
            subplot(3,4,9)
            plot(r,yinit(9,:))
            title('Initial b''(\zeta)');
            subplot(3,4,10)
            plot(r,yinit(10,:))
            title('Initial u(\zeta)');
            subplot(3,4,11)
            plot(r,yinit(11,:))
```

```
655             title('Initial u''(\zeta)');
656             y = 1;
657         end
658     end
659
660
661     function yinit = fcnsinit(x)
662         % The initial functions for all of the solutions
663         % y1 = H, y2 = H', y3 = H'',
664         % y4 = G, y5 = G',
665         %
666         % Build a switch function that changes from 0 to 1 at x = x0
667         gammy = 10;
668         x0 = 0.3;
669         w = (tanh(gammy*(x-x0)) + 1)/2;
670         wp = 1/2*(sech(gammy*(x-x0))).^2.*gammy;
671         %
672         % y6 = c, y7 = c'
673         % y8 = b, y9 = b'
674         % y10= u, y11= u'
675         %
676         % The asymptotic behaviour for for x < 1
677         a1 = 0.510232618867;
678         b1 = -0.615922014399;
679         yAinit = [ -a1*x.^2 + x.^3/3 + b1*x.^4/6
680             -2*a1*x + x.^2 + 2*b1*x.^3/3
681             -2*a1 + 2*x + 2*b1*x.^2
682             1 + b1*x + a1*x.^3/3
683             b1 + a1*x.^2
684             c0*(1-w) + cinf*w
685             c0*(0-wp) + cinf*wp
686             b0*(1-w) + binf*w
687             b0*(0-wp) + binf*wp
688             u0*(1-w) + uinf*w
689             u0*(0-wp) + uinf*wp];
690         % The asymptotic behaviour for for x >> 1
691         a0 = 0.884919;
692         A1 = 0.93344;
693         B1 = 1.21046;
694         C = A1^2+B1^2;
695         yBinit = [ -a0 + 2*A1*exp(-a0*x)/a0 - C*exp(-2*a0*x)/2/a0^3
696             -2*A1*exp(-a0*x) + C*exp(-2*a0*x)/a0^2
697             2*a0*A1*exp(-a0*x) - 2*C*exp(-2*a0*x)/a0
698             B1*exp(-a0*x) - B1*C*exp(-3*a0*x)/12/a0^4
699             -a0*B1*exp(-a0*x) + B1*C*exp(-3*a0*x)/4/a0^3
```

```
            c0*(1-w) + cinf*w
            c0*(0-wp) + cinf*wp
            b0*(1-w) + binf*w
            b0*(0-wp) + binf*wp
            u0*(1-w) + uinf*w
            u0*(0-wp) + uinf*wp];
        % Switch from one to the other depending on x
        yinit = yAinit*diag(x<1) + yBinit*diag(1-(x<1));
    end

    function [y] = geth0(u0t,flags_details1,flags_details2)
        %
        % Given a value for u0, determine h0, b0 and c0
        %--------------------------------------------------------------------
        % Find the value of h0 (Dimensionless hydrogen level when c0 = c0max and
        %--------------------------------------------------------------------
        % When u0 = 1 this should return h0 = Hinf/H0, b0 = 1, c0 = 1
        if flags_details1 == 1, fprintf('\nSolving for h0,b0,c0\n'), end
        gam = sqrt(K2*KP*Cl/2/Ksp);
        if u0t < (KW/gam/Cl)^2
            lam = (KW*u0t/gam/Cl)^(1/3);
        else
            lam = sqrt(u0t);
        end
        j = 1;f = 1;
        if flags_details1 == 1, fprintf('Newton iterations to compute h0\n'), end
        while (j < 20 && abs(f) > eps)
            if flags_details1==1, fprintf('j = %3i lam = %16.13e err = %5.3e\n',j,
            f = lam^4 + lam^3*gam/Cl*u0t - lam^2*u0t - (KW*u0t+KP*u0t^2)/Cl/gam*la
            fp = 4*lam^3 + 3*lam^2*gam/Cl*u0t - 2*lam*u0t - (KW*u0t+KP*u0t^2)/Cl/g
            if lam~=0
                lam = lam - f/fp;
            end
            j = j + 1;
        end
        h0temp = lam*gam/H0;
        if u0t == 0
            c0temp = 1;
            b0temp = 0;
        else
            c0temp = (H0/Hinf)^2*h0temp^2/u0t;
            b0temp = (Hinf/H0)*u0t/h0temp;
        end
        if flags_details1 == 1
            if abs(f) > eps
```

```
745                 fprintf('ERROR: h0 DID NOT CONVERGE\n')
746             else
747                 fprintf('j = %3i lam = %16.13e err = %5.3e\n',j,lam,f)
748             end
749             fprintf('Computed h0 = %16.13e\n',h0temp)
750         end
751         if flags_details1 == 1 && flags_details2 == 1
752             fprintf('\nTest of consistency (h0 values).\n')
753             fprintf('(Calculated)           (Thesis section 4.4.3)\n')
754             fprintf('u0=%16.13e u0=%16.13e\n',u0t,u0t)
755             fprintf('h0=%16.13e h0=%16.13e\n',h0temp,Hinf/H0*sqrt(u0t))
756             %    fprintf('(OH)  =%16.13e (OH)  =%16.13e\n',KW/H0,KW/Cl)
757             fprintf('b0=%16.13e b0=%16.13e\n',b0temp,sqrt(u0t))
758             %    fprintf('(CO3) =%16.13e (CO3) =%16.13e\n\n',K2*KP/H0^2,K2*KP/Cl^2)
759             fprintf('c0=%16.13e c0=%16.13e\n',c0temp,1)
760             %fprintf('\nBEFORE: \nu0 = %10.6e, h0 = %10.6e,\nb0 = %10.6e, c0 = %10.6e\
761             %fprintf('h(approx)=%5.3e b(approx)=%5.3e c(approx)=%5.3e\n',Hinf*sqrt(u0)
762             fprintf('Saturation condition  Hinf*c0*b0/H0 - h0 = %5.3e\n',Hinf*c0temp*b0t
763             fprintf('Equilibrium condition Hinf*u0/H0 - b0*h0 = %5.3e\n\n',Hinf*u0t/H0 -
764         end
765         y(1) = h0temp;
766         y(2) = b0temp;
767         y(3) = c0temp;
768     end
769
770     function [y] = gethinf(cinftemp,flags_details1,flags_details2)
771         %
772         % Given a value for cinf, determine hinf, binf assuming uinf = 1
773         %-------------------------------------------------------------------------
774         % Find the value of hinf (Dimensionless hydrogen level when uinf = 1 and cinf
775         %-------------------------------------------------------------------------
776         % When cinf = 0 this should return hinf = 1, binf = Hinf/H0
777         if flags_details1==1, fprintf('Solving for hinf,binf\n'), end
778         lam = (1-cinftemp)/2 + 1/2*sqrt((1-cinftemp)^2+4*KP/H0^2);
779         j = 1;f = 1;
780         if flags_details1 == 1, fprintf('Newton iterations to compute hinf\n'), end
781         while (j < 20 && abs(f) > eps)
782             if flags_details1==1, fprintf('j = %3i lam = %16.13e err = %5.3e\n',j,lam,f)
783             f = lam^3 + (2*Ksp*Hinf^2*cinftemp/K2/KP/H0-Cl/H0)*lam^2 - (KW+KP)/H0^2*lam
784             fp = 3*lam^2 + 2*(2*Ksp*Hinf^2*cinftemp/K2/KP/H0-Cl/H0)*lam - (KW+KP)/H0^2;
785             lam = lam - f/fp;
786             j = j + 1;
787         end
788         hinftemp = lam;
789         binftemp = (Hinf/H0)*1/hinftemp;
```

```
790         if flags_details1 == 1
791             if abs(f) > eps
792                 fprintf('ERROR: hinf DID NOT CONVERGE\n')
793             else
794                 fprintf('j = %3i lam = %16.13e err = %5.3e\n',j,lam,f)
795             end
796             fprintf('Computed hinf = %16.13e\n',hinftemp)
797         end
798         if flags_details1 == 1 && flags_details2 == 1
799             fprintf('Comparison: Exact                Approximate\n')
800             fprintf('      hinf: %16.13e %16.13e\n',hinftemp,1-cinftemp)
801             fprintf('      binf: %16.13e %16.13e\n',binftemp,Hinf*1/H0*(1+cinftemp
802             fprintf('      cinf: %16.13e ---\n',cinftemp)
803             fprintf('Equilibrium condition Hinf*uinf/H0 - binf*hinf = %5.3e\n\n',H
804         end
805         y(1) = hinftemp;
806         y(2) = binftemp;
807         y(3) = cinftemp;
808     end
809 end
810
811
812
813 %-------------------------------------------------------------------------
814 % EXTERNAL FUNCTIONS
815 %-------------------------------------------------------------------------
816
817 function [x] = rock_kcarbonatevals(Tc,idx,debug)
818 %
819 % Returns the rate k1, k-1, k2, k-2 of the various carbonate reactions,
820 % the equilibrium constants KW, K2, K5, KH, and finally Ksp
821 %
822 % If no arguments then supply all values at 25 C
823 % If one argument then supply all values at Tc
824 % If two arguments then only supply that index
825 % If three arguments then output verbose messages
826 if nargin < 3, debug = 0; end;
827 if nargin < 2
828     N = 9;
829     x = zeros(N,1);
830 else
831     N = 1;
832 end
833 if nargin < 1, Tc = 25; end;
834 T = Tc + 273.16;
```

```
% 1: k1  (carbon dioxide to bicarbonate via water)
% 2: k-1 (bicarbonate to carbon dioxide via water)
% 3: k2  (carbon dioxide to bicarbonate via hydroxide)
% 4: k-2 (bicarbonate to carbon dioxide via hydroxide)
% 5: KW  (Dickson and Riley 1979)
% 6: K2  (Plummer and Busenberg 1982)
% 7: K5  (Kern 1960 theory with modern rate constants)
% 8: KH  (Henry's constant for the dissolution of CO2 in water)
% 9: Ksp (Solubility product from Patnaik 2003 handbook
for loop = 1:N
    if nargin < 2, idx = loop; end
    switch idx
        case 1 %log_10 k1
            if debug==1, disp('k1'); end
            y = 329.850 - 110.54*log10(T) - 17265.4./T; % Usdowski 1982
        case 2 %log_10 k-1 Usdowski 1982
            if debug==1, disp('k-1'); end
            y = 13.558 - 3617.1./T; % Usdowski 1982
        case 3 %log_10 k2
            if debug==1, disp('k2'); end
            y = 13.635 - 2895./T; % Usdowski 1982
        case 4 %log_10 k-2
            if debug==1, disp('k-2'); end
            y = 14.09 - 5308./T; % Usdowski 1982
        case 5 %log_10 KW
            if debug==1, disp('KW'); end
            %logKW = 22.801 - 4787.3./T - 0.010365*T - 7.1321*log10(T); % Harned and H
            lnKWn = 148.9802 - 13847.26./T - 23.6521*log(T); % Dickson and Riley 1979
            y = log10(exp(lnKWn));
        case 6 %K2 P&B 1982
            if debug==1, disp('K2'); end
            y = -107.8871 + 5151.59./T - 0.03252849*T + 38.92561*log10(T) - 563713.9./T.
            %logK22 = -2902.39./T - 0.02379*T + 6.4980; % Harned and Scholes, 1941
        case 7 %K5
            if debug==1, disp('K5'); end
            %y = log10(1.707e-4)*ones(length(T)); % P&B 1982
            % Kern 1960 theory with modern rate constants
            %K5  = k2*km1*KW/km2/k1
            %K5' = k2*KW/km2
            log10k1 = 329.850 - 110.54*log10(T) - 17265.4./T;
            log10km1 = 13.558 - 3617.1./T;
            log10k2 = 13.635 - 2895./T;
            log10km2 = 14.09 - 5308./T;
            lnKWn = 148.9802 - 13847.26./T - 23.6521*log(T);
            log10KW = log10(exp(lnKWn));
```

```
880             y = log10km1 + log10k2 + log10KW - log10km2 - log10k1;
881         case 8 %KH
882             if debug==1, disp('KH'); end
883             y = 108.3865 - 6919.53./T + 0.01985076*T - 40.45154*log10(T) + 669365.
884         case 9 %Ksp
885             if debug==1, disp('Ksp'); end
886             y = log10(4.47e-9);
887     end
888     if nargin < 2
889         x(loop) = 10.^y;
890     else
891         x = 10.^y;
892     end
893 end
894 % Extra possible sets of values
895 % From Johnson 1982
896 % @article{johnson1982carbon,
897 %   title={Carbon dioxide hydration and dehydration kinetics in seawater},
898 %   author={Johnson, K.S.},
899 %   journal={Limnology and Oceanography},
900 %   pages={849--855},
901 %   year={1982},
902 %   publisher={JSTOR}
903 % }
904 % T = 25+273.16; S = 0;
905 % A = [1246.98 -930.13 1346.24 -2225.22];
906 % B = [0 0.110 -0.126 -0.049];
907 % D = [-6.19 3.10 -6.44 8.91]*1e4;
908 % E = [-183 140.9 -196.4 336.6];
909 % logkco2 =  A(1) + B(1)*sqrt(S) + D(1)/T + E(1)*log(T);
910 % logkohKW = A(2) + B(2)*sqrt(S) + D(2)/T + E(2)*log(T);
911 % logkd =    A(3) + B(3)*sqrt(S) + D(3)/T + E(3)*log(T);
912 % logkhco3 = A(4) + B(4)*sqrt(S) + D(4)/T + E(4)*log(T);
913 % kco2 = exp(logkco2)
914 % kohKW = exp(logkohKW)
915 % kd = exp(logkd)
916 % khco3 = exp(logkhco3)
917
918 % For Soli
919 % @article{soli2002co,
920 %   title={CO< sub> 2</sub> system hydration and dehydration kinetics and the eq
921 %   author={Soli, A.L. and Byrne, R.H.},
922 %   journal={Marine chemistry},
923 %   volume={78},
924 %   number={2},
```

```
%   pages={65--73},
%   year={2002},
%   publisher={Elsevier}
% }
% T = 25+273.16;
% lnkd = 30.15-8018/T;
% logKa = -0.994-610.5/T
% lnkh = 22.66-7799/T;
% K5 = 10^logKa
% kd = exp(lnkd)
% kh = exp(lnkh)
% K = kd/kh
% K5p = K5/(1+K)
% logK1 = log10(K5p)
end

function [x] = rock_carbonatedissnparams(Tc,rpm)
%
% Returns the physical parameters of the experiment
% 1A: DCO2 (Diffusion coefficient of dissolved CO2: Zeebe, 2011)
% 1B: nu (Viscosity of water: Kreslin, 1978)
% 1: Sc (Schmidt number)
% 2: Re (Reynolds number)
% 3: omega (Rotation rate in rad/sec)
% 4: cs (Molarity of calcium in a calcite crystal)
% 5: Rd (Radius of sample)
% 6: Rv (Radius of container)
T = Tc + 273.16;
DCO2 = 14.8836*((T/217.2056)-1).^1.9970;
DCO2 = DCO2*1e-9;
nu = 9.82e-7;
Sc = nu/DCO2; % Schmidt number
omega = 2*pi*rpm/60;
rhos = 2.7102e3; % Density kg/m^3
Ms = 100.0869; % Molecular weight g/mol
cs = rhos/Ms; % moles/l
Rd = 1.5*2.54/2*1e-2; %1.5 inches in diameter expressed in metres
Rv = 5*2.54/2*1e-2; %5 inches in diameter expressed in metres
Re = omega*Rd^2/nu;
x(1) = Sc;
x(2) = Re;
x(3) = omega;
x(4) = cs;
x(5) = Rd;
x(6) = Rv;
```

```
970 end
```

APPENDIX G

List of Publications

1. Yazdani, Camelia and Bohun, C.Sean "Modelling Calcite Dissolution in a Rotating Disk Reaction Vessel." The IV AMMCS International Conference, Aug 20-25, 2017.